University of Szeged

Faculty of Pharmacy

Department of Pharmaceutical Technology

Head: Prof. Dr. habil. Piroska Szabó-Révész D.Sc.

Ph.D. Thesis

Investigation of the skin barrier function and transdermal drug delivery techniques

By

Boglárka Balázs
pharmacist

Supervisors:

Dr. habil. Erzsébet Csányi
Dr. Szilvia Berkó Ph. D.

Szeged

2016

PUBLICATIONS RELATED TO THE SUBJECT OF THESIS

I. **Boglárka Balázs,** Gabriella Farkas, Ottó Berkesi, Rolland Gyulai, Szilvia Berkó, Mária Budai-Szűcs, Piroska Szabó-Révész, Lajos Kemény, Erzsébet Csányi: Protein structure is changed in psoriatic skin on the unaffected region – imaging possibility with ATR-FTIR spectroscopy. MICROCHEMICAL JOURNAL 117. 183–186. (2014)
IF: 2.746 Citations: 3

II. Corina Danciu, Marius Biriş, **Boglárka Balázs**, Erzsébet Csányi, Ioana Zinuca Pavel, Georgeta Pop, Codruta Soica, Lavinia Ceuta, Lucian Nita, Claudiu Morgovan, Dana Stoian: Pro-apoptotic Effect of Soy Total Extract Incorporated in Lyotropic Liquid Crystals Formulation, REVISTA DE CHIMIE 66. 1038–1041. (2015)
IF: 0.810

III. Corina Danciu, Szilvia Berkó, Gábor Varju, **Boglárka Balázs**, Lajos Kemény, István Balázs Németh, Andreea Cioca, Alexandra Petruş, Cristina Dehelean, Citu Ioan Cosmin, Elena Amaricai, Claudia Crina Toma: The Effect of Electroporation of a Lyotroic Liquid Crystal Genistein-Based Formulation in the Recovery of Murine Melanoma Lesions, INTERNATIONAL JOURNAL OF MOLECULAR SCIENCES 16. 15425–15441. (2015)
IF: 2.862

IV. **Boglárka Balázs**, Eszter Csizmazia, Szilvia Berkó, Mária Budai-Szűcs, Piroska Szabó-Révész, Erzsébet Csányi: New approach of sucrose myristate as a promising penetration enhancer in dermal preparations, TENSIDE SURFACTANTS DETERGENTS 52. 375–379. (2015)
IF: 0.739

V. **Boglárka Balázs**, Péter Sipos, Corina Danciu, Stefana Avram, Codruta Soica, Cristina Dehelean, Gábor Varju, Gábor Erős, Mária Budai-Szűcs, Szilvia Berkó, Erzsébet Csányi: An ATR-FTIR and Raman spectroscopic investigation of the electroporation-mediated transdermal delivery of a nanocarrier system

containing an antitumour drug, BIOMEDICAL OPTICS EXPRESS 7. 67–78. (2016)
IF: 3.648

VI. **Boglárka Balázs**, Gábor Vizserálek, Szilvia Berkó, Mária Budai-Szűcs, András Kelemen, Bálint Sinkó, Krisztina Takács-Novák, Piroska Szabó-Révész, Erzsébet Csányi: Investigation of the efficacy of transdermal penetration enhancers through the use of human skin and a skin mimic artificial membrane, JOURNAL OF PHARMACEUTICAL SCIENCES 105. 1134–1140. (2016)
IF: 2.590

PRESENTATIONS RELATED TO THE SUBJECT OF THESIS

I. Corina Danciu, Ciurlea Sorina, Erzsébet Csányi, **Boglárka Balázs**, Avram Ştefana, Camelia Peev, Dehelean Cristina: A new approch in the recovery of murine melanoma lesions: electroporation of lyotropic liquid crystals genistein based formulation, 5th BBBB International Conference, Athen, Greece, 26-28. September 2013. (poster)

II. **Balázs Boglárka**: A pszoriázisos bőr fehérje struktúrájának újszerű vizsgálati lehetősége, XX. Szent-Györgyi Napok, Szeged, 2013. november 15. (verbal presentation)

III. **Balázs Boglárka**, Csizmazia Eszter, Berkó Szilvia, Szabóné Révész Piroska, Csányi Erzsébet: Szacharóz-zsírsavészterek penetrációfokozó hatásának vizsgálata, XV. Congressus Pharmaceuticus Hungaricus, Budapest, 2014. április 10-12. (poster)

IV. **Boglárka Balázs**, Eszter Csizmazia, Szilvia Berkó, Piroska Szabó-Révész, Erzsébet Csányi: Penetration enhancer effect of sucrose esters, Skin Forum 14th Annual Meeting, Prague, Czech Republic, 4-5. September 2014. (poster)

V. **Boglárka Balázs**, Szilvia Berkó, Mária Budai-Szűcs, Piroska Szabó-Révész, Erzsébet Csányi: Drug diffusion and permeation studies of Genistein containing Lyotropic liquid crystals, 5th International Conference and Exhibition on

Pharmaceutics & Novel Drug Delivery Systems, Dubai, UAE, 16-18. March 2015 (poster)

VI. **Boglárka Balázs**, Mónika Bakonyi, Eszter Csizmazia, Szilvia Berkó, Mária Budai-Szűcs, Piroska Szabó-Révész, Erzsébet Csányi: Non-invasive in vivo comparison of penetration enhancers containing hydrogel formulations, 1st European Conference on Pharmaceutics - Drug Delivery, Reims, France, 13-14. April 2015. (poster)

VII. **Balázs Boglárka**: Szacharóz-zsírsavészterek penetrációfokozó hatásának vizsgálata, Richter Gedeon Centenáriumi Alapítvány előadóülés, Budapest, 2015. március 05. (verbal presentation)

VIII. Csupor Dezső, Jedlinszki Nikoletta, **Balázs Boglárka**, Csányi Erzsébet: Veszélyes-e a nadálytő? Egy farmakokinetikai vizsgálat tanulságai, XIV. Magyar Gyógynövény Konferencia, Pannonhalma, Magyarország, 2015. május 29-30. (poster)

IX. **Boglárka Balázs**, Attila Léber, Szilvia Berkó, Mária Budai-Szűcs, Piroska Szabó-Révész, Erzsébet Csányi: In vivo investigation of newly developed microemulsion and lyotropic liquid crystal systems, 4th International Conference and Expo on Cosmetology & Trichology, Philadelphia, USA, 22-24. June 2015. (poster)

X. Nikoletta Jedlinszki, Anikó Dobó Beretka, **Boglárka Balázs**, Dezső Csupor: Absorption of lycopsamine from a comfrey ointment through human skin, 63rd International Congress and Annual Meeting of the Society for Medicinal Plant and Natural Product Research (GA2015), Budapest, Hungary, 23-27. August 2015. (poster)

XI. Léber Attila, **Balázs Boglárka**, Berkó Szilvia, Csányi Erzsébet: Új típusú nanohordozó rendszerek bőrre gyakorolt hatásának tanulmányozása non-invazív NIR spektroszkópiai és *in vivo* vizsgálati módszerekkel, Gyógyszertechnológiai és Ipari Gyógyszerészeti Konferencia, Siófok, 2015. október 15-17. (poster)

XII. **Balázs Boglárka**, Berkó Szilvia, Csányi Erzsébet: Elektoporáció, mint a bőrön keresztüli hatóanyag bejuttatás új típusú lehetősége, Gyógyszertechnológiai és Ipari Gyógyszerészeti Konferencia, Siófok, 2015. október 17. (verbal presentation)

TABLE OF CONTENTS

ABBREVIATIONS

API active pharmaceutical ingredient
ATR-FTIR attenuated total reflection Fourier transform infrared
BR Britton-Robinson buffer
CAM chorioallantoic membrane
C_d drug concentration of the donor phase
CPE chemical penetration enhancer
CRH40 Cremophor RH 40
CT conventional treatment
EF enhancement factor
EI enhancer index
EP electroporation
FSD Fourier self-deconvolution
GEN genistein
GLY glycerol
HLB hydrophilic-lipophilic balance
IBU ibuprofen
IPM isopropyl myristate
J steady state flux
K_p permeability coefficient
K_{pe} K_p of the hydrogel with the CPE
K_{pef} K_p of the CPE-free hydrogel
LLC lyotropic liquid crystal
LLC-GEN genistein-containing lyotropic liquid crystal
MCR-ALS multivariate curve resolution – alternating least squares
PBS phosphate buffer solution
Q cumulative amount of API diffused/penetrated per cm^2
R^2 determination coefficient
SC stratum corneum
SD standard deviation
SE sucrose fatty acid ester
SEM standard error of the mean
Skin PAMPA skin parallel artificial membrane permeability assays
SL sucrose laurate
SLS sodium lauryl sulfate
SM sucrose myristate
TEWL transepidermal waterloss
TR Transcutol
XYL xylitol

1. INTRODUCTION

Great attention is currently paid to skin care and skin disease prevention. Physical and psychological health are affected to considerable extents by the integrity of the skin. An appropriate skin condition is therefore essential for healthy skin.

From a pharmaceutical industrial standpoint, the skin is a desirable target for drug delivery. The first transdermal drug was approved by the US Food and Drug Administration over 35 years ago. Today, transdermal products represent a growing, multibillion dollar market. The US transdermal drug delivery market approached $1.2 billion in 2001, $6.7 billion in 2006 and nearly $7.9 billion in 2010. By 2015, the global transdermal market is expected to reach $32 billion (Walter et al., 2015).

Not surprisingly, transdermal drug delivery has received increased attention in recent years thanks to its numerous advantages over the oral and injection routes, such as avoidance of the hepatic "first-pass" metabolism, sustained drug delivery, protection of the gastrointestinal tract from drugs and good patient compliance. Unfortunately, the number of drugs which can be administered by this route is limited. Increase of the number of transdermally applied drugs and the optimization of drug delivery through the human skin are therefore important research opportunities in modern therapy. Ideal transdermal drug delivery systems must be designed to overcome the skin barrier and deliver a therapeutically effective amount of drug through the skin, while skin barrier repair must be facilitated and a good skin condition ensured.

In order to enhance transdermal drug absorption, different methodologies have been investigated and developed. Improvements in physical penetration enhancement technology have led to renewed interest in transdermal drug delivery. Some of these novel advanced transdermal penetration enhancement techniques include iontophoresis, electroporation (EP), ultrasound, microneedles to open up the skin, and more recently the use of transdermal nanocarriers.

More complex drug–device combinations are being developed to overcome the natural barrier function of the skin. From a pharmaceutical technological viewpoint, it is an interesting task to investigate the new transdermal drug delivery techniques, in the interest of the optimization and development of these strategies.

2. LITERATURE BACKGROUND

2.1. Skin structure and barrier function

The skin, which forms the barrier between the body and the environment, is the largest organ of the body with a surface area of 2 m^2; it accounts for about 16% of the body weight. It consists of three main layers: the epidermis, the dermis and the subcutaneous layer (**Fig. 1**).

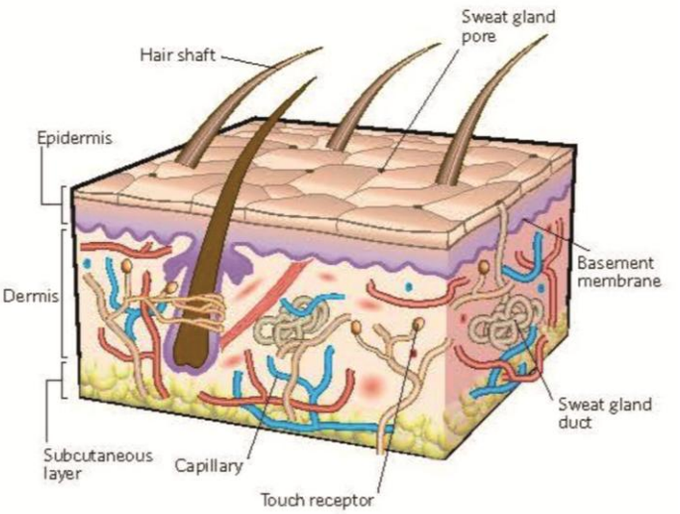

Figure 1. Sectional view of the skin (MacNeil, 2007).

The epidermis is the 0.05–1.5 mm thick external layer, which serves as the physical and chemical barrier between the interior body and the exterior environment (**Fig. 2**). It is mainly composed of keratinocytes (about 90%), but also contains melanocytes (about 8%), Langerhans cells and Merkel cells (Tortora et al., 2014). It consists of five major layers, but the main penetration barrier for most drugs is the stratum corneum (SC), the outermost 10–15 μm thick zone of the epidermis (Barry, 1983). The SC consists of several layers of almost nonpermeable, nonviable cornified cells (corneocytes) embedded in an intercellular matrix of lipids. These lipids comprise approximately 50% ceramides, 25% cholesterol, 15% free fatty acids and some minor components (Prausnitz et al., 2012).

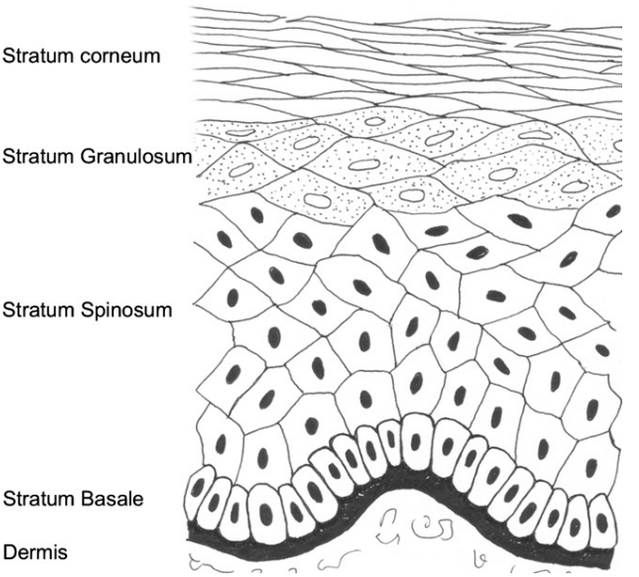

Figure 2. Sectional view of the epidermal layers. The clear layer (not shown) is found only in the very thick epidermis of the palms and soles (Wickett et al., 2006).

The dermis, which is 3–5 mm thick, is composed of connective tissue containing collagen and elastic fibers. It is situated below the epidermis and contains sweat glands, hair roots, nerve cells, fibers, and blood and lymph vessels. Its main functions are the regulation of body temperature, the supply of oxygen and nutrients to the skin, and the removal of toxic products.

The subcutaneous layer (hypodermis) is not part of the skin but, as one of its functions, it attaches the skin to the underlying tissues and organs. It is made up of loose connective tissue and fat, which can be up to 3 cm thick on the abdomen (Tortora et al., 2014).

The SC protective barrier may undergo disorganization as a result of several skin diseases (such as atopic dermatitis, psoriasis and contact dermatitis), environmental or intrinsic factors, psychological stress and aging (Grice, 1980; Ghadially et al., 1995; Denda et al., 1998; Denda et al., 2000). The skin condition affects the overall confidence of the majority of people. At a global level, skin conditions are the fourth leading cause of nonfatal diseases. Skin disease prevention and the development of a targeted dermal system which ensures individual patient treatment are therefore needed to prevent human skin problems in the world today (**Fig. 3**) (Hay et al., 2014).

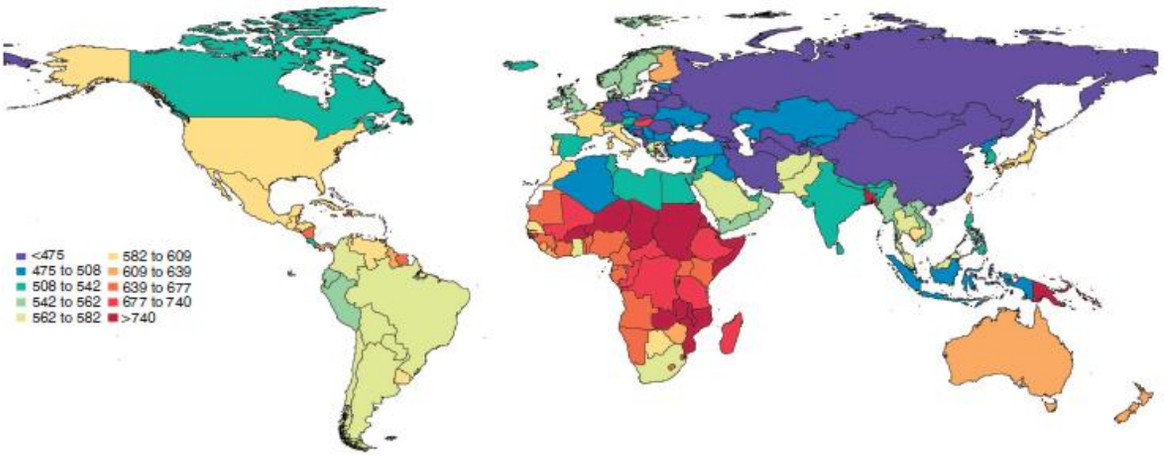

Figure 3. Disability-adjusted life year rate per 100,000 individuals in 2010 (all skin conditions combined) (Hay et al., 2014).

Psoriasis, one of the most common chronic inflammatory skin diseases, with a frequency of approximately 1-2% of the population in the developed world, is characterized by regular exacerbations of cutaneous symptoms and frequent articular involvement. The diagnosis is usually made on clinical grounds, though rarely a skin biopsy is necessary. The disease has a polygenic inheritance, and the expression of the symptoms is greatly influenced by environmental factors, such as stress or streptococcal infections (Schön et al., 2005; Bernard et al., 2007).

Histologically, the disease is characterized by keratinocyte hyperproliferation, lymphocyte and granulocyte infiltration of the epidermis and dermis, and vasodilation of the dermal blood vessels. It is well known that multiple lipid bilayers play an important role in the permeability of the skin, and psoriatic skin is more permeable than healthy skin (Bernard et al., 2007). A number of studies have demonstrated that psoriatic skin exhibits alterations in lipid metabolism (Motta et al., 1994; Holtje et al., 2001), whereas the changes in the proteins and their conformations in the SC of psoriatic skin have not been well studied to date.

2.2. Drug penetration through the skin

Increasing the transdermal delivery of the drug through the skin is a challenging obstacle because very few drugs fit the criteria. The best candidate drug for transdermal delivery has the following properties (Guy, 1996; Finnin et al., 1999; Bos et al., 2000; Benson, 2005):

- molecular weight < 500 Da,
- melting point < 200 °C,

- log $P_{\text{octanol/water}}$ between 1 and 4,
- a dose < 50 mg per day, and ideally < 10 mg per day,
- ≤ 2 hydrogen-bonding groups,
- not an irritant to the skin,
- and does not stimulate an immune reaction in the skin.

The three potential pathways by which drugs can cross the SC are the intercellular, transcellular and transappendageal routes (**Fig. 4**). The intercellular route is the predominant penetration pathway of drug molecules under normal circumstances. In this pathway, the drug overcomes the SC by passing between the corneocytes. This route involves sequential diffusion and partitioning between the polar head groups and the alkyl chains of the intercellular lipids, and the diffusional path length is therefore much longer than the simple thickness of the SC and has been estimated as long as 500 μm (Hadgraft, 2004).

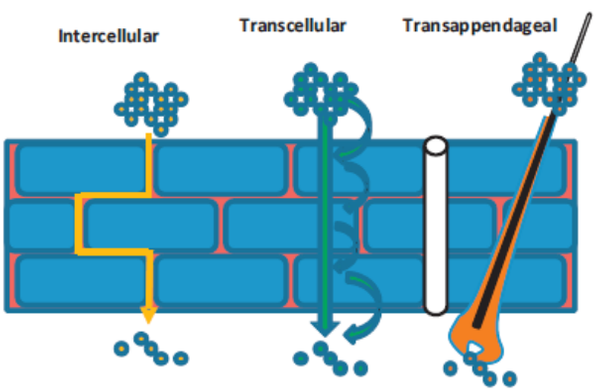

Figure 4. Different transport pathways through the SC (Lane, 2013).

The shortest route for drugs is the transcellular pathway. This is a direct route where the drug has to cross the skin by directly passing through both the lipid structures of the SC and the cytoplasm of the dead keratinocytes. However, drugs resist penetration because they have to cross both lipophilic and hydrophilic structures (Trommer et al., 2006).

The transappendageal route is considered to be minor (Moser et al., 2001) because sweat glands and hair follicles occupy only 0.1% of the total surface area of the human skin (Scheuplein, 1967). However, the hair follicles have been shown to be a relevant penetration pathway for particles and also an important long-term reservoir (Lademann et al., 2011). Furthermore, iontophoretic drug delivery uses an electrical charge to drive molecules into the skin primarily via the transappendageal route as this provides less electrical resistance (Benson, 2005).

2.3. Transdermal drug delivery strategies

2.3.1. Passive methods

The conventional means of applying drugs to the skin include vehicles such as ointments, creams, gels and patch technology. Such dosage forms have recently been developed and/or modified to enhance the driving force of drug diffusion (thermodynamic activity) and/or increase the permeability of the skin. The passive strategies most widely applied with the aim of improving drug penetration involve the skin hydration and the use of chemical penetration enhancers (CPEs). Increased tissue hydration tends to increase skin penetration and is the safest method through which to increase the transdermal delivery of both hydrophilic and lipophilic compounds. The ideal semisolid dermal drug delivery system should moisturize the skin well in order to enhance drug penetration (Barry, 2001).

More than 360 CPEs have been demonstrated to enhance the skin permeability (Karande et al., 2005). Their mechanisms of action involve disruption of the intercellular lipids of the highly ordered SC, or interaction with intracellular proteins, or improvement of the drug partition into the SC (Garg et al., 2013).

The ideal CPE should be nonirritating, nontoxic and nonallergenic, should have rapid, unidirectional working with predictable duration and have no pharmacological activity, and should be compatible with both excipients and drugs. Not surprisingly, to date only few have been routinely incorporated in the currently marketed transdermal products (Williams et al., 2004). Investigations of the efficacy of CPEs are therefore highlighted that will promote the rational selection of CPEs and ultimately the development of safer and more efficacious formulations. **Table 1** summarizes the classification of CPEs based on the chemical class to which the compounds belong.

Transcutol (TR) and sucrose esters (SEs) are biocompatible CPEs. TR is a powerful solubilizing agent that enhances the percutaneous penetration of various drugs, especially when it is used in combination with suitable surfactants (Touitou et al., 1994; Cázares-Delgadillo et al., 2005).

SEs, a new generation of nonionic surfactants, are likewise favorable CPEs. They consist of a sugar substituent, sucrose as the hydrophilic group and a fatty acid as the lipophilic group (Mitsubishi-Kagaku Foods Co., 1982). These natural compounds possess many advantages, such as low toxicity, good biocompatibility and excellent biodegradability (Kanikkannan et al., 2002; Youan et al., 2003). Ionic surfactants (e.g. sodium lauryl sulfate,

SLS) are generally more potent CPEs than their nonionic counterparts, but these agents can damage the barrier of the skin if applied for a long time. SEs, which cause less dermatological damage, act by altering the ordered structure of the intercellular region of the SC (Csóka et al., 2007). Their hydrophilic-lipophilic balance (HLB) value ranges from 1 to 16 (Ganem-Quintanar et al., 1998). SEs are widely used in the food and cosmetic industries and have recently received increased attention in the pharmaceutical field (Szűts et al., 2012).

Glycerol (GLY), which is also applied in several external formulations, hydrates the skin because it acts as a humectant (Rawlings et al., 2004; Andersen et al., 2007). Moreover, it improves the barrier function, exerts an anti-irritant effect, stabilizes the skin collagen and accelerates wound healing (Fluhr et al., 1999; Fluhr et al., 2008). Xylitol (XYL) is a naturally occurring polyol, which is a widely used substitute of sugar. Recent studies indicated that XYL can also be utilized as a humectant and moisturizer (Cohen et al., 1993; Leite e Silva et al., 2009).

Table 1. The classification of CPEs (Marwah et al., 2015).

Chemical class	Compounds
Water	Water
Hydrocarbons	Alkanes, Alkenes, Squalene, Mineral oil, Halogens
Alcohols	Glycerols, Glycols, Polyglycols, Ethanol, Caprylic alcohol
Acids	Oleic acid, Undecanoic acid and other fatty acids
Amines	Primary, secondary and tertiary, cyclic and acyclic amines
Amides	Pyrrolidone(*N*-methyl-2-pyrrolidone, 2-pyrrolidon), azones (Azone) (1-dodecylazacycloheptan-2- one)), Urea
Ethers	Diethylene glycol monoethyl ether (Transcutol)
Esters	Isopropyl myristate, Sucrose fatty acid esters
Surfactants (anionic, cationic, non-ionic, Zwitterionic)	Sodium lauryl sulfate, Cetyltrimethyl ammonium bromide, Sorbitan monolaurate, Polysorbate 80, Dodecyl dimethyl ammoniopropane sulfate
Terpenes, terpenoids and essential oils	Menthol, Limonene
Sulfoxides	Dimethyl sulfoxide, Dodecyl methyl sulfoxide
Lipids	Phospholipids

Another convenient method of increasing drug transport across the skin is the use of carrier formulations as skin delivery systems. In this respect, an interesting possibility is offered by lyotropic liquid crystals (LLCs). They are characterized by the properties of both liquids and solids, i.e. they exhibit in part a structure typical of fluids and also the structured, crystalline state of solids (Tadwee et al., 2012). LLCs are usually formed from water and one or two surfactants and possibly cosurfactants and oils. The advantageous qualities of such formulations include their amphiphilic nature, the similarity to colloidal systems existing in living organisms, the various structures of liquid crystal states, and their thermodynamic stability (Makai et al., 2003; Vicentini et al., 2007). LLCs display good solubilizing effects and the sustained release and enhanced bioavailability of other lipophilic drugs (Boyd et al., 2006).

Other passive possibilities are outlined in **Table 2**. However, the amounts of drugs that can be delivered by these methods are limited because the barrier properties of the skin are not fundamentally changed, which has led to studies involving alternative strategies, referred to as active methods.

Table 2. Passive transdermal drug delivery strategies (Barry, 2001).

Passive method	**Type**
Drug-vehicle interactions	Drug/prodrug selection Ion pairs Eutectic systems
Vesicles and particles	Liposomes and analogues High velocity particles
SC modification	Hydration Chemical penetration enhancers

2.3.2. Active methods

These strategies have been shown to deliver macromolecules (> 500 Da, polar or apolar molecules) by the use of external energy to act as a driving force and/or reduce the barrier nature of the SC. The active methods cause stronger disruption of the SC barrier, while still protecting deeper tissues. The development of active methods was made possible by the emergence of technologies to localize effects to the SC combined with the safety issue (Brown et al., 2006). **Table 3** shows various active methods of enhancing drug transport through the skin.

Table 3. Active transdermal drug delivery strategies (Brown et al., 2006).

Active method	Type
Electrical methods	Iontophoresis Electroporation
Mechanical methods	Microneedle/puncture/perforation Abrasion Needless injection Suction Stretching
Miscellaneous	Ultrasound Magnetophoresis Radio frequency Laser and photomechanical waves Temperature

Electroporation (EP) is currently one of the most promising modes of active enhancement for the noninvasive transdermal delivery of lipophilic, hydrophilic, charged or neutral molecules or macromolecules. EP involves the application of short (microsecond to millisecond) pulses of high voltage (100–1500 V) to achieve a transitory structural perturbation of the lipid bilayer membranes (Prausnitz et al., 1993; Neumann et al., 2000). Its main advantages are that it is an easy and rapid technique which is able to open the lipid bilayer membranes. Appropriate transdermal transport necessitates adjustment of the voltage, the pulse duration and the number of series of impulses (Wong, 2014). The appropriate skin EP for the transdermal transport of drugs with molecular weights up to 40 kDa across the skin can thereby be increased by several orders of magnitude (Lombry et al., 2000; Denet et al., 2004).

Currently the most rapidly developing area of EP is electrochemotherapy, which is an effective way of treating cutaneous and subcutaneous tumors. This method consists in applying high voltage pulses to permeabilize tumor cells to an impermeable cytotoxic drug which is given by injection either into a vein or directly into a tumor (Mir et al., 1999).

2.3.3. Future prospects – combinations of enhancing methods

Recent studies have suggested that suitably designed combinations of enhancing methods are safer and more effective than each of them alone (Prausnitz et al., 2008). The synergistic effects between EP and ultrasound, EP and iontophoresis or EP and pre/cotreatment with CPEs have been reported earlier (Vanbever et al., 1997; Zewert et al., 1999; Mitragotri, 2000; Sen et al., 2002). However, not only the combination of two active

methods or an active and a passive method can be successful. The high-throughput screening of 500 different pairs of CPEs was studied by Karande et al., who reported that a combination of appropriate CPEs could increase the skin permeability to macromolecules (~ 1–10 kDa) by up to ~ 100-fold without inducing skin irritation. For example, the potency and safety of a combination of sodium laureth sulfate and phenylpiperazine (a compound containing aromatic nitrogen) were confirmed by the transdermal delivery of leuprolide acetate (Karande et al., 2004). Screening to find such synergistic combinations is continuing because it provides useful information for the development of a transdermal dosage form (Kling et al., 2007).

3. EXPERIMENTAL AIMS

The primary aim of my study was to investigate promising transdermal penetration enhancer techniques. To achieve this, the skin barrier structure was examined and different types of novel penetration enhancers were tested alone or in combination from the aspect of the achievement of the effective transdermal drug delivery. The following steps were set.,

1. In the first part of my Ph.D. work, the healthy and the diseased skin, especially the unaffected area in the psoriatic skin was studied in order to gain a deeper insight into the highly perturbed functions of the diseased SC, and to help to find the healthy volunteers for the skin measurements.
2. In the second part, different penetration-enhancing strategies were optimized to ensure appropriate transdermal drug delivery. The aims were:
    - to compare the penetration-enhancing effect of a newly developed SE, sucrose myristate (SM), with the generally used sucrose laurate (SL);
    - to investigate the behavior of TR and SEs applied alone or in combination through the use of a Skin PAMPA artificial membrane system and human skin;
    - to examine the possibility of the spectral analysis of the effects of polyols in SLS-induced acute irritation;
    - to develop a suitable carrier for the poorly water-soluble, lipophilic phytocompound genistein (GEN);
    - to investigate the transdermal delivery of an LLC-based GEN-containing formulation (LLC-GEN) alone or in combination with EP; and
    - to test the recovery effect of LLC-GEN application and its combination with EP on murine melanoma lesions.

My Ph.D. work plan is summarized in **Fig. 5.**

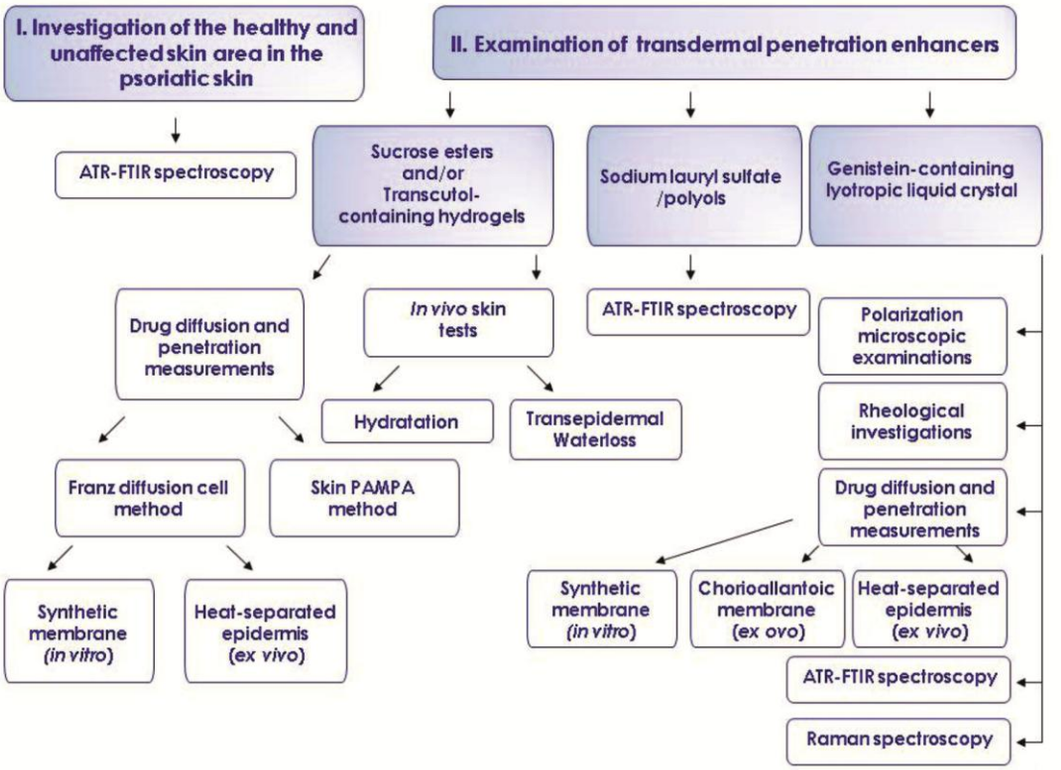

Figure 5. Overall scheme of the Ph.D. work.

4. MATERIALS AND METHODS

4.1. Materials

4.1.1. Sucrose esters and/or Transcutol-containing hydrogels

A CPE-free hydrogel (Control gel) was prepared by the following procedure. 5 wt.% Ibuprofen (IBU, Sigma-Aldrich, St Louis, MO, USA) was dissolved in polyethylene glycol 400 (20 wt.%) (Hungaropharma Ltd., Budapest, Hungary) and this solution was added to a 3 wt.% Carbopol 971 (Lubrizol Corporation/Azelis, Budapest, Hungary) hydrogel prepared with distilled water. The pH was adjusted to 7.0 by adding trolamine (7 wt.%) (Hungaropharma Ltd., Budapest, Hungary).

Two SEs, SL and SM, were purchased from Mitsubishi-Kagaku Foods Corporation, Tokyo, Japan. To compare the two SEs, 2.64 wt.% of each was incorporated individually in Carbopol 971-based hydrogel (SL gel and SM gel). 2.64 wt.% was chosen because this gave the maximum SE concentration-containing hydrogel which did not require a centrifugation process to remove the bubbles. Similar compositions were prepared by using 10 wt.% TR

(Gattefossé and Lubrizol Corporation/Azelis, Budapest, Hungary) (TR gel). 2.64 wt.% SE + 10% TR-containing gels were prepared too (SL + TR and SM + TR gel).

Different concentrations of SE-containing gels were also prepared by a similar method (SL 1; 2; 4; 6; 8; or 10 wt.% gel, SM 0.25; 0.5; 1; 2; 4; 6; or 10 wt.% gel) to investigate the *in vitro* diffusion influenced by the CPE contents.

4.1.2. Genistein-containing lyotropic liquid crystal formulation

GEN was purchased from Extrasynthèse (Genay, France; purity > 95%), and the nonionic surfactant Cremophor RH 40 (CRH40; Polyoxyl 40 Hydrogenated Castor Oil USP/NF) from BASF (Ludwigshafen, Germany). The aqueous phase of the systems was distilled water, and the oil phase was isopropyl myristate (IPM; Merck Kft., Budapest, Hungary).

A GEN-free LLC was prepared by the following procedure. The oil–surfactant mixture (oil:surfactant ratio = 2:1) was homogenized with a magnetic stirrer at room temperature. 10 wt.% of water was then added in small amounts to this mixture during stirring. A similar composition was prepared by using 3 wt.% GEN incorporated in the oil–surfactant mixture with a magnetic stirrer.

4.2. Methods

4.2.1. Drug diffusion and penetration investigations

4.2.1.1. Franz diffusion cell method

Membrane diffusion and permeability studies of active pharmaceutical ingredients (APIs) were carried out with a vertical Franz diffusion cell system (Hanson Microette TM Topical & Transdermal Diffusion Cell System, Hanson Research Co., Chatsworth, CA, USA). A stirring rate of 450 rpm was used. The receptor medium temperature was maintained at 37 ± 0.5 °C throughout the experiments to support the physiological skin temperature (32 ± 0.5 °C) on the membrane in the Franz cell (Mura et al., 2009). The donor phase was 0.30 g of sample, which was placed on a cellulose acetate membrane (Porafil, Machenerey-Nagel, Düren, Germany, and Pall Life Sciences, Washington, NY, USA) itself (*in vitro*), or in the case of *ex ovo* and *ex vivo* measurements the chorioallantoic membrane (CAM) and the epidermis were supported with the Porafil membrane filter. Samples of 0.8 ml were taken from the acceptor phase by the autosampler (Hanson Microette Autosampling System, Hanson Research Co., Chatsworth, CA, USA) and replaced with fresh receiving medium. Five parallel

measurements were made of the amount of drug that penetrated over a time period. The absorbance of the API content was measured with a Unicam Helios α Thermospectronic UV-spectrophotometer v4.55 (Unicam, Thermo Fisher Scientific, Waltham, MA, USA). The further details of the investigations are summarized in **Table 4**.

Table 4. Detailed parameters of drug diffusion and penetration investigations (BR: Britton-Robinson buffer, PBS: phosphate buffer solution, SD: standard deviation, SEM: standard error of the mean).

	SEs and/or TR-containing hydrogels			**LLC-GEN**		
Drug diffusion/penetration studies	*in vitro*	*ex vivo*	Skin PAMPA	*in vitro*	*ex ovo*	*ex vivo*
API	IBU	IBU	IBU	GEN	GEN	GEN
Surface area	1.767 cm^2	1.767 cm^2	-	1.33 cm^2	1.33 cm^2	1.33 cm^2
Acceptor phase	PBS (pH = 7.4)	PBS (pH = 7.4)	BR (pH = 7.4)	10 wt.% ethanol-containing PBS (pH = 7.4)	10 wt.% ethanol-containing PBS (pH = 7.4)	10 wt.% ethanol-containing PBS (pH = 7.4)
Time	24 h	16 h	16 h	24 h	24 h	48 h
Absorbance of the API content	263 nm	263 nm	263 nm	261 nm	261 nm	261 nm
Results	means ± SD	means ± SD	means ± SD	means ± SEM	means ± SEM	means ± SEM

4.2.1.2. Skin PAMPA method

The Skin PAMPA model involves recently published artificial membrane-based technology for the fast prediction of skin penetration. The method was reported previously (Vizserálek et al., 2015).

4.2.1.3. Preparation of chorioallantoic membrane

The CAM for the *ex ovo* experiment, was provided by Victor Babes University of Medicine and Pharmacy, Timisoara, Romania. The method of its preparation was described previously (Balázs et al., 2015).

4.2.1.4. Preparation of heat-separated epidermis

Excised human skin was obtained during abdominal plastic surgery on a Caucasian female patient. This was approved in advance by the Ethical Committee of the Human Investigation Review Board at Albert Szent-Györgyi Clinical Center, University of Szeged. The subcutaneous fat tissue was separated from the outer skin layers after the excision, and the skin was stored at −20 °C overnight. Then, after thorough defrosting, membrane separation was achieved with a previously reported method (Kligman et al., 1963). Individual portions were immersed in water at 60 °C for 90 s. After removal of the skin from the water, it

was placed SC side up on a filter paper, and the epidermis (comprising the SC and the viable epidermis) was gently removed from the underlying dermis with the use of forceps. The latter was discarded and the epidermal membrane was floated onto the surface of PBS (pH = 7.4) for at least 20 min and then placed on a supporting Porafil membrane (cellulose acetate, pore diameter 0.45 μm) (Brain et al., 2007; Schroeder et al., 2007).

4.2.1.5. Analysis of drug penetration

In vitro IBU diffusion parameters were obtained from the cumulative amount of IBU diffused per cm^2 (Q) versus time plots. The steady state flux (J) was obtained from the slope of the linear regression versus $t^{1/2}$. The permeability coefficient (K_p) was calculated according to Fick's first law of diffusion, based on J and the applied drug concentration (C_d) of the donor phase (Wagner et al., 2001):

$$K_p = J/C_d \quad (1)$$

The effectiveness of CPEs was determined by comparing the K_p in the presence and absence of the CPE. This was defined as the enhancer index (EI), which was calculated by using the K_p of the hydrogel with the CPE (K_{pe}) and the K_p of the CPE-free Control gel (K_{pef}) (Vaddi et al., 2002):

$$EI = K_{pe}/ K_{pef} \quad (2)$$

Ex vivo/Skin PAMPA penetration parameters of IBU were obtained from the cumulative amount of IBU penetrated per cm^2 (Q) versus time plots. The J was calculated from the slope of the concentration versus time profile in the receiver compartment, and expressed in $\mu g\ cm^{-2}\ h^{-1}$. For the linear regression analysis, the linear range of the incubation period from 1 to 6 h was selected, and this range was used to calculate the flux data of the compounds.

The effectiveness of the CPE was determined by comparing the flux of IBU in the presence and in the absence of the CPE. This was defined as the enhancement factor (EF), which was calculated via the following equation (Yan et al., 2007).

$$EF = (\text{flux of the penetrant from the gel containing the CPE})/(\text{flux of the penetrant from the Control gel without the CPE}) \quad (3)$$

The flux data from the GEN investigations were obtained as described above in connection with the *ex vivo*/Skin PAMPA penetration parameters of IBU.

Two-way ANOVA was performed to identify any significant difference in the diffused and penetrated amounts of IBU (Q) between the Control gel and the test preparations using

GraphPad Prism software (Graph-Pad Software Inc., La Jolla, CA, USA). Differences were regarded as significant if $p < 0.05$*, $p < 0.01$* or $p < 0.001$***.

The correlation between the data on the Skin PAMPA model and the human epidermis was calculated via the following expression:

$$R = \frac{\sum(x - \overline{x})(y - \overline{y})}{\sqrt{\sum(x - \overline{x})^2 \sum(y - \overline{y})^2}} \quad (4)$$

where R is the correlation, x and y are the amounts of penetrated drug as a function of time in the case of the human epidermis and the Skin PAMPA model, respectively, and $\overline{x}$ and $\overline{y}$ are the average values of x and y.

4.2.2. Skin hydration and transepidermal waterloss (TEWL) measurements

Skin hydration was measured with a Corneometer® CM 825 (Courage and Khazaka Electronic GmbH, Cologne, Germany). The TEWL measurements were performed with the Tewameter® TM 300 instrument (Courage and Khazaka Electronic GmbH, Cologne, Germany). The TEWL is an indicator of the integrity of the skin barrier, and measurement of the TEWL is an easy and rapid noninvasive means of examining the effects of newly developed transdermal systems (Tanojo et al., 1998; Yilmaz et al., 2006). Measurements were performed under standardized conditions (room temperature of 21–23 °C, and 40–50% relative humidity). Seven healthy female volunteers aged between 23 and 60 years with no history of dermatological diseases or allergy participated in the experiment. Informed consent was obtained from all these volunteers and the study was approved by the local ethics committee (the Regional and Institutional Human Medical Biological Research Ethics Committee at the University of Szeged). The volunteers were asked not to apply any moisturizer or cosmetic product for at least 24 h before the process. They were given 30 min to adapt to the measurement room conditions. During the experiment, samples (0.30 g) were applied to the dorsal region of the hand (a 3 x 3 cm area) of all the subjects. The electrical capacitance of the SC, indicating the hydration level of the SC, was determined before and 30, 90 and 150 min after the sample application. The measured values were compared with the values detected on the non-treated skin, and the changes in hydration were expressed as percentages. TEWL values were determined on the same area of the skin before and 30 and 150 min after the sample application. The measured values were compared with the values detected on the non-treated skin, and the changes in TEWL were expressed as percentages (Nicander et al., 2004; Savic et al., 2004; Betz et al., 2005). Two-way ANOVA was

performed to determine the statistical difference between the data for the various preparations and the Control gel; *, ** and *** indicate $p < 0.05$, $p < 0.01$ and $p < 0.001$, respectively (GraphPad Prism software).

4.2.3. Polarization microscopic examinations

The structures of the LLC samples were examined with a polarization microscope (LEICA Q500 MC Image Analyzer System) at room temperature. The magnification was 20x.

4.2.4. Rheological investigations

The rheological profiles of the samples were studied with a PaarPhysica MCR101 rheometer (Anton Paar GmbH, Graz, Austria). The measuring device was of plate–plate type (diameter 25 mm, gap distance 0.2 mm). The measurements were carried out at 25 °C. The linear viscoelastic range was determined in the first step by examining the complex modulus as a function of the shear stress at a given frequency (1 Hz). On the basis of these experiments, the shear stress was set at 1 Pa during the dynamic testing as this value was always within the linear viscoelastic range. The storage and loss moduli values were examined as a function of frequency (0.01–10 Hz).

4.2.5. Electroporation parameters

The Mezoforte Duo EP device (Serial Number Mez 120905-D) produced by Dr Derm Equipment Ltd. (Budapest, Hungary) was provided by the Derm Clinic of Anti-Aging Dermatology, Aesthetic Laser and Plastic Surgery (Budapest, Hungary). The device operates on the basis of a pulsed electromagnetic field. The polypropylene-covered treating handpiece contains a 25 mm diameter plate electrode in direct contact with the treated surface. Modulation was achieved with high-voltage pulses with a voltage pulse duration of 5 ms, followed by a 20 ms break.

4.2.6. Attenuated total reflection Fourier transform infrared (ATR-FTIR) spectroscopy measurements

ATR-FTIR spectroscopy is a suitable tool for studies of the structure of the SC at the molecular level, in order to characterize its lipids, proteins and water content (Dias et al., 2008). The method allows analysis of the penetration of drugs into the skin and the biochemical modifications induced by the penetration (Csizmazia et al., 2012). ATR-FTIR combined with tape-stripping is essentially a nondestructive sampling technique which serves as a rapid, simple, noninvasive *in vivo* method for studies of the skin. Sequential tape-

stripping permits the acquisition of SC layers from the deeper regions. The ATR device allows spectra to be taken from the surface of a sample without any preparation (Bommannan et al., 1990).

ATR-FTIR spectra were recorded with an Avatar 330 FT-IR spectrometer (Thermo Nicolet, Waltham, MA, USA) equipped with a horizontal ATR crystal (ZnSe, 45°), between 4000 and 400 cm^{-1}, at an optical resolution of 4 cm^{-1}. 128 scans or in the case of investigations of GLY and XYL, 64 scans were co-added and all spectral manipulations were performed with the Thermo Scientific's GRAMS/AI Suite software. No ATR correction was performed.

For the investigation of *human psoriatic skin*, the components of the amide-I band and their relative intensities were estimated semiquantitatively in the 1695–1600 cm^{-1} region of the FTIR spectra by a curve-fitting algorithm, using Gaussian–Lorenzian mixing functions. The best fits were found by an iterative process minimizing the standard error. The results of curve-fitting were evaluated and analyzed statistically by Student's t-test (Graph-Pad Software Inc., La Jolla, CA, USA). The data given are the averages of the results of 13 parallel (3 psoriatic and 10 healthy) experiments ± SD ($p < 0.05$*, $p < 0.01$**).

For *animal experiments*, in order to obtain a reference spectrum of the API, KBr pellets containing 0.5 mg of SLS or GEN were prepared and used. The spectra of treated and untreated samples were also recorded. Each average layer spectrum of the treated SC was corrected with the corresponding average layer spectrum of the untreated SC. To ensure that no absorbances from the skin itself remained and interfered with the results, the spectra of untreated control skin samples were subtracted from the spectra of water-treated control skin samples.

4.2.6.1. Human experiments

Psoriatic SC samples were obtained from 6 untreated psoriatic patients (3 males and 3 females) aged between 32 and 64 years. Normal SC samples were collected from 20 healthy volunteers (10 males and 10 females) aged between 21 and 42 years with no history of dermatological disease. The study was approved by the local ethics committee (Government Office of Csongrád County Policy Administration Services of Public Health, PSO-SPEKT-001). All volunteers were asked not to apply any moisturizer or cosmetic product for at least 24 h before the process. The forearm skin of each volunteer was stripped with adhesive cellophane tape; this was repeated up to 25 strips. In the case of the psoriatic patients, the

samples were taken from the unharmed skin of the forearm. Every first tape with one strip was discarded because of the possibility of surface contamination. Every second adhesive tape with three strips was analyzed, because this gave the most intensive IR spectrum.

4.2.6.2. Animal experiments

12–15 week old male SKH-1 hairless mice were housed in plastic cages in a thermoneutral environment with a 12 h light-dark cycle and had access to standard laboratory chow and water *ad libitum*. All interventions were in full accordance with the NIH guidelines and the protocols were approved in advance by the Ethical Committee for the Protection of Animals in Scientific Research at the University of Szeged (licence number: V./145/2013).

4.2.6.2.1. Spectroscopic investigations of the effects of polyols in sodium lauryl sulfate-induced acute irritation

Mice were randomly allocated into six groups. Group 1 (n = 23) served as a control treated with purified water. Group 2 (n = 23) was exposed to a 5 wt.% solution of SLS. In group 3 (n = 23), the solution applied to the skin contained 5 wt.% SLS and 5 wt.% GLY. The animals in group 4 (n = 23) received a solution containing 5 wt.% SLS and 8.26 wt.% XYL. Group 5 (n = 23) was treated with 5 wt.% SLS and 10 wt.% GLY, while in group 6 (n = 23), 5 wt.% SLS and 16.52 wt.% XYL were applied to the skin. The SLS and the polyols were dissolved in purified water. The appropriate GLY and XYL solutions were equiosmolar. In each group, 15 mice were randomly chosen for patch testing. In closed patch tests, extra-large Finn Chambers (diameter 18 mm) and corresponding filter discs soaked with 120 μl of the test solutions were applied to the dorsal region for 3 h, using Scanpore tape (SmartPractice, Phoenix, AZ, USA). The relative humidity was 40–50% and the ambient temperature was kept at 20–22 °C. The patch testing was followed by ATR-FTIR. The corneocytes were obtained from the dorsal region of the patch-tested mice with adhesive cellophane tape. This was repeated up to 25 strips, an IR spectrum being recorded after each third tape strip. Every first tape with one strip was discarded because of the possibility of surface contamination. The untreated dorsal skin of the mice was stripped and measured with the same method. Data analysis was performed with SigmaStat (Systat Software Inc., Chicago, IL, USA). Differences between groups were analyzed with Kruskal-Wallis one-way analysis of variance on ranks, followed by the Dunn method for pairwise multiple comparison. $p < 0.05^*$ was considered statistically significant.

4.2.6.2.2. Investigations of Genistein-containing lyotropic liquid crystal

The mice involved in this study were divided into 5 groups as follows:

Group I: mice treated with dermally applied LLC-GEN for 2 min (conventional treatment)

Group II: mice treated with LLC-GEN and EP at 700 V for 1 min

Group III: mice treated with LLC-GEN and EP at 900 V for 1 min

Group IV: mice treated with LLC-GEN and EP at 700 V for 2 min

Group V: mice treated with LLC-GEN and EP at 900 V for 2 min

5 mice were randomly assigned to each experimental condition. Corneocytes were collected from the uppermost layer of their dorsal skin with the use of adhesive tape (D Squames, CuDerm Corporation, Dallas, TX, USA) immediately after treatment. The treated and the untreated dorsal skin of each mouse was stripped with adhesive tape; this procedure was repeated up to 18 strips, an IR spectrum being recorded after every third tape strip. Every first tape with one strip was discarded because of the possibility of surface contamination. Two-way ANOVA was used to identify any significant differences in the total penetrated amount of GEN between the conventional treatment and the combined EP treatments by using GraphPad Prism software. Differences were regarded as significant if $p < 0.05$*.

4.2.7. Raman measurements

For Raman measurements, 2 mice were randomly assigned to each of groups I, III and V as described in section 4.2.6.2.2. *"Investigations of Genistein-containing lyotropic liquid crystal"*. At the end of the observation period, the animals in these groups were sacrificed and full-thickness skin samples were excised from the treated areas. The samples were embedded in Cryomatrix resin (Thermo Fisher Scientific Inc., Waltham, MA, USA) and cryosections of 6 μm were made.

Raman spectra were acquired with a Dispersive Raman Microscope (Thermo Fisher Scientific Inc., Waltham, MA, USA) equipped with a CCD camera and a diode laser operating at 780 nm. The spectra of CRH40, IPM and GEN were collected with an exposure time of 6 s, with 48 scanning and cosmic ray and fluorescence corrections. Raman measurements were carried out with a laser power of 12 mW at a slit width of 25 μm. The localization of GEN in the skin samples was investigated by confocal Raman mapping. For mapping, the microtomed skin samples as depth sections were rotated by 90° and placed on an aluminum surface with the SC toward the top of the plate. Thus, a 1000 μm length of the sample specimen corresponds to a 1000 μm depth into the skin. The mapping was achieved in

a point-by-point mode, using a step size of 10 μm perpendicular and parallel to the SC. Raman maps of skin with dimensions 30–40 μm parallel and 900–1300 μm perpendicular to the SC surface were generated one by one. The spectrum acquisition time was 3 s per spectrum, and 24 spectra were accumulated and averaged at each measured point, these parameters ensuring an acceptable signal-to-noise ratio. The mapping was carried out with a laser power of 24 mW at a slit width of 25 μm. The vibrational chemical images were studied by a multivariate curve resolution – alternating least squares (MCR-ALS) chemometric method; the purpose was to identify GEN in the Raman spectra.

4.2.8. Murine melanoma investigations

Animal studies were conducted on 7–8 week old C57BL/6J female mice with an average weight of 20–25 g, purchased from Charles River (Sulzfeld, Germany). The experiments were conducted in accordance with the rules of the Ethical Committee of Victor Babes University of Medicine and Pharmacy, Timisoara, Romania. The number of mice involved in the study was 30, divided equally into 6 groups of 5 animals as follows:

Group A: blank group

Group B: mice inoculated with B164A5 cells and otherwise not treated

Group C: mice inoculated with B164A5 cells and treated with LLCs without GEN

Group D: mice inoculated with B164A5 cells and treated with LLCs with 3 wt.% GEN

Group E: mice inoculated with B164A5 cells and treated with LLCs without GEN and EP at 900 V for 6 min

Group F: mice inoculated with B164A5 cells and treated with LLCs with 3 wt.% GEN and EP at 900 V for 6 min

On day 0 of the experiment, the mice in groups B–F received a subcutaneous (s.c.) inoculation of 0.1 ml containing $1*10^6$ cells/mouse into the depilated lateral abdomen. For the mice in groups C–F, treatment with 2 ml of a 3 wt.% LLC-GEN formulation was administered from day 2 post-inoculation, using 6 min of high voltage EP or the classical application as described above. The mice were inspected daily for the development of tumors or other changes. Results are presented as means ± SD. One-way ANOVA followed by the Bonferroni test was used to determine the statistical difference between the various experimental and control groups; *, ** and *** indicate $p < 0.05$, $p < 0.01$ and $p < 0.001$. Tumor growth was measured daily in millimeters, using calipers, and the tumor volume was estimated by the formula: length x $width^2/2$. The mice were subsequently sacrificed by cervical dislocation.

5. RESULTS AND DISCUSSION

5.1. Investigation of the unaffected skin area in the psoriatic skin

One of the most common applications of FTIR spectroscopy in protein studies is the analysis of secondary structure. FTIR spectroscopy involves the measurement of the wavelength and intensity of the absorption of IR radiation by a sample. The amide-I band region (1700−1600 cm^{-1}) is the spectral region most sensitive to the secondary structural components of the proteins; this is due very largely (approximately 80%) to the C=O stretch vibrations of the peptide linkages. Fourier self-deconvolution (FSD), a band-narrowing method, has not only enriched the qualitative interpretation of IR spectra, but has also provided a basis for the semiquantitative estimation of the secondary structure of proteins (Kong et al., 2007; Hadgraft et al., 2011).

The amide-I band appears clearly in the ATR-FTIR spectrum of the skin in consequence of the coupling of the transition dipole moments of the amide groups within the protein backbone. Various protein secondary structures have their own characteristic amide-I bands. However, because of the strong overlap between the characteristic bands, the amide-I bands of the recorded IR spectra are too complex to permit the direct determination of the components with various secondary structures (Barth, 2007).

Band-narrowing procedures such as FSD and curve-fitting greatly enhance the potential of this band as a meaningful structural probe. Such mathematical processes increase the degree of separation by narrowing the half-bandwidths of the individual components for easier visualization without seriously distorting the spectrum. The main disadvantage of this procedure is its tendency to magnify both the signal and the noise in the spectrum. This causes a dramatic increase in the noise level, which necessitates coupling the FSD with a smoothing function (Lamba et al., 1993; Al-Mustafa, 2002; Kong et al., 2007).

FSD of the corresponding ranges of the recorded spectra was used to determine the approximate frequencies of the components of the amide-I bands indicating the presence of protein chain sections with various secondary structures (Pelton et al., 2000; Barth, 2007). Seven bands were fitted to all the spectra and their areas were compared (**Fig. 6**). The ratios of the integrated band areas provide an estimate of the proportions of the parts with various secondary protein structures.

A protein molecule is formed from a chain of amino acids. The secondary structure of a protein is determined by the set of dihedral angles (φ and ψ) which define the spatial

orientation of the peptide backbone, and the presence of specific hydrogen-bonds. Regular secondary structures include α-helices and β-sheets. An ideal α-helix has 3.6 residues per turn, and is built up from a contiguous amino acid segment via backbone−backbone hydrogen-bond formation between amino acids in positions i and i + 4. The residues taking part in an α-helix have φ angles around −60° and ψ angles around −45°.

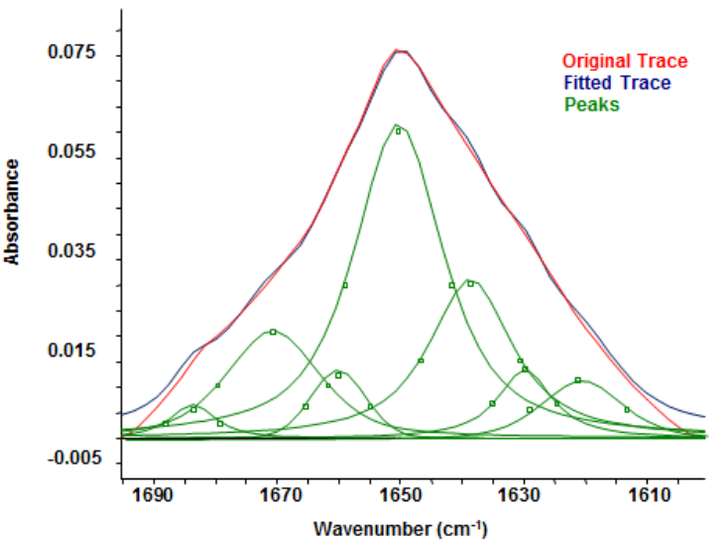

Figure 6. The original FTIR spectra of the SC and the deconvolved and curve-fitted components.

β-sheets are created when atoms of β-strands are hydrogen-bonded. β-sheets may consist of parallel strands, antiparallel strands or a mixture of parallel and antiparallel strands. In parallel β-sheets the strands run in one direction, whereas in antiparallel sheets they run in alternating directions. The dihedral angles of the β-sheet are φ ~ −130° and ψ ~ −120°, forming an extended structure with some right-handed twist.

Turns allow a protein to fold back on itself and are stabilized by a hydrogen-bond that holds the ends together. They are classified according to the number of residues involved in the hydrogen-bonded structure. Unordered structure is generally defined as a conformation that is not helix, sheet or turn (Pelton et al., 2000).

In the SC, greater flexibility is achieved through loose packing of the keratin filaments and a lower number of disulfide crosslinks. It was observed that the overall intensities of the amide-I bands were lower for the psoriatic SC than for the healthy SC (**Fig. 7**), but the peak at 1660 cm^{-1} exhibited the most pronounced alteration, as shown in **Fig. 8**.

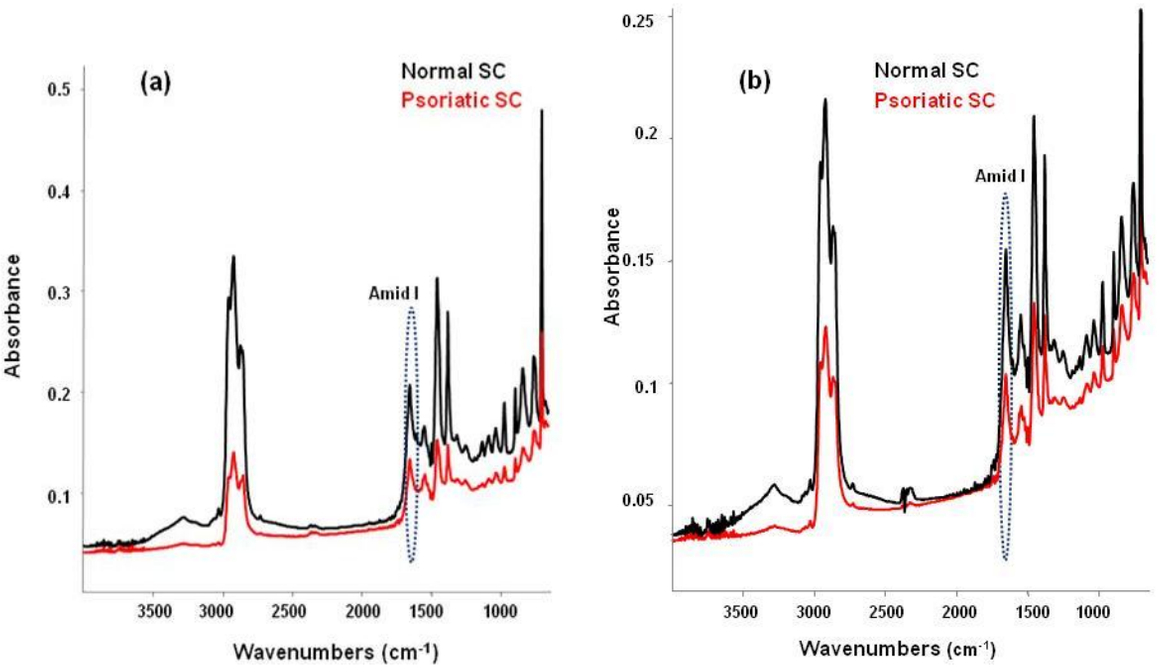

Figure 7. Differences in intensity between a normal SC and a psoriatic SC spectrum: (a) man; (b) woman.

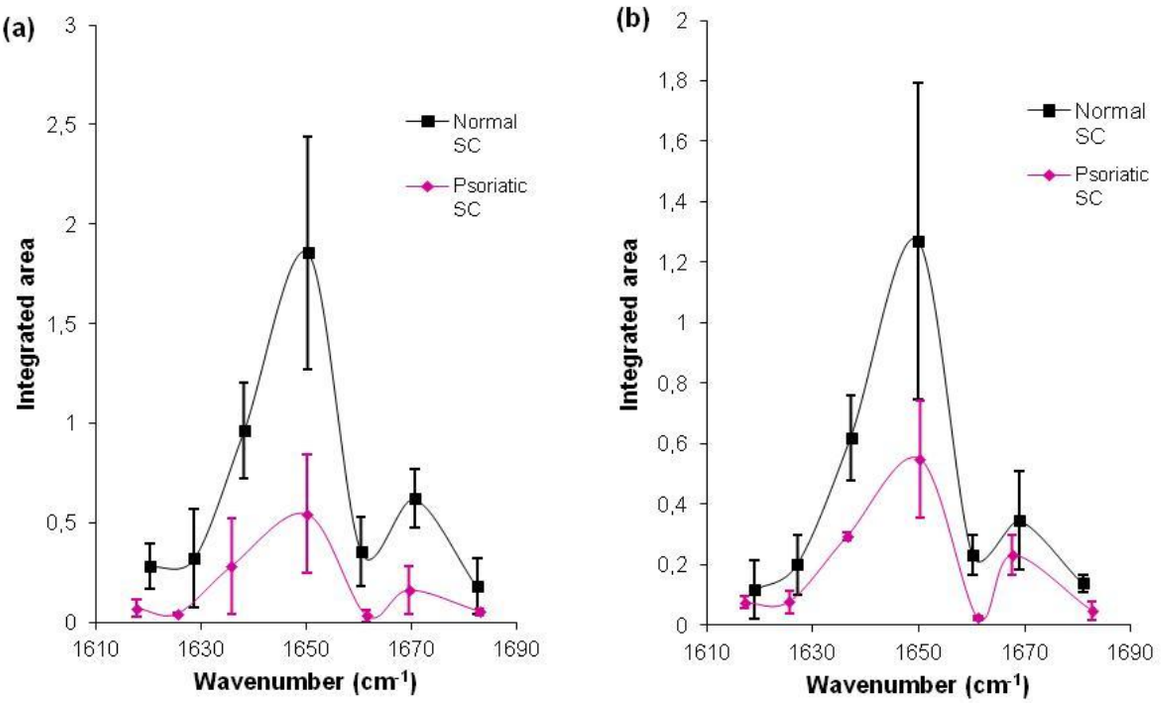

Figure 8. Areas of the fitted components of the amide-I band in the cases of normal and psoriatic SC: (a) man; (b) woman.

The proteins in the SC are mainly in α-helical conformation (Gniadecka et al., 1998). The peak at 1650 cm^{-1} indicates the presence of an α-helix (**Fig. 8**), which always has the largest area. We focused on the peak at 1660 cm^{-1}, characteristic of the turns in the protein chain (Pelton et al., 2000). It was observed that the overall intensities of the amide-I bands were lower for the psoriatic SC than for the healthy SC, but the peak at 1660 cm^{-1} exhibited the most pronounced alteration, as shown in **Fig. 8**. The intensity of this peak decreases almost to zero in psoriatic patients, indicating the drop in concentration in the turn protein regions (**Table 5**). The results for men and women are given separately, because of the differences in skin between the genders (Tur, 1997).

Table 5. Decreased integrated area of amide-I protein structures in psoriatic skin.

Conformation	β-sheet		α-helix	Turns		β-sheet	Turn
Wavenumber [cm^{-1}]	1620	1640	1650	1670	1680	1630	1660
Healthy men mean integrated area (±SD)	0,28 (0,11)	0,96 (0,24)	1,85 (0,58)	0,62 (0,15)	0,18 (0,14)	0,32 (0,25)	0,36 (0,17)
Psoriatic men mean integrated area (±SD)	0,07 (0,04)	0,28 (0,24)	0,54 (0,30)	0,16 (0,12)	0,05 (0,02)	0,04 (0,005)	0,03 (0,03)
Integrated area percentage (%) of psoriatic over healthy	**24,6**	**29,4**	**29,3**	**25,9**	**29,3**	**13,2**	**9,2**
Healthy women mean integrated area (±SD)	0,12 (0,10)	0,62 (0,14)	1,27 (0,52)	0,34 (0,16)	0,14 (0,03)	0,20 (0,10)	0,23 (0,06)
Psoriatic women mean integrated area (±SD)	0,07 (0,02)	0,29 (0,01)	0,55 (0,19)	0,23 (0,06)	0,05 (0,03)	0,08 (0,04)	0,02 (0,01)
Integrated area percentage (%) of psoriatic over healthy	**64,4**	**47,4**	**43,1**	**67**	**33,9**	**3,9**	**9,7**

Fig. 9 compares the areas of the peak at 1660 cm^{-1} for the healthy control group and the psoriatic patients. As a result of the presence of psoriasis, the intensity of this band is significantly lower for both males ($p < 0.05$*) and females ($p < 0.01$**). The areas of all the amide-I band components are less in the psoriatic group, but the decrease is especially marked in the cases of the bands at 1630 and at 1660 cm^{-1} (**Fig. 8**). The former is in the middle of the region characteristic of the β-sheet structure, and the latter reflects the turn structure. The fall in the intensity of the latter suggests the loss of those parts of the protein structure even in the unharmed psoriatic SC which provide the protein with flexibility.

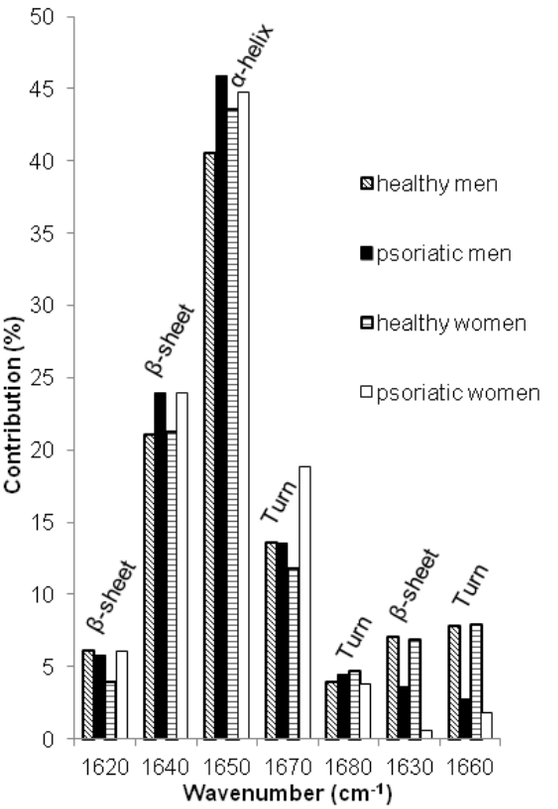

Figure 9. Percentage contributions of the components of the amide-I band for psoriatic and healthy patients of both genders.

5.2. Examination of transdermal penetration enhancers

5.2.1. Study of Sucrose esters and/or Transcutol-containing hydrogels

5.2.1.1. Drug diffusion and penetration measurements

The *in vitro* and *in vivo* skin permeability of IBU is improved by the use of a hydrophilic vehicle alone (Lee et al., 1993), but it is increased even more by the application of CPEs such as SEs (Csizmazia et al., 2012). First, in order to investigate how the SEs influenced the diffusion of IBU *in vitro*, we tested the 2.64 wt.% SE content formulations. **Fig. 10** presents the cumulative amount per unit area of IBU diffused through the synthetic membrane from the different formulations against time. Without CPEs, the drug liberation was about 6687.58±823.86 μg cm^{-2} in 24 h. Both 2.64 wt.% SE-containing hydrogels increased IBU diffusion, but in this concentration great differences were not observed between the different SEs. Although the SL-containing hydrogel caused a slightly slower drug release than the Control gel in the first few hours, the cumulative drug amount in 24 h was greater than that in the case of the Control gel. The diffused drug amounts were not statistically significant in this case. However, when SM was used, the amount of the liberated

drug was similar to that in the case of the Control gel in the first 3 h, but after 9 h the difference between the amounts of IBU diffused from the Control gel and the SM gel was statistically significant ($p < 0.05$*).

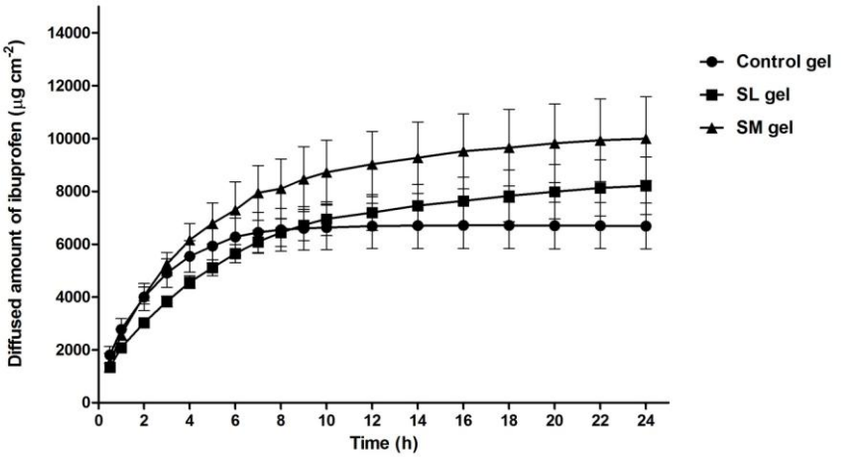

Figure 10. The cumulative diffused amount of IBU through synthetic membrane.

Next, to examine the effects of the CPE concentrations on the *in vitro* drug diffusion, we carried out *in vitro* tests with both SE gels in different concentrations. The *in vitro* fluxes (representing the absorption rate per unit area) and the EIs suggest that SL has a concentration-dependent enhancing effect (**Table 6**). It can be seen that from 2 wt.% SL content the EI values and the amount of IBU diffused after 24 h were better than in the case of the CPE-free hydrogel. We observed a maximum curve and the best penetration of IBU was strengthened by the 6 wt.% SL gel (**Fig. 11**). This gel showed the highest IBU diffusion profile and after 10 h the results were significant. The 8 wt.% and 10 wt.% SL-containing hydrogels resulted in lower penetration parameters than those with the 6 wt.% SL gel.

The studies with SM revealed the same tendency. A maximum curve was again observed, but this curve reached the maximum at much lower SE concentration, 0.5 wt.%. The diffusion profile of IBU from the 0.5 wt.% SM-containing gel revealed the highest drug release and after 3 h this formulation showed the earliest significantly increased diffused IBU amount ($p < 0.05$*) relative to the Control gel (**Fig. 11**). This gel gave the best IBU diffusion profile and enhanced the IBU diffusion 1.5-fold as compared with the EI value of the 6 wt.% SL gel. The EIs further demonstrated that SM up to 4 wt.% is more effective than SL for enhancing the diffusion of IBU through a synthetic membrane (**Table 7**).

Table 6. Parameters of IBU diffusion from different SL-containing hydrogels after 24 h.

Formulation	Q (μg cm^{-2})	J (μg cm^{-2} h^{-1})	Kp · 10^{-3} (cm h^{-1})	Enhancer Index (EI)
Control gel	6687.59 ± 869.12	971.73	19.43	1.00
SL 1% gel	2443.09 ± 425.22	117.05	2.34	0.12
SL 2% gel	7002.61 ± 1674.47	1248.60	24.97	1.28
SL 2.64% gel	8213.55 ± 1092.08	1629.60	32.59	1.68
SL 4% gel	8331.24 ± 478.75	1619.40	32.39	1.67
SL 6% gel	10824.16 ± 1130.68	2282.30	45.65	2.35
SL 8% gel	10317.58 ± 1736.76	2233.70	44.67	2.29
SL 10% gel	7542.37 ± 930.57	1575.60	31.51	1.62

Table 7. Parameters of IBU diffusion from different SM-containing hydrogels after 24 h.

Formulation	Q (μg cm^{-2})	J (μg cm^{-2} h^{-1})	Kp · 10^{-3} (cm h^{-1})	Enhancer Index (EI)
Control gel	6687.59 ± 869.12	971.73	19.43	1.00
SM 0.25% gel	11075.59 ± 1251.89	2166.20	43.32	2.76
SM 0.5% gel	14166.39 ± 549.12	2792.30	55.85	3.56
SM 1% gel	11753.84 ± 1152.88	2192.80	43.86	2.79
SM 2% gel	10449.58 ± 766.22	2109.20	42.18	2.69
SM 2.64% gel	9999.87 ± 1581.83	1932.80	38.66	2.46
SM 4% gel	9675.14 ± 1784.70	1927.90	38.56	2.46
SM 6% gel	7198.69 ± 1070.05	1387.00	27.74	1.77
SM 10% gel	1619.33 ± 282.15	312.24	6.24	0.39

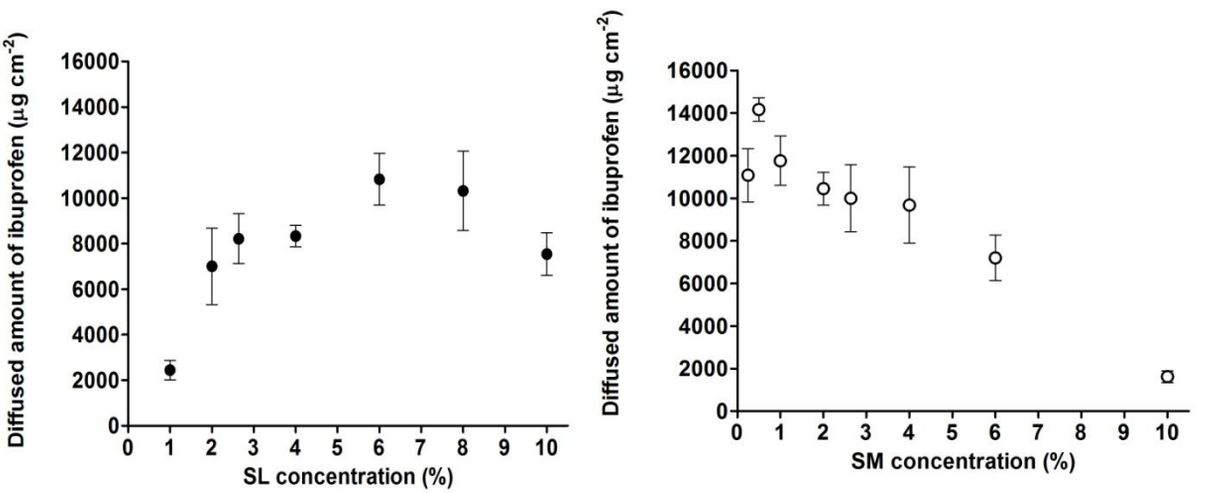

Figure 11. The amount of IBU diffused from different SL and SM-containing hydrogels after 24 h.

Table 8 presents the parameters of IBU penetration through excised human epidermis. The SE gels increased the penetration of IBU through the skin appreciably as compared with the CPE-free Control gel, but the TR gel did not enhance the IBU penetration. TR is thought to give rise to its penetration-enhancing function by increasing the solubility of the applied drug. However, TR has also been observed to display an accumulation property by increasing

the skin accumulation of topically applied drugs without a concomitant increase in transdermal penetration. TR causes the swelling of intercellular SC lipids, and lipophilic drugs such as IBU are trapped within the swollen SC lipids (Godwin et al., 2002).

Table 8. Parameters of IBU penetration through the human epidermis after 16 h.

Formulation	Q (μg cm^{-2})	J (μg cm^{-2} h^{-1})	EF
Control gel	463.95±110.50	42.72	-
TR gel	193.36±87.13	14.23	0.33
SL gel	866.79±320.42	67.93	1.59
SM gel	889.22±348.09	54.28	1.27
SL + TR gel	825.08±384.67	54.38	1.27
SM + TR gel	1527.19±764.62	91.59	2.14

As regards SEs, SL (C = 12, HLB = 16) and SM (C = 14, HLB = 16) were selected because SEs with lower C numbers and higher HLB values increase the drug release more than do SEs with longer fatty acids and lower HLBs (Csóka et al., 2007). SL has been reported to maximize the effect of a surfactant on membrane permeability (Park et al., 2000). SEs may act by disrupting the ceramide–cholesterol or cholesterol–cholesterol interaction. Increase of the carbon chain length of the fatty acids results in their molecular weights increasing, and their mobility within the skin layers is expected to decrease, which may explain their lower penetration enhancement effect (El-Laithy et al., 2009). *Ex vivo* fluxes reveal that SL induces faster IBU release than does SM, whereas the amount of penetrated IBU after 16 h was higher in the case of the SM gel. The *ex vivo* drug release behavior data indicated that SL was not a better penetration enhancer for IBU than SM (**Table 8**).

In contrast with the application of TR alone, it has been reported that its combination with SE resulted in facilitated surfactant absorption into the deeper layers of the SC. This synergistic enhancement between SE and TR affects only the penetration depth of the formulation and does not increase the amount of drug that penetrates (Ayala-Bravo et al., 2003). The SM + TR gel exhibited the best penetration parameters (**Table 8**). The SL + TR gel resulted in a lower penetration than that with the SL gel, but the difference was not statistically significant. A possible reason for this phenomenon could be that the TR depot effect predominated in the case of the SL + TR gel, because SL is not able to cause so much lipid disruption. In contrast with SL, SM may cause a greater extent of lipid alteration through its higher carbon chain and this prevents the TR depot effect. Furthermore, SM in combination with TR proved to penetrate the skin well, and there was a marked increase in

IBU release from the SM + TR gel as compared with the Control gel. The *ex vivo* statistical analysis indicated that only the SM + TR gel resulted in a significantly ($p < 0.001$***) higher penetrated IBU amount relative to the Control gel after 7 h.

Table 9 presents the penetration data on the different transdermal formulations tested with the Skin PAMPA system. Lower standard deviation and higher penetration data are observed with the PAMPA model than with the Franz cell method, which may be caused by the differences in the membrane structure in the two procedures. However, the penetration profiles obtained with the Skin PAMPA and *ex vivo* Franz cell methods were in good agreement in most cases (**Fig. 12**).

Table 9. Parameters of IBU penetration through the Skin PAMPA model after 16 h.

Formulation	Q (μg cm^{-2})	J (μg cm^{-2} h^{-1})	EF
Control gel	5204.95±311.23	432.35	-
TR gel	4941.95±966.97	329.95	0.76
SL gel	5642.38±383.43	517.06	1.20
SM gel	5812.12±150.72	512.81	1.19
SL + TR gel	5616.67±208.33	483.72	1.12
SM + TR gel	6062.98±121.23	563.1	1.30

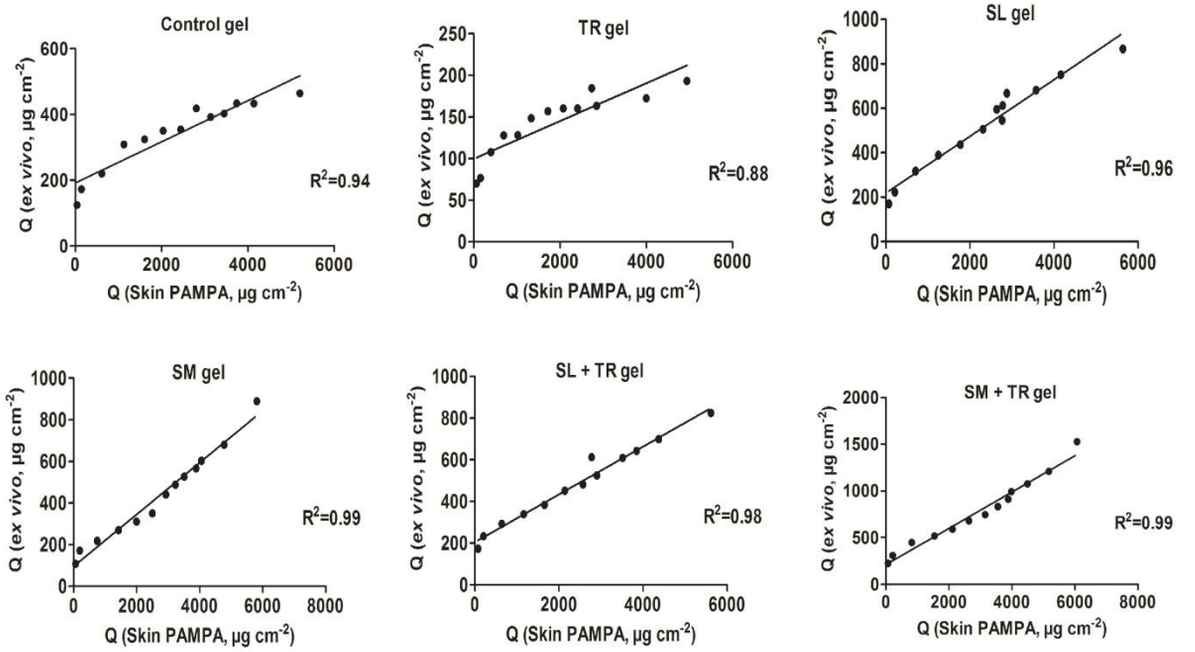

Figure 12. The correlations between the amounts of IBU penetrated through human skin and Skin PAMPA.

The differences between the PAMPA and Franz cell results clearly indicate the TR depot phenomena which can not be observed through the synthetic membrane (Park et al., 2000). The decreased amount of IBU that penetrated from the TR gel relative to the Control gel was statistically significant after 3 h ($p < 0.001$***). The penetration-enhancing effect of the SEs is clear. Whereas SL rather hampers the penetration through the synthetic membrane, it increases the penetration of IBU efficiently through the Skin PAMPA or the human epidermis (Park et al., 2000). The SM gel caused only a slightly lower flux than that with the SL gel, yielding a significantly higher penetration profile as compared with the Control gel after 4 h ($p < 0.01$**) and as compared with the SL gel after 7 h ($p < 0.001$***). The combination SL + TR also demonstrated a lower penetration profile, as can be seen in the case of the *ex vivo* result. The penetration profile of IBU from the SM + TR gel showed the earliest significantly increased diffused IBU amount ($p < 0.001$**) after 3 h as compared with the Control gel, and after 7 h as compared with the SM gel. The highest average penetration profile of IBU was seen with this gel. This result was verified by both the Skin PAMPA and the Franz cell method.

The determination coefficients (R^2) of linear regression of the correlation between the amount of IBU that penetrated through the human skin and the amount of IBU that penetrated through the Skin PAMPA indicated a good correlation. The determination coefficients between the *in vitro* PAMPA and the *ex vivo* Franz cell methods were in the range 0.88–0.99 (**Fig. 12**). The EF values observed with the *ex vivo* and *in vitro* methods were of the same order of magnitude in all five cases (**Fig. 13**).

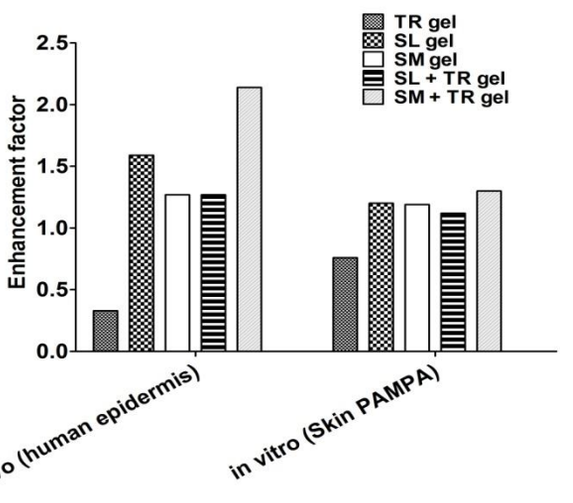

Figure 13. *Ex vivo* (human epidermis) and *in vitro* (Skin PAMPA) enhancement factors of different formulations.

5.2.1.2. *In vivo* skin tests

The penetration of a drug into the deeper layers can be enhanced through a well-hydrated skin, too. During moisturizing, the intercellular space between the corneocytes increases due to the swelling of the SC. **Fig. 14** shows that every investigated sample increased the hydrated state of the skin and ensured a good, lasting moisturizing effect. The greatest increase in skin water content were obtained with the 2.64 wt.% SM gel and the SM + TR gel. The application of the 2.64 wt.% SM gel or SM + TR gel results in significantly higher skin hydration relative to the Control gel after 30, 90 and 150 min ($p < 0.001$***). The Control gel and the 2.64 wt.% SL gel showed a similar hydration state after 30 min, but after 90 min the 2.64 wt.% SL gel achieved a greater and more enduring moisturizing effect than that with the Control gel. However, the results were not statistically significant as compared with the SE free hydrogel (**Fig. 14a**).

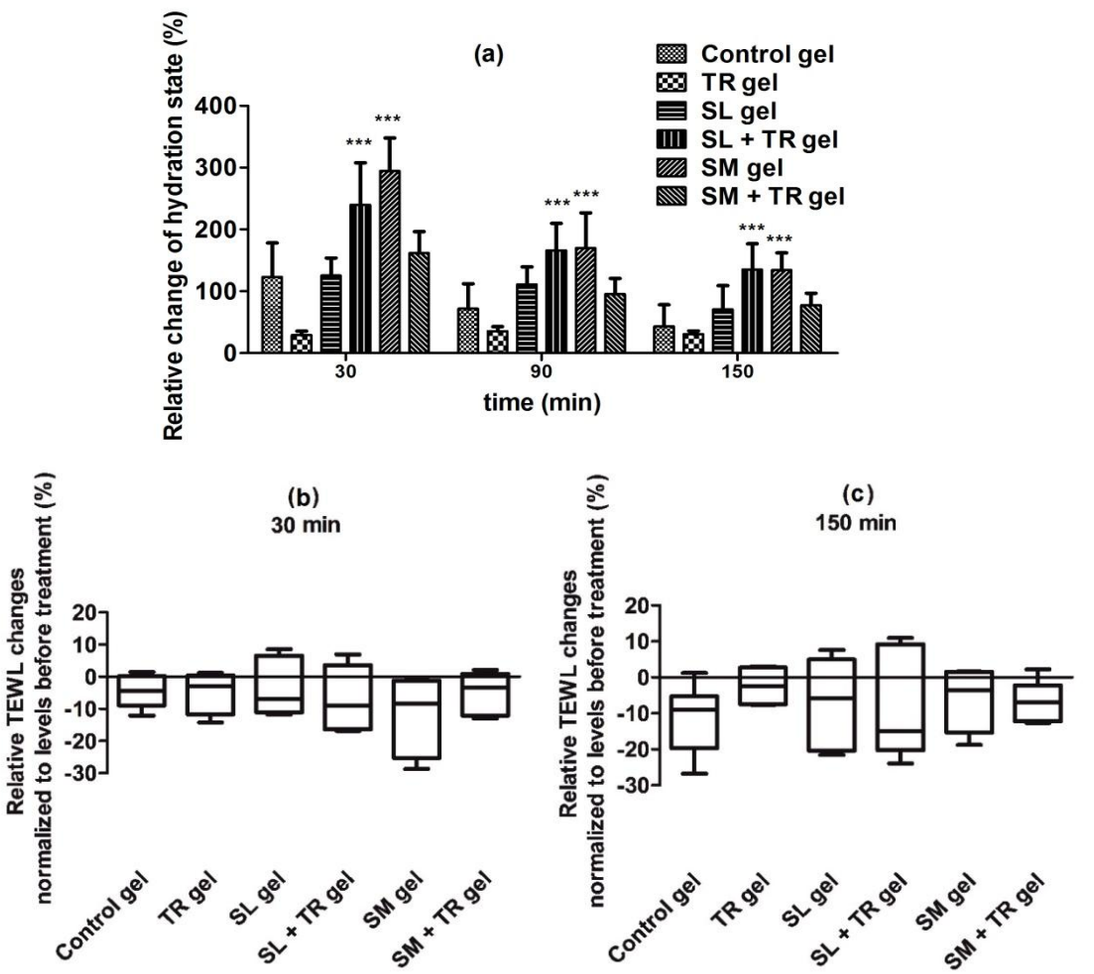

Figure 14. Skin water hydration (a) and TEWL measurement after (b) 30 min and (c) 150 min treatment with the single application of six IBU-free topical formulations.

It was proved earlier that SL acts as an effective and non-irritating hydration and penetration enhancer for IBU through the skin (Csizmazia et al., 2011). From our results, it can be concluded that the SEs incorporated into the hydrogel vehicle interact synergistically to modify the skin barrier, but statistically SM achieved a higher skin water-holding capacity increase. The SEs have the same HLB value (HLB = 16), but with the 14 C-atom-long fatty acid chains, SM in a hydrogel formulation is probably able to integrate into the SC lipid bilayer more efficiently than SL (C = 12).

TEWL measurement is the most appropriate noninvasive model with which to study the skin barrier function and its change effected in the dermal preparation. Application of the control formulation leads to lower TEWL values than the level before treatment. Even after 150 min, the skin was well protected and lastingly by the Control gel. This phenomenon can be seen in the cases of TR, SM and the combination SM + TR. Treatment with SL or SL + TR-containing gels resulted in only slight increases in TEWL. The changes were not statistically significant as compared with the Control gel. The skin barrier structure remained basically unaltered for all the tested formulations. Although TR and the SEs caused minimal modifications in the SC barrier structure (Cázares-Delgadillo et al., 2005; Csizmazia et al., 2011), these hydrogel-based trandsdermal preparations protected the special SC structure (**Fig. 14b, c**).

5.2.2. Spectroscopic investigations of the effects of polyols in sodium lauryl sulfate-induced acute irritation

The penetration of the dermal preparation components emerge as viewpoint from pharmaceutical technology development of dermal formulations. The penetration characteristics of SLS, as frequently used components, in the presence of the polyols were therefore studied with combined tape stripping and ATR-FTIR spectroscopy (Dias et al., 2008; Balázs et al., 2014). ATR-FTIR spectroscopy revealed the most characteristic bond of SLS assigned to the SO_2 stretch (asymmetric) at 1220 cm^{-1} (**Fig. 15**) (Bhise et al., 2009). It was found that both lower concentration polyol treatments modified the SLS penetration, but a significant decrease in the amount of SLS in the deeper layers was observed when higher polyol treatments were applied (**Table 10**).

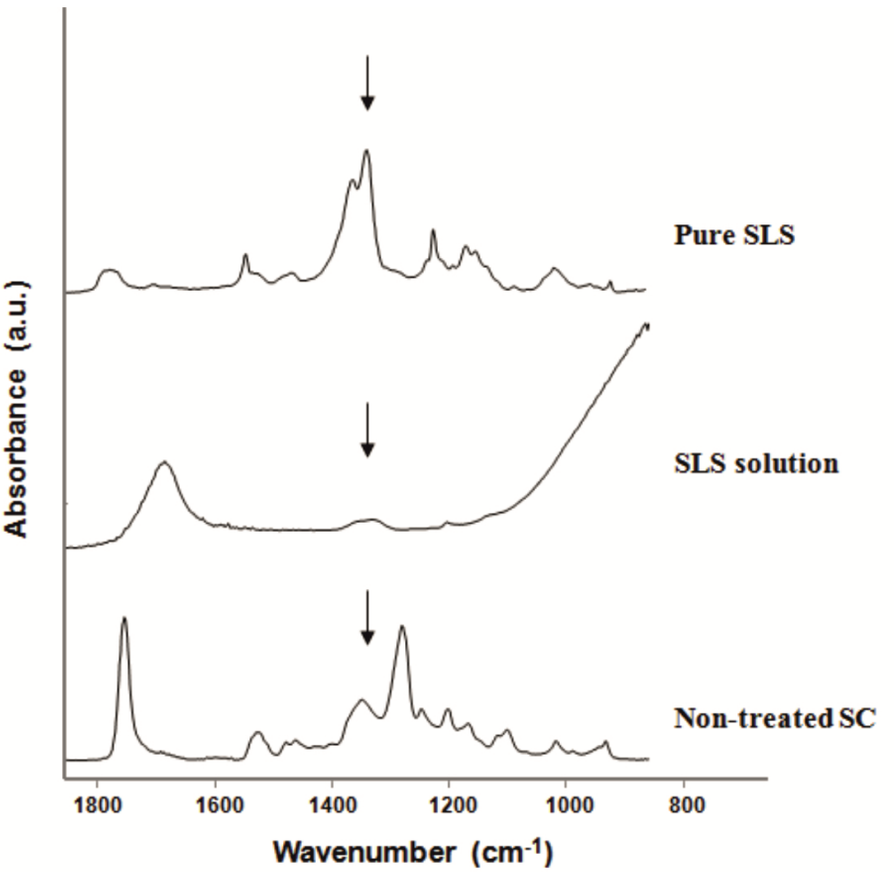

Figure 15. ATR-FTIR spectra of pure SLS, a 5 wt.% solution of SLS and the non-treated SC.

Table 10. Intensities in the upper and lower layers of the treated SC (relative absorbance of SLS at 1220 cm^{-1}). Median values (M) with 25th and 75th percentiles.

	Group 2 (SLS 5 %)		**Group 3** (SLS + GLY 5 %)		**Group 4** (SLS + XYL 8.26 %)		**Group 5** (SLS + GLY 10 %)		**Group 6** (SLS + XYL 16.52 %)	
Number of layers	M	25p; 75p	M	25p; 75p	M	25p; 75p	M	25p; 75p	M	25p; 75p
1-4	0.0226	0.0137 0.0264	0.0309	0.0187; 0.0518	0.0318	0.0181; 0.0468	0.0319	0.0161; 0.0532	0.0196	0.0134; 0.0360
5-8	0.0234	0.0140 0.0433	0.0223	0.0122; 0.0300	0.0241	0.0149; 0.0454	0.00601 *	0.00143; 0.0134	0.000 *	0.000; 0.0133

GLY may reduce the average aqueous pore radius in the SC, thereby decreasing the penetration of irritants (Ghosh et al., 2007), it may be presumed that the anti-irritant and anti-inflammatory effects of GLY and XYL are just elucidated by the hampered penetration of SLS. The penetration of SLS to the deeper SC layers decreased significantly at higher polyol concentrations, which is a novel feature for XYL. However, this result is not completely in

accordance with the previous observed effects of polyols, where XYL merely proved to be effective at lower concentration. In addition, the hydrating effects of polyols are independent of their action on SLS penetration.

5.2.3. Investigations of Genistein-containing lyotropic liquid crystal

5.2.3.1. Polarization microscopic examinations

In the development of the dermal delivery, we prepared an LLC formulation which is capable of suspending and partly dissolving GEN in a concentration of 3 wt.%. **Fig. 16** presents a polarization microscopic picture of the developed LLC structure, revealing a lamellar LLC pattern with a characteristic ribbon structure in polarized light.

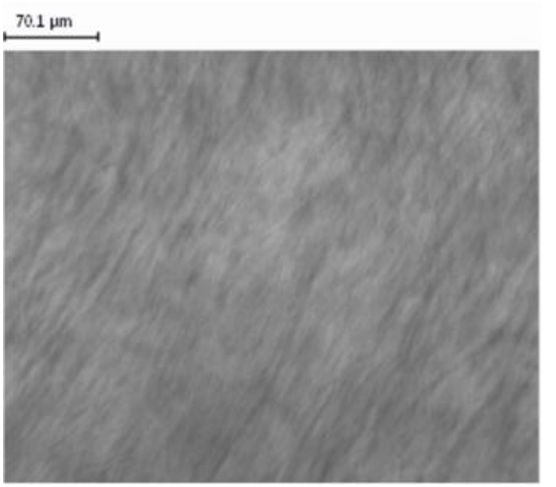

Figure 16. Polarizing microscopic examination of blank LLC at a magnification of 20x.

5.2.3.2. Rheological investigations

The characteristics of the LLC system include the frequency-dependent storage and loss moduli. In the investigated frequency range, the blank LLC system is more elastic than viscous. The solubilization of GEN in the LLC system led to a consistency increase (**Fig. 17**).

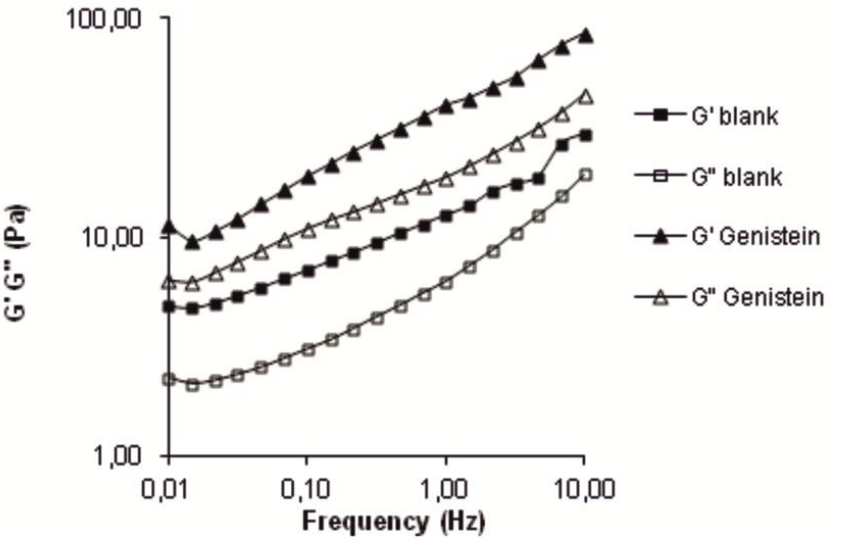

Figure 17. Rheological characterization of the blank and GEN-containing LLC formulations.

5.2.3.3. Drug diffusion and penetration measurements

The membrane diffusion investigations indicated that good drug release and diffusion was attained through the synthetic membrane *in vitro*, 713.26±90.73 μg cm^{-2} being liberated in 24 h (**Fig. 18a**). Somewhat less drug was observed after 24 h (491.26±15.55 μg cm^{-2}) in the case of *ex ovo* penetration (**Fig. 18b**). In the e*x vivo* investigations which revealed not only the amount of drug that diffused through the skin, but also the interaction with the skin and the incidental reservoir function of the SC, only a small amount of drug penetrated through the human epidermis (8.93±1.81 μg cm^{-2} after 24 h and 15.68±3.09 μg cm^{-2} after 48 h), but the penetration profile was similar to that for *ex ovo* penetration and sustained drug release was achieved (**Fig. 18c**). The J values showed that the drug penetration was slowed down by the application of the biological membrane, and that LLC-GEN alone was not sufficient to reach an appropriate plasma concentration.

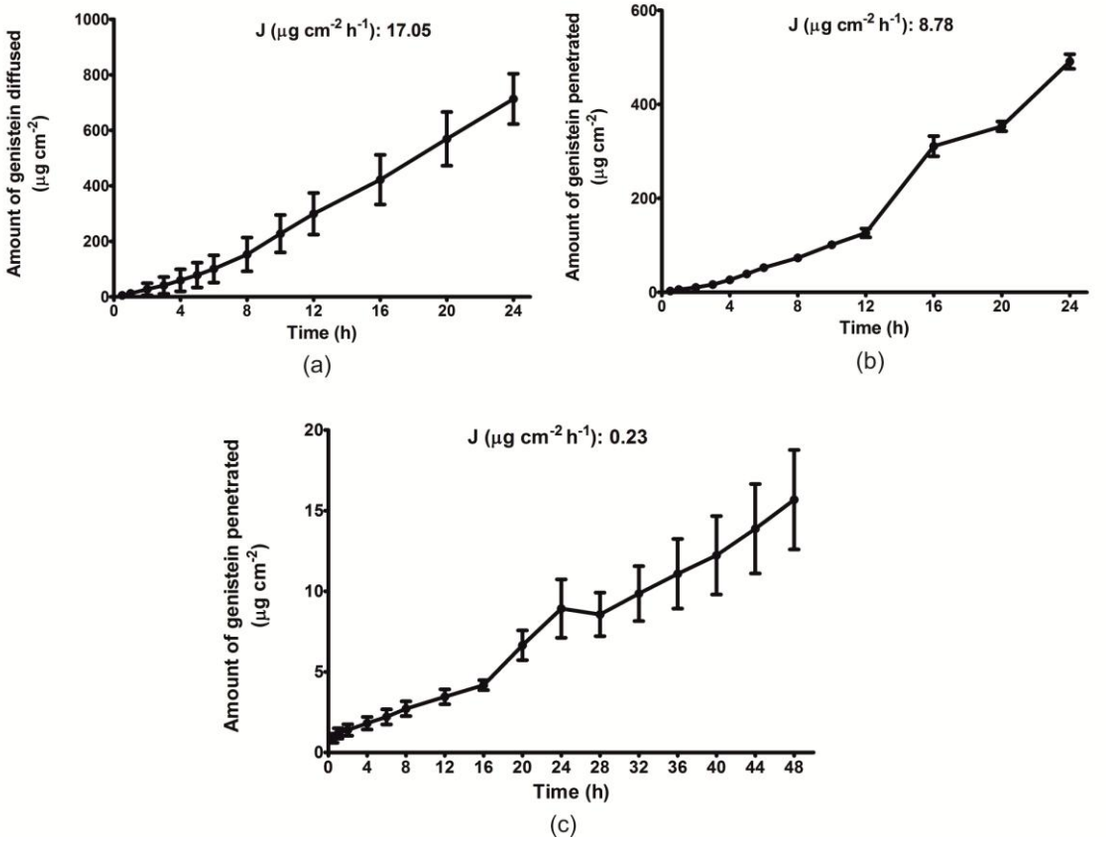

Figure 18. Amount of GEN diffused *in vitro* (a), or penetrated *ex ovo* (b) or *ex vivo* (c).

5.2.3.4. ATR-FTIR spectroscopy

The results showed that the traditionally used LLC-GEN was not effective alone. The LLC-GEN formulation was therefore combined with an active penetration-enhancing method, EP. Different treatment times and voltages were used. The penetration profile of GEN within the different layers of the SC was established with a combination of tape stripping and ATR-FTIR spectroscopy. The most characteristic peaks in the ATR-FTIR spectrum of GEN were assigned to the C1=C2 stretch at 1652 cm^{-1}, and the C=O stretch, O7-H22 bend, and ring A C-C stretch at 1518 cm^{-1} (**Fig. 19**) (Surendra Babu et al., 2012).

Table 11 presents the relative absorbances in the SC layers at 1652 cm^{-1} and 1518 cm^{-1}, which correspond to the amounts of GEN that penetrated into the SC after conventional and EP treatments (**Fig. 20**). The drug delivery and the onset time for transport depend on the electrical parameters of the pulses and the physicochemical properties of the drug (Denet et al., 2004). It was found that EP treatment at 700 V for 1 min did not enhance the GEN transdermal delivery relative to the conventional treatment. This may be explained by the high

viscosity of the drug carrier, which decreases the efficacy of EP on the skin (Vanbever et al., 1995). Slightly deeper GEN penetration was ensured by EP treatment at 900 V for 1 min, but the total amount of GEN did not exceed that for conventional treatment with LLC-GEN. However, EP treatment at 700 V for 2 min resulted in a deeper penetration of a 2-fold amount of the drug than without EP treatment (revealed at both characteristic bonds of GEN). The best penetration profile of GEN was obtained on EP treatment at 900 V for 2 min, when the total amount of the drug was 3-fold greater as compared with conventional treatment at both assigned bonds ($p < 0.001$*** and $p < 0.05$*), but the GEN distribution was not consistent. The presence of GEN was not seen in the 5th and 6th tape strips, whereas the drug appeared again in the 7th strips. This phenomenon could be explained by the electrical breakdown of the SC layers. Furthermore, the amount of drug that penetrated increased with increasing voltage of the pulses (Prausnitz et al., 1993; Vanbever et al., 1996).

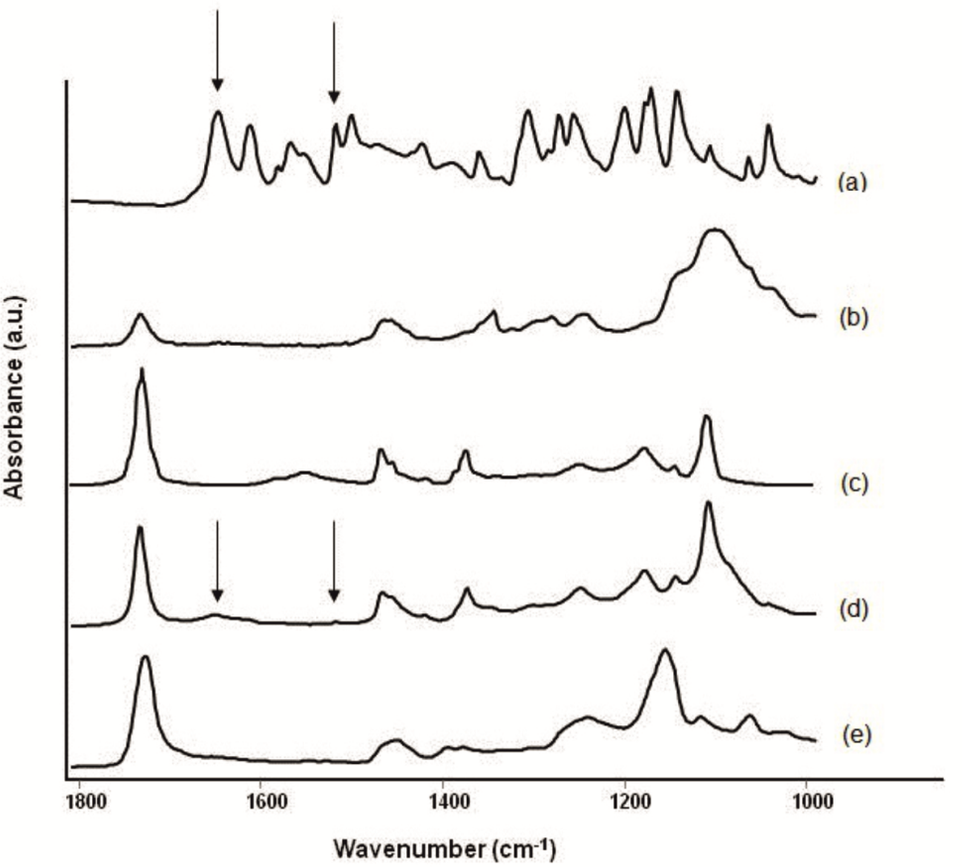

Figure 19. ATR-FTIR spectra of pure GEN (a), CRH40 (b), IPM (c), LLC-GEN composition (d) and non-treated SC (e).

Table 11. Intensities of GEN in the different layers of the treated SC (average value ± SD, n = 3) (CT = conventional treatment).

	Treated with LLC-GEN (CT, 2 min)		Treated with LLC-GEN + EP (700 V, 1 min)		Treated with LLC-GEN + EP (900 V, 1 min)		Treated with LLC-GEN + EP (700 V, 2 min)		Treated with LLC-GEN + EP (900 V, 2 min)	
No. of tape strips	**Absorbance at**		**Absorbance at**		**Absorbance at**		**Absorbance at**		**Absorbance at**	
	1652 cm^{-1} GEN	**1518 cm^{-1} GEN**	**1652 cm^{-1} GEN**	**1518 cm^{-1} GEN**	**1652 cm^{-1} GEN**	**1518 cm^{-1} GEN**	**1652 cm^{-1} GEN**	**1518 cm^{-1} GEN**	**1652 cm^{-1} GEN**	**1518 cm^{-1} GEN**
1	0.06±0.03	0.05±0.02	0.05±0.05	0.04±0.04	0.04±0.01	0.03±0.00	0.15±0.02	0.12±0.02	0.22±0.10	0.18±0.08
2	0.03±0.01	0.03±0.01	0.02±0.02	0.02±0.01	0.01±0.01	0.01±0.01	0.04±0.02	0.04±0.02	0.08±0.06	0.07±0.05
3	0.03±0.02	0.02±0.01	-	-	0.03±0.00	0,03±0.00	0.06±0.00	0.05±0.00	0.06±0.00	0.05±0.00
4	-	-	-	-	0.03±0.00	0.02±0.00	0.02±0.00	0.02±0.00	0.03±0.01	0.03±0.01
5	-	-	-	-	-	-	0.01±0.00	0.01±0.00	-	-
6	-	-	-	-	-	-	-	-	-	-
7	-	-	-	-	-	-	-	-	0.02±0.02	0.02±0.01
8	-	-	-	-	-	-	-	-	-	-

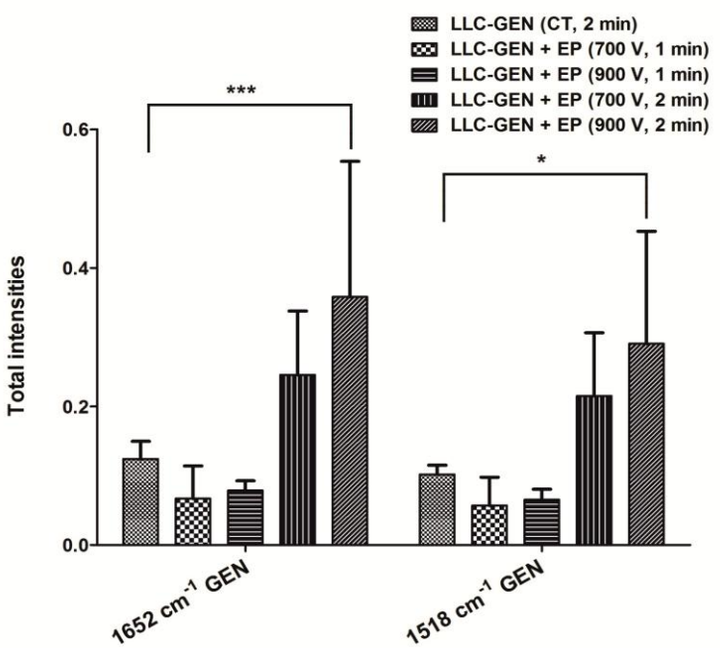

Figure 20. Total intensities of GEN at 1652 cm^{-1} and at 1518 cm^{-1}. CT was used as a control. $p < 0.001$*** and $p < 0.05$* vs. EP-treated group.

5.2.3.5. Raman spectroscopy

Mouse skin treated with LLC-GEN combined with EP was examined by Raman spectroscopy. The deeper skin penetration of LLC-GEN containing the ingredients CRH40 and IPM was studied in Raman scattering experiments. Raman chemical mapping was employed to confirm the localization of GEN at various depths of the skin specimens. Since ATR-FTIR demonstrated that EP treatment at 900 V ensured deeper penetration than that at 700 V, EP treatments at 900 V for 1 and 2 min were chosen for comparison with conventional treatment by Raman spectroscopy.

Fig. 21 depicts the experimental Raman spectra of pure CRH40, IPM and GEN in the wavenumber range 2000–200 cm^{-1}. As model solution, GEN was dissolved in CRH40 and IPM containing LLC (GEN content 3 wt.%) to observe the physical state of GEN. Six common characteristic ranges can be seen in the spectra of CRH40 and IPM, with peaks centered at 1733, ~1442–1437, 1300, 1063 and 843–823 cm^{-1}, and the spectra of CRH40, IPM and the LLC-GEN composition are very similar. **Table 12** lists the Raman bands of the components and the LLC-GEN composition. The lipid components used in this study have similar chemical structures and therefore similar Raman bands.

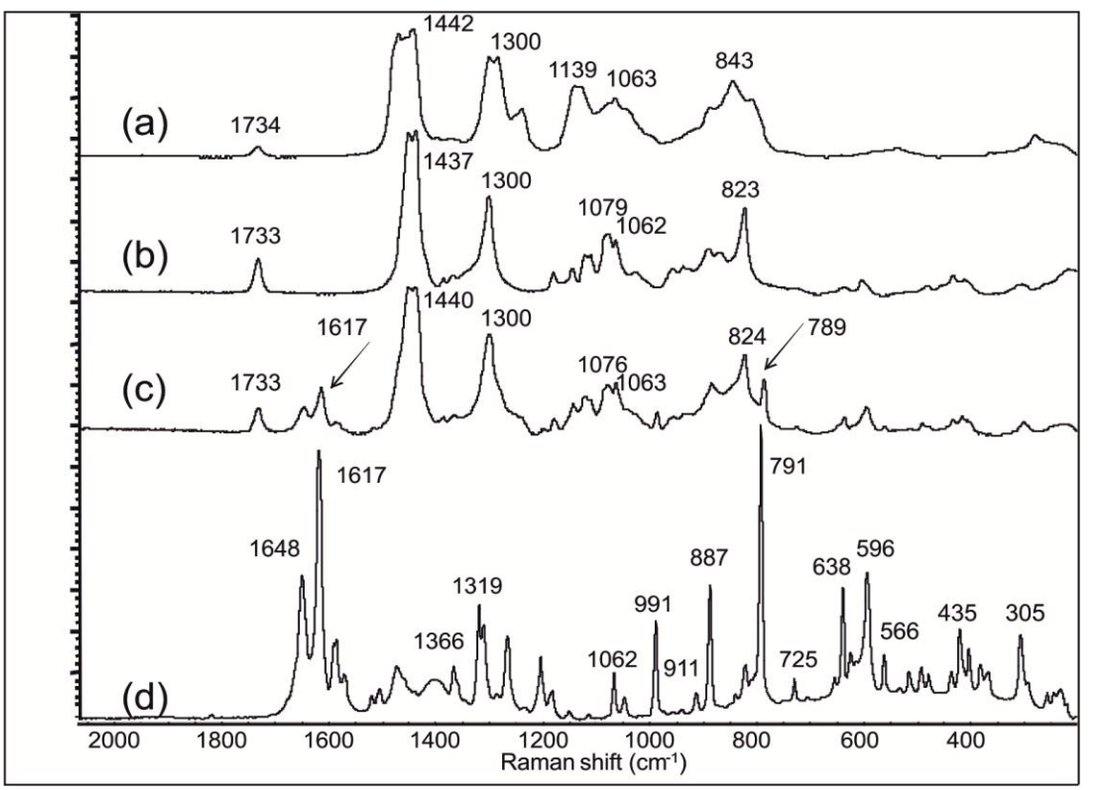

Figure 21. Experimental Raman spectra of CRH40 (a), IPM (b), LLC-GEN composition (c) and pure GEN (d).

Table 12. Observed Raman peaks and peak assignments of individual components and LLC-GEN (*str* = stretching, *def* = deformation, *tw* = twisting).

Assignment	CRH40	IPM	LLC-GEN	GEN
str C=O (ester)	1734	1733	1733	-
str C=C (ring A)	-	-	1648	1648
str C=C (ring B)	-	-	1617	1617
def CH2-CH3	1442	1437	1440	-
str C=C	-	-	-	1366
	-	-	-	1319
def CH2 and *tw* CH3	1300	1300	1300	-
str C-C	1139	-	-	-
		1079	1076	-
str O-C	1063	1062	1063	1062
str C=C and C-C-C (ring A)	-	-	991	991
str C=C (ring A) and C-C-C (ring C)	-	-	887	887
str C-CH (aromatic ring)	843	-	-	-
	-	823	824	-
str C-C-C (C ring), *str* C=O	-	-	789	791
str C-C-C and C=C (ring A)	-	601	596	596
str C-C-C (rings A and C)	-	-	-	566

The Raman spectrum of the LLC-GEN is basically the sum of the individual spectra, with minor shifts at around 1440 and 1079 cm^{-1} (**Fig. 21c**), indicating that the CH_2-CH_3 bonds of the LLC ingredients were affected by the interaction. Only a few Raman peaks of GEN were observed in the spectrum of LLC-GEN, at around 1617, 1062, 991, 887 and 789 cm^{-1}. For GEN, two characteristic peaks, centered at 1617 and 789 cm^{-1}, were assigned to the vibration of the C=C bond in ring B and the C-C-C, C-C and C=O bonds in ring C of the isoflavonoid molecule. These bands, free from interference from LLC ingredient bands, were chosen to confirm the localization of GEN in the skin specimen.

Raman spectra were acquired from skin treated with LLC-GEN and from non-treated intact *ex vivo* skin (**Fig. 22**), both perpendicular to the SC at equivalent depth (1000 μm). In the Raman spectrum of the treated skin, characteristic peaks of GEN and the LLC ingredients were observed at around 1670–1650 and 1470–1410 cm^{-1}, respectively. The band of interest centred at 1440 cm^{-1} was assigned to the vibration of the amide functional group due to C=O stretching and $–CH_2$, $-CH_3$ bending of the skin lipid constituents. The C=C stretching observed at 1617 cm^{-1} arose predominantly from the GEN isoflavonoid. The chemical mapping therefore confirmed the presence of the characteristic GEN band at around 1617 cm^{-1}. This peak is close to the vibrations of the native skin components. The skin component peaks at 1608 and 1453 cm^{-1} are well known to be associated with the C=C vibration of phenylalanine, the CH_2 scissoring of lipids and the CH_2, CH_3 deformation of proteins in the native skin.

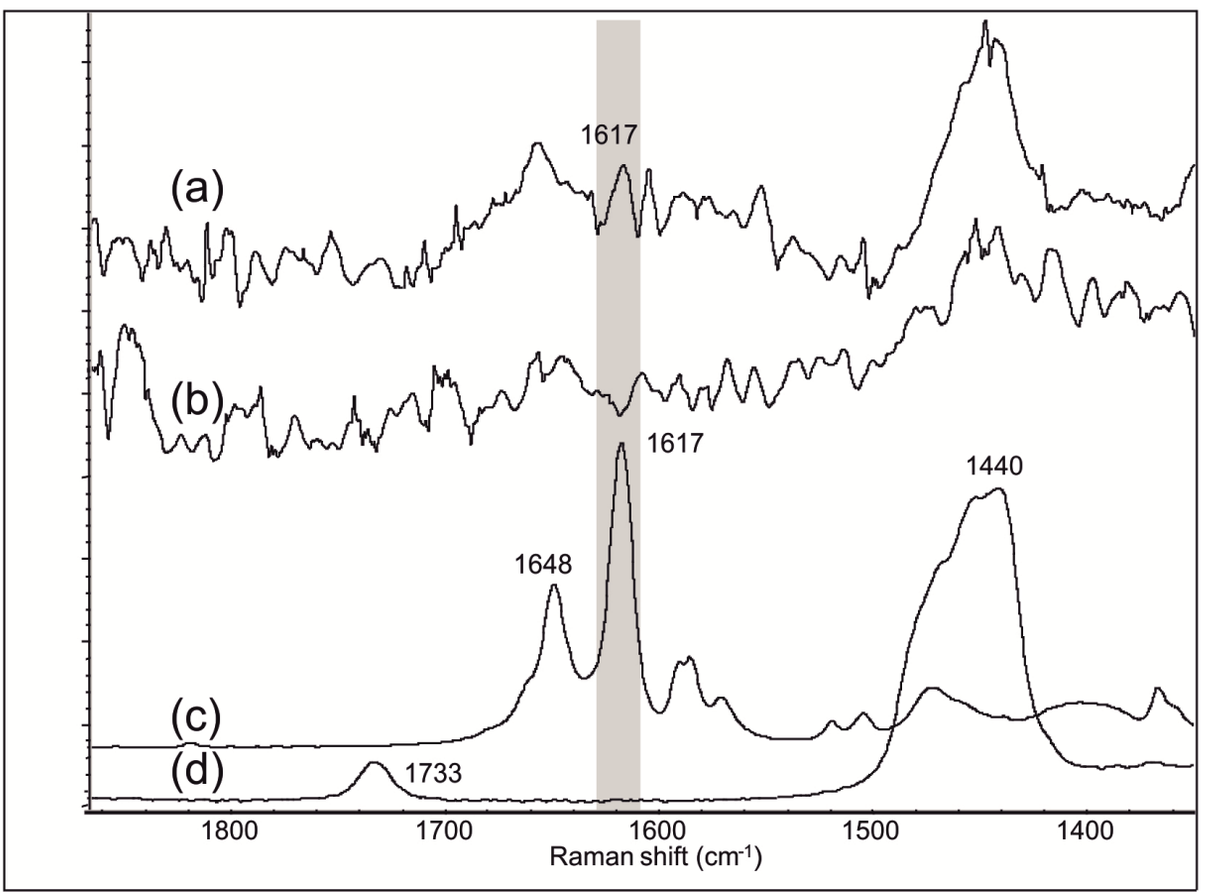

Figure 22. Raman spectra of GEN-treated skin (900 V, 2 min, 1000 μm depth) (a), non-treated skin specimen as control (1000 μm depth) (b), pure GEN (c) and GEN-free LLC composition (d) in the range 1900–1350 cm^{-1}.

Fig. 23 displays qualitative distribution maps of the LLC components and GEN in animal skin specimens after different EP protocols, at 10-fold magnification. It was of interest to determine whether GEN diffusion is limited to the SC or to the epidermis or dermis. As discussed in the Materials and Methods section, as the skin specimens were planar, there was no need for the z-axis and adjustment of the depth values. 1300 µm deep sections of the skin specimen were investigated, from top to bottom corresponding to the SC → epidermis → dermis. In order to confirm GEN diffusion, the chemical maps were resolved. The characteristic bands obtained for GEN at around 1617 cm^{-1} were used to visualize the spatial distribution of GEN from the Raman chemical mapping. The resolution of the chemical map and hence the identification of the ingredients present were achieved by using an MCR-ALS chemometric method. This method furnishes the response profiles of different components in complex samples, and provides information about the composition.

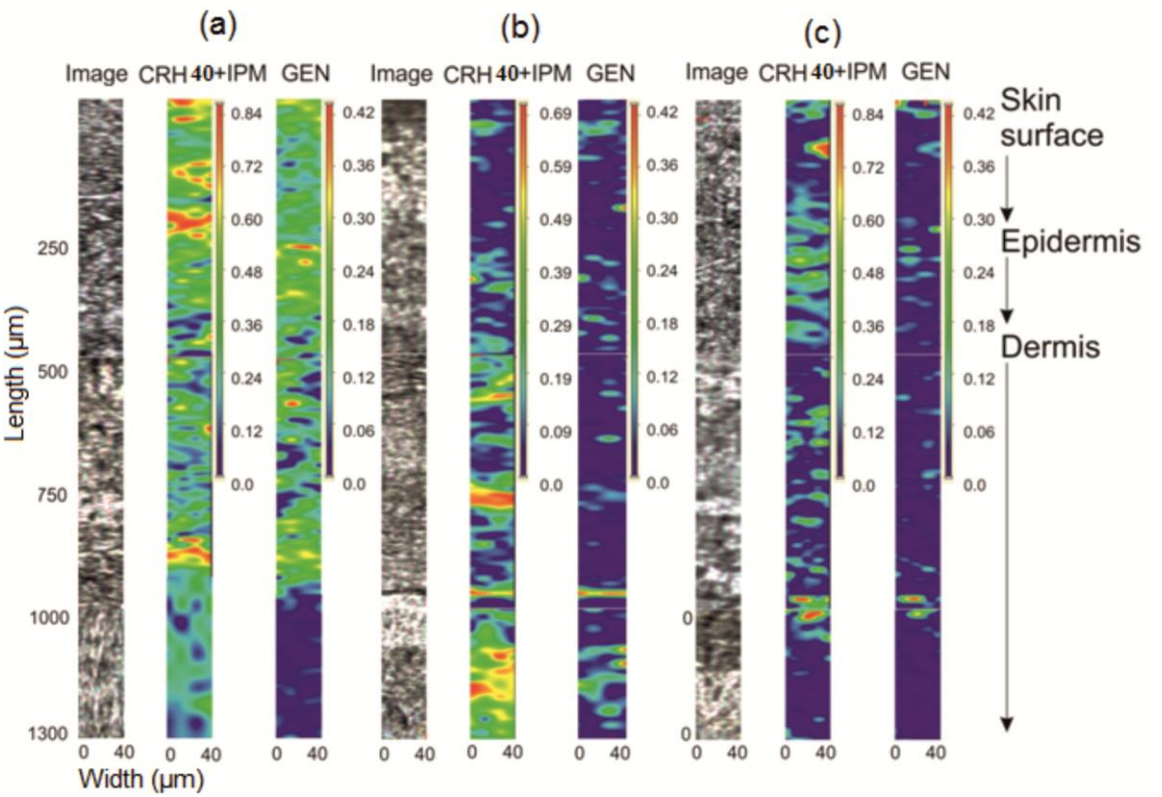

Figure 23. Qualitative Raman maps of GEN distribution in animal skin specimens following different EP protocols (at 10-fold magnification). Conventionally treated skin as control (a), skin treated with EP at 900 V for 1 min (b) and skin treated with EP at 900 V for 2 min (c). Color coding of content: red > yellow > green > blue.

The presence of bands due to GEN and the LLC components in the upper layer of the skin (0–1000 μm) clearly indicates a good distribution following conventional treatment of the LLC-GEN composition (**Fig. 23a**). After the 900 V process for 1 min, GEN was accumulated in the middle section of the dermis (**Fig. 23b**). The penetration of GEN into the dermis was slowed by the dermis being a dense network of collagen fibers. The GEN and LLC component contents of the skin specimen (to a depth of 1300 μm) were relatively low after the 900 V EP process for 2 min (**Fig. 23c**), indicating that the GEN penetrated into the deep layer of the dermis. Although the difference between the EP processes for 1 and 2 min may seem minor, the slower diffusion of GEN may be presumed because of the enrichment of the LLC components (as vehicles of GEN) in the 1000–1300 μm deep section. In the absence of the EP process, the epidermal and upper dermal regions serve as a tight barrier, impeding deep GEN delivery. Thus, slow diffusion of the GEN took place.

5.2.3.6. Effect of electroporation treatment on murine melanoma

In each of the inoculated mice, the volume of the tumor was observed to be increased, to an extent directly proportional to the number of days of the examination. Tumors appeared on day 8 post-inoculation in both the treated and the untreated groups, with the exception of the mice in group F; in these mice, which were inoculated with B164A5 cells and treated with LLC-GEN and EP for 6 min at high voltage, the tumors appeared on day 10 post-inoculation. The mean tumor volume in group F was 83.33±28.86 mm^3, in contrast with 466.66±208.16 mm^3 in group B, 589.78±204.67 mm^3 in group C, 309.00±207.81 mm^3 in group D and 603.23±264.57 mm^3 in group E. Comparison of the curves corresponding to the different treatment approaches reveals that the LLC-GEN formulation decreased the tumor volume, but following EP of this formulation, the results were even better. On day 21 of the experiment, the tumor volumes were 1001.58±409.26 mm^3 in group B, 1000.86±404.96 mm^3 in group C, 866.66±256.58 mm^3 in group D, 999.87±408.95 mm^3 in group E and 751.00±151.03 mm^3 in group F. Significant results ($p < 0.05$) between the different experimental groups were found, as shown in **Fig. 24**.

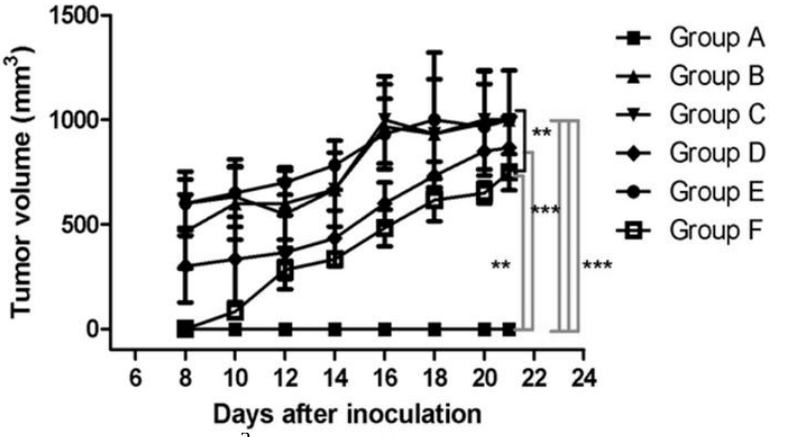

Figure 24. Tumor volumes (mm^3) in the different experimental groups on day 21 of the experiment.

6. SUMMARY

The main aim of my research work was to achieve a better understanding of the SC structure and its barrier function against drug penetration. I compared the unharmed SC in untreated psoriatic patients with that in the healthy control group. A further goal was to investigate different methods of increasing the drug penetration through the skin.

1. Using the components of the amide-I band, intact psoriatic skin was investigated to determine the changes in the secondary structure of the proteins by combining tape stripping and ATR-FTIR spectroscopy. FSD of the amide-I band was followed by curve-fitting to generate the underlying components. Integration of band areas provided an estimate of the secondary structure.

To summarize this part of my Ph.D. work, new results were achieved:

- The protein structure is changed on the unaffected area in psoriatic skin disease.
- The results indicated decreases in all amide-I band components, the peak at 1660 cm^{-1} revealing the most dramatic change. This peak is characteristic of the turn structure in the protein chain. The decrease is marked in the case of the β-sheet structure at 1630 cm^{-1} too.
- The combination of tape stripping and ATR-FTIR spectroscopy could serve as an appropriate, rapid, simple noninvasive method for the study of psoriasis and give the possibility to follow up the efficiency of treatment.

2. In the second part of my Ph.D. work, different types of transdermal drug delivery techniques were tested in order to increase the drug penetration through the skin.

2.1. IBU-containing hydrogels were used with SEs and TR as biocompatible penetration enhancers. The effects of the SE concentrations were examined through a synthetic membrane (*in vitro*) by the Franz cell method and the effects of SE hydrogel formulations on the skin

were evaluated by noninvasive *in vivo* tests. Furthermore, the behavior of these promising CPEs was tested through the use of two different skin test systems.

- The SE concentration influenced the *in vitro* diffusion process markedly. SL showed the highest penetration effect at 6 wt.%. concentration, while SM presented the best enhancing effect at 0.5 wt.%. It is not useful to use these SEs at higher concentrations as CPEs.
- The *ex vivo* and Skin PAMPA drug penetration results revealed that TR as cosolvent with SM significantly improved the penetration of the surfactant into the skin and promoted attainment of the maximum penetration effect. SM + TR could be a potential CPE combination for IBU in a dermally used hydrogel.
- Skin PAMPA can serve as an effective and quick prediction model for the monitoring of CPEs and of drug penetration through the skin. The findings with the new artificial PAMPA membrane correlated closely with those with an *ex vivo* human skin membrane.
- The *in vivo* results demonstrated that the incorporation of SEs (and especially SM) into a hydrogel extends and increases the hydration phenomenon. SM significantly improved the moisturizing effect of the hydrogel vehicle.

2.2. Penetration of SLS was investigated combined with polyols. It was concluded from ATR-FTIR spectroscopy that the use of GLY and XYL can decrease SLS penetration. Different concentrations of GLY and XYL were studied and higher polyol treatments decreased the penetration of SLS to the deeper layers of the SC.

2.3. A lamellar LLC was prepared in order to increase the solubility of the lipophilic phytocompound GEN. In order to verify the efficacy of this formulation, membrane diffusion and penetration studies were carried out with a Franz diffusion cell, through a synthetic membrane *in vitro*, a CAM *ex ovo*, and *ex vivo* excised human epidermis. Thereafter, LLC-GEN was combined with EP to enhance the transdermal drug delivery.

- The synergistic effect of EP was verified by *in vivo* ATR-FTIR and *ex vivo* Raman spectroscopy on hairless mouse skin. The penetration through the skin was ensured by the application of LLC-GEN alone. However, combination of the LLC nanocarrier system with EP resulted in rapid and more effective transdermal drug transport than that with the LLC-GEN formulation alone.
- It was confirmed by murine melanoma investigations that EP could be a good method for the delivery of GEN because it delayed the appearance of the tumors and ensured the drug penetration to the deeper layers of the skin.

7. REFERENCES

Al-Mustafa J.I.: FTIR investigation of the conformational properties of the cyanide bound human hemoglobin. *Vib. Spectrosc.* 30. 139–146. (2002)

Andersen F., Hedegaard K., Petersen T.K., Bindslev-Jensen C., Fullerton A., Andersen K.E.: Comparison of the effect of glycerol and triamcinolone acetonide on cumulative skin irritation in a randomized trial. *J. Am. Acad. Dermatol.* 56. 228–235. (2007)

Ayala-Bravo H.A., Quintanar-Guerrero D., Naik A., Kalia Y.N., Cornejo-Bravo J.M., Ganem-Quintanar A.: Effects of sucrose oleate and sucrose laureate on in vivo human stratum corneum permeability. *J. Pharm. Res.* 20. 1267–1273 (2003)

Balázs B., Farkas G., Berkesi O., Gyulai R., Berkó Sz., Budai-Szűcs M., Szabó-Révész P., Kemény L., Csányi E.: Protein structure is changed in psoriatic skin on the unaffected region – imaging possibility with ATR-FTIR spectroscopy. *Microchem. J.* 117. 183–186. (2014)

Balázs B., Sipos P., Danciu C., Avram S., Soica C., Dehelean C., Varju G., Erős G., Budai-Szűcs M., Berkó Sz., Csányi E.: An ATR-FTIR and Raman spectroscopic investigation of the electroporation-mediated transdermal delivery of a nanocarrier system containing an antitumour drug. *Biomed. Opt. Express* 7. 67–78. (2016)

Barry B.W. Dermatological Formulations–Percutaneous Absorption, Marcel Dekker, New York (1983)

Barry B.W.: Novel mechanisms and devices to enable successful transdermal drug delivery *Eur. J. Pharm. Sci.* 14. 101–114. (2001)

Barth A.: Infrared spectroscopy of proteins. *Biochim. Biophys. Acta* 1767. 1073–1101. (2007)

Benson H.A.E.: Transdermal drug delivery: penetration enhancement techniques. *Curr. Drug Deliv.* 2. 23–33. (2005)

Bernard G., Auger M., Soucy J., Pouliot R.: Physical characterization of the stratum corneum of an in vitro psoriatic skin model by ATR-FTIR and Raman spectroscopies. *Biochim. Biophys. Acta* 1770. 1317–1323. (2007)

Betz G., Aeppli A., Menshutina N., Leuenberger H.: In vivo comparison of various liposome formulations for cosmetic application. *Int. J. Pharm.* 296. 44–54. (2005)

Bhise S.B., Mookkan S.: Formulation and evaluation of novel FDCs of antitubercular drug. *J. Pharm. Res.* 2. 437–444. (2009)

Bommannan D., Potts R.O., Guy R.H.: Examination of stratum corneum barrier function in vivo by infrared spectroscopy. *J. Invest. Dermatol.* 95 403–408. (1990).

Bos, J.D., Meinardi M.M.: The 500 Dalton rule for the skin penetration of chemical compounds and drugs. *Exp. Dermatol.* 9. 165–169. (2000)

Boyd B.J., Whittaker D.V., Khoo S.M., Davey G.: Lyotropic liquid crystalline phases formed from glycerate surfactants as sustained release drug delivery systems. *Int. J. Pharm.* 309. 218–226. (2006)

Brain K.R., Green D.M., Lalko J., Api A.M.: In-vitro human skin penetration of the fragrance material geranyl nitrile. *Toxicol. In Vitro* 21. 133–138. (2007)

Brown M.B., Martin G.P., Jones S.A., Akomeah F.K.: Dermal and transdermal drug delivery systems: current and future prospects. *Drug Deliv.* 13. 175–187. (2006)

Cázares-Delgadillo J., Naik A., Kalia Y.N., Quintanar-Guerrero D., Ganem-Quintanar A.: Skin permeation enhancement by sucrose esters: a pH-dependent phenomenon. *Int. J. Pharm.* 297. 204–212. (2005)

Cohen S., Marcus Y., Migron Y., Dikstein S., Shafran A.: Water sorption, binding and solubility of polyols. *J. Chem. Soc. Faraday Trans.* 89. 3271–3275. (1993)

Csizmazia E., Erős G., Berkesi O., Berkó Sz., Szabó-Révész P., Csányi E.: Penetration enhancer effect of Sucrose laurate and Transcutol on Ibuprofen. *J. Drug Del. Sci. Tech.* 21 411–415. (2011)

Csizmazia E., Erős G., Berkesi O., Berkó Sz., Szabó-Révész P., Csányi E.: Ibuprofen penetration enhance by sucrose ester examined by ATR-FTIR in vivo. *Pharm. Dev. Technol.* 17. 125–128 (2012)

Csóka G., Marton S., Zelko R., Otomo N., Antal I.: Application of sucrose fatty acid esters in transdermal therapeutic systems. *Eur. J. Pharm. Biopharm.* 65. 233–237. (2007)

Denda M., Tshuchiya T., Hosoi J., Koyama J.: Immobilization-induced and crowded environment-induced stress delay barrier recovery in murine skin. *Br. J. Dermatol.* 138. 780–785. (1998)

Denda M., Tsuchiya T., Elias P.M., Feingold K.R.: Stress alters cutaneous permeability barrier homeostasis. *Am. J. Physiol. Regul. Integr. Comp. Physiol*..278. R367–R372. (2000)

Denet A.R., Vanbever R., Préat V.: Skin electroporation for transdermal and topical delivery. *Adv. Drug Deliv. Rev.* 56. 695–674. (2004)

Dias M., Naik A., Guy R.H., Hadgraft J., Lane M.E.: In vivo infrared spectroscopy studies of alkanol effects on human skin. *Eur. J. Pharm. Biopharm.* 69. 1171–1175 (2008)

El-Laithy H.M.: Novel transdermal delivery of Timolol maleate using sugar esters: preclinical and clinical studies. *Eur. J. Pharm. Biopharm.* 72. 239–245. (2009)

Finnin B.C., Morgan T.M.: Transdermal penetration enhancers: applications, limitations, and potential. *J. Pharm. Sci.* 88. 955–958. (1999)

Fluhr J.W., Gloor M., Lehmann L., Lazzerini S., Distante F., Berardesca E.: Glycerol accelerates recovery of barrier function in vivo. *Acta Derm. Venereol.* 79. 418–421. (1999)

Fluhr J.W., Darlenski R., Surber C.: Glycerol and the skin: holistic approach to its origin and functions. *Br. J. Dermatol.* 159. 23–34. (2008)

Ganem-Quintanar A., Quintanar-Guerrero D., Falson-Rieg F., Buri P.: Ex vivo oral mucosal permeation of lidocaine hydrochloride with sucrose fatty acid esters as absorption enhancers. *Int. J. Pharm.* 173. 203–210. (1998)

Garg T., Singh S., Goyal A.K.: Stimuli-sensitive hydrogels: an excellent carrier for drug and cell delivery. *Crit. Rev. Ther. Drug Carrier Syst.* 30. 369–409. (2013)

Ghadially R., Brown B.E., Sequeira-Martin S.M., Feingold K.R., Elias P.M.: The aged epidermal permeability barrier. Structural, functional, and lipid biochemical abnormalities in humans and a senescent murine model. *J. Clin. Invest.* 95. 2281–2290. (1995)

Ghosh S., Blankschtein D.: The role of sodium dodecyl sulfate (SDS) micelles in inducing skin barrier perturbation in the presence of glycerol. *J. Cosmet. Sci.* 58. 109–133. (2007)

Gniadecka M., Faurskov Nielsen O., Christensen D.H., Wulf H.C.: Structure of water, proteins, and lipids in intact human skin, hair, and nail. *J. Invest. Dermatol.* 110. 393–398. (1998)

Godwin D.A., Kim N-H., Felton L.A.: Influence of Transcutol CG on the skin accumulation and transdermal permeation of ultraviolet absorbers. *Eur. J. Pharm. Biopharm.* 53. 23–27. (2002)

Grice K.A.: Transepidermal Water Loss in Pathologic Skin. In: Jarrett A.: The Physiology and Pathophysiology of the Skin. Academic Press, London, 2147–2155. (1980)

Guy R.H. Pharm. Res. 13. 1765–1769. (1996)

Hadgraft J.: Skin deep. *Eur. J. Pharm. Biopharm.* 58. 291–299. (2004)

Hadgraft J., Lane M.E.: Skin Permeation: Spectroscopic Methods. In: Benson H.A.E., Watkinson A.C.: Transdermal and Topical Drug Delivery. John Wiley & Sons, Inc., Hoboken, 155–166. (2011)

Hay R.J., Johns N.E., Williams H.C., Bolliger I.W., Dellavalle R.P., Margolis D.J., Marks R., Naldi L., Weinstock M.A., Wulf S.K., Michaud C., Murray C.J.L., Naghavi M.: The global burden of skin disease in 2010: an analysis of the prevalence and impact of skin conditions. *J. Invest. Dermatol.* 134. 1527–1534. (2014)

Holtje M., Forster T., Brandt B., Engels T., von Rybinski W., Holtje H.D.: Molecular dynamics simulations of stratum corneum lipid models: fatty acids and cholesterol. *Biochim. Biophys. Acta* 1511. 156–167. (2001)

Kanikkannan N., Singh M.: Skin permeation enhancement effect and skin irritation of saturated fatty alcohol. *Int. J. Pharm.* 248. 219–228. (2002)

Karande P., Jain A., Mitragotri S.: Discovery of transdermal penetration enhancers by high-throughput screening. *Nat. Biotechnol.* 22. 192–197. (2004)

Karande P., Jain A., Ergun K., Kispersky V., Mitragotri S.: Design principles of chemical penetration enhancers for transdermal drug delivery. *Proc. Natl. Acad. Sci. USA* 102. 4688–4693. (2005)

Kligman A.M., Christophers E.: Preparation of isolated sheets of human stratum corneum. *Arch. Dermatol.* 88. 702–705. (1963)

Kling J., DeFrancesco L.: High-throughput path to acquisition. *Nat. Biotechnol.* 25. 1223. (2007)

Kong J., Yu S.: Fourier transform infrared spectroscopic analysis of protein secondary structures. *Acta Bioch. Bioph. Sin.* 39. 549–559. (2007)

Lademann J., Richter H., Schanzer S., Knorr F., Meinke M., Sterry W., Patzelt A.: Penetration and storage of particles in human skin: perspectives and safety aspects. *Eur. J. Pharm. Biopharm.* 77. 465–468. (2011)

Lamba O.P., Borchman D., Sinha S.K., Shah J., Renugopalakrishnan V., Yappert M.C.: Estimation of the secondary structure and conformation of bovine lens crystallins by infrared spectroscopy: quantitative analysis and resolution by Fourier self-deconvolution and curve fit. *Biochim. Biophys. Acta* 1163. 113–123. (1993)

Lane M.E.: Skin penetration enhancers. *Int. J. Pharm.* 447. 12–21. (2013)

Lee C.K., Uchida T., Kitagawa K., Yagi A., Kim N.S., Goto S.: Effect of hydrophilic and lipophilic vehicles on skin permeation of tegafur, alclofenac and ibuprofen with or without permeation enhancers. *Biol. Pharm. Bull.* 16. 1264–1269. (1993)

Leite e Silva R.S., Ferelli C., Gimenis J.M., Ruas G.W., Baby A.R., Velasco M.V., Taqueda M.E., Kaneko T.M.: Hydrating effects of moisturizer active compounds incorporated into hydrogels: in vivo assessment and comparison between devices. *J. Cosmet. Dermatol.* 8. 32–39. (2009)

Lombry C., Dujardin N., Préat V.: Transdermal delivery of macromolecules using skin electroporation. *Pharm. Res.* 17. 32–37. (2000)

MacNeil S.: Progress and opportunities for tissue-engineered skin. *Nature* 445. 874–880. (2007)

Makai M., Csányi E., Németh Z., Pálinkás J., Erős I.: Structure and drug release of lamellar liquid crystals containing glycerol. *Int. J. Pharm.* 256. 95–107. (2003)

Marwah H., Garg T., Goyal A.K., Rath G.: Permeation enhancer strategies in transdermal drug delivery. *Drug Deliv.* 21. 1–15. (2015)

Mir L., Orlowski S.: Mechanisms of electrochemotherapy. *Adv. Drug Deliv. Rev.* 35. 107–118. (1999)

Mitragotri S.: Synergistic effect of enhancers for transdermal drug delivery. *Pharm. Res.* 17. 1354–1359. (2000)

Mitsubishi-Kagaku Foods Corporation, Ryoto Sugar Ester Technical Information. Nonionic surfactant/Sucrose fatty acid ester/Food additive. http://www.mfc.co.jp/english (1982)

Moser K., Kriwet K., Naik A., Kalia Y.N., Guy R.H.: Passive skin penetration enhancement and its quantification in vitro. *Eur. J. Pharm. Biopharm.* 52. 103–112. (2001)

Motta S., Sesana S., Monti M., Giuliani A., Caputo R., Interlamellar lipid differences between normal and psoriatic stratum corneum. *Acta Derm. Venereol. Suppl. (Stockh)* 186. 131–132. (1994)

Mura S., Manconi M., Sinico C., Valenti D., Fadda A.M.: Penetration enhancer-containing vesicles (PEVs) as carriers for cutaneous delivery of minoxidil. *Int. J. Pharm.* 380. 72–79. (2009)

Neumann E., Kakorin S., Toensing K.: Principles of Membrane Electroporation and Transport of Macromolecules. In: Jaroszeski M.J., Heller R., Gilbert R.: Electrochemotherapy, electrogenetherapy and transdermal drug delivery: Electrically mediated delivery of molecules to cells. Humana Press, Totowa, 1–35. (2000)

Nicander I., Ollmar S.: Clinically normal skin vs. non-atopic skin as seen through electrical impedance. *Skin Res. Technol.* 10. 178–183. (2004)

Park E-S., Chang S-Y., Hahn M., Chi S-C.: Enhancing effect of polyoxyethylene alkyl ethers on the skin permeation of ibuprofen. *Int. J. Pharm.* 209. 109–119. (2000)

Pelton J.T., McLean L.R.: Spectroscopic methods for analysis of protein secondary structure. *Anal. Biochem.* 277. 167–176. (2000)

Prausnitz M.R., Bose V.G., Langer R., Weaver J.C.: Electroporation of mammalian skin: a mechanism to enhance transdermal drug delivery. *Proc. Natl. Acad. Sci.* USA 90. 10504–10508. (1993)

Prausnitz M.R., Langer R.: Transdermal drug delivery. *Nat. Biotechnol.* 26. 1261–1268. (2008)

Prausnitz M.R., Elias P.M., Franz T.J., Schmuth M., Tsai J-C., Menon G.K., Holleran W.M., Feingold K.R.: Skin barrier and transdermal drug delivery. In Bolognia J.L., Jorizzo J.L., Schaffer J.V.: Dermatology, 3rd ed. Elsevier Health Sciences, St. Louis, 2065–2073. (2012)

Rawlings A.V., Canestrari D.A., Dobkowski B.: Moisturizer technology versus clinical performance. *Dermatol. Ther.* 17. 49–56. (2004)

Savic S., Tamburic S., Savic M., Cekic N., Milic J., Vuleta G.: Vehicle-controlled effect of urea on normal and SLS-irritated skin. *Int. J. Pharm.* 271. 269–280. (2004)

Scheuplein R.J.: Mechanism of percutaneous absorption. II. Transient diffusion and the relative importance of various routes of skin penetration. *J. Invest. Dermatol.* 48. 79–88. (1967)

Schön M.P., Boehncke W.H.: Psoriasis. *N. Engl. J. Med.* 352. 1899–1912. (2005)

Schroeder I.Z., Franke P., Schaefer U.F., Lehr C-M.: Delivery of ethinylestradiol from film forming polymeric solutions across human epidermis in vitro and in vivo in pigs. *J. Control. Rel.* 118. 196–203. (2007)

Sen A., Zhao Y-L., Hui S.W.: Saturated anionic phospholipids enhance transdermal transport by electroporation. *Biophys. J.* 83. 2064– 2073. (2002)

Surendra Babu N., Abute Lelisho T.: Computational studies of solvent effects on structure and Vibrational Spectra of isofavonoid 5,7-Dihydroxy-3-(4-hydroxyphenyl)chromen-4-one(Genistein) by ab intio HF and DFT methods. *Adv. Appl. Sci. Res.* 3. 3916–3934 (2012)

Szűts A., Szabó-Révész P.: Sucrose esters as natural surfactants in drug delivery systems – a mini-review. *Int. J. Pharm.* 433. 1–9. (2012)

Tadwee I., Shahi S., Ramteke V., Syed I.: Liquid crystals pharmaceutical application: A review. *Int. J. Pharm. Res. & All. Sci.* 1. 06–11. (2012)

Tanojo H., Boelsma E., Junginger H.E., Ponec M., Bodde H.E.: In vivo human skin barrier modulation by topical application of fatty acids. *Skin Pharmacol. Appl. Skin Physiol.* 11. 87–97. (1998)

Tortora G.J., Derrickson B. H.: Principles of Anatomy and Physiology 14th ed. John Wiley & Sons, Inc., New York (2014)

Touitou E., Levi-Schaffer F., Dayan N., Alhaique F., Riccieri F.: Modulation of caffeine skin delivery by carrier design: liposomes versus permeation enhancers. *Int. J. Pharm.* 103. 131–136. (1994)

Trommer H., Neubert R.H.H.: Overcoming the stratum corneum: the modulation of skin penetration. A review. *Skin Pharmacol. Physiol.* 19. 106–121. (2006)

Tur E.: Physiology of the skin–-differences between women and men. *Clin. Dermatol.* 15. 5–16. (1997)

Vaddi H.K., Ho P.C., Chan Y.W., Chan S.Y.: Terpens in ethanol:haloperidol permeation and partition through human skin and stratum corneum changes. *J. Control. Rel.* 81. 121–133. (2002)

Vanbever R., Préat V.: Factors affecting transdermal delivery of metoprolol by electroporation. *Bioelectrochem. Bioenerg.* 38. 223–228. (1995)

Vanbever R., LeBoulenge E., Préat V.: Transdermal delivery of fentanyl by electroporation: I. Influence of electrical factors. *Pharm. Res.* 13. 559–565. (1996)

Vanbever R., Prausnitz M.R., Préat V.: Macromolecules as novel transdermal transport enhancers for skin electroporation. *Pharm. Res.* 14. 638– 644. (1997)

Vicentini F., Casagrande R., Georgetti S.R., Bentley V., Fonseca M.V.: Influence of vehicle on antioxidant activity of quercetin: a liquid crystalline formulation. *Lat. Am. J. Pharm.* 26. 805–810. (2007)

Vizserálek G., Berkó Sz., Tóth G., Balogh R., Budai-Szűcs M., Csányi E., Sinkó B., Takács-Novák K.: Permeability test for transdermal and local therapeutic patches using Skin PAMPA method. *Eur. J. Pharm. Sci.* 76. 165–172. (2015)

Wagner H., Kostka K.-H., Lehr C.-M., Schaefer U.F.: Interrelation of permeation and penetration parameters obtained from in vitro experiments with human skin and skin equivalents. *J. Control. Rel.* 75. 283–295. (2001)

Walter J.R., Xu S.: Therapeutic transdermal drug innovation from 2000 to 2014: current status and outlook. *Drug Discov. Today* 20. 1293–1299. (2015)

Wickett R.R., Visscher M.O.: Structure and function of the epidermal barrier. *Am. J. Infect. Control* 34. 98–110 (2006)

Williams A.C., Barry B.W.: Penetration enhancers. *Adv. Drug Deliv. Rev.* 56. 603–618. (2004)

Wong T.W.: Electrical, magnetic, photomechanical and cavitational waves to overcome skin barrier for transdermal drug delivery. *J. Control. Rel.* 193. 257–269. (2014)

Yan K-S, Yan T-X, Guo H, Li J-Z, Wei L-L, Wang C, Nie S-F, Pan W-S.: Evaluation of transdermal permeability of pentoxifylline gel: in vitro skin permeation and in vivo microdialysis using Wistar rats. *Drug Discov. Ther.* 1. 78–83. (2007)

Yilmaz E., Borchert H-H.: Effect of lipid-containing, positively charged nanoemulsions on skin hydration, elasticity and erythema--an in vivo study. *Int. J. Pharm.* 307. 232–238. (2006)

Youan B.C., Hussain A., Nguyen N.T.: Evaluation of sucrose esters as alternative surfactants in micro-encapsulation of proteins by the solvent evaporation method. *AAPS Pharmsci.* 5. 123–131. (2003)

Zewert T.E., Pliquett U.F., Vanbever R., Langer R., Weaver J.C.: Creation of transdermal pathways for macromolecule transport by skin electroporation and a low toxicity, pathway-enlarging molecule. *Bioelectrochem. Bioenerg.* 49. 11– 20. (1999)

ACKNOWLEDGMENTS

I would like to thank the Head of the Department of Pharmaceutical Technology and the Head of the Pharmaceutical Technology PhD Program, **Professor Piroska Szabó-Révész** for providing me with the opportunity to work in this department and to complete my work under her guidance.

I would like to express my warmest thanks to my supervisors, **Associate Professor Dr. Erzsébet Csányi,** and **Assistant Professor Dr. Szilvia Berkó** for their constant advice during my Ph.D. work, and for critically reviewing my manuscripts. I owe my thanks to their, for their great help, support, guidance, encouragement and kindness.

I am very grateful to all of my **co-authors** for their kind collaboration.

I thank **all members** of the Department of Pharmaceutical Technology for their help and friendship.

I would like to thank **Richter Gedeon Plc.** for supporting my Ph.D. study.

I am deeply grateful to **my family** for their love, encouragement, support and understanding and for providing me with a peaceful background.

ANNEX

I.

Microchemical Journal 117 (2014) 183–186

Contents lists available at ScienceDirect

Microchemical Journal

journal homepage: www.elsevier.com/locate/microc

Protein structure is changed in psoriatic skin on the unaffected region — Imaging possibility with ATR-FTIR spectroscopy

Boglárka Balázs [a,b], Gabriella Farkas [a], Ottó Berkesi [c], Rolland Gyulai [d], Szilvia Berkó [a], Mária Budai-Szűcs [a], Piroska Szabó-Révész [a], Lajos Kemény [e], Erzsébet Csányi [a,*]

[a] Department of Pharmaceutical Technology, University of Szeged, Eötvös utca 6., H-6720 Szeged, Hungary
[b] Gedeon Richter Ltd., Gyömrői út 17-19., H-1103 Budapest, Hungary
[c] Department of Physical Chemistry and Materials Science, University of Szeged, Aradi Vt. 1., H-6720 Szeged, Hungary
[d] Department of Dermatology, Venereology and Oncodermatology, Medical School, University of Pécs, Kodály Z. u. 20., H-7624 Pécs, Hungary
[e] Department of Dermatology and Allergology, University of Szeged, Korányi fasor 6., H-6720 Szeged, Hungary

ARTICLE INFO

Article history:
Received 8 May 2014
Accepted 2 July 2014
Available online 9 July 2014

Keywords:
ATR-FTIR spectroscopy
Psoriatic skin
Protein structure
Amide-I band
Fourier self-deconvolution

ABSTRACT

Psoriasis is a T lymphocyte-mediated inflammatory disorder that affects the skin. A number of studies have demonstrated the occurrence of lipid alterations in psoriatic skin, resulting in a highly perturbed stratum corneum (SC). Relatively little attention has been paid to the protein conformation of the SC. In this study, the attenuated total reflection Fourier transform infrared (ATR-FTIR) spectrum of the untreated psoriatic patients' unharmed SC was obtained after tape stripping. We focused on the amide-I band components in order to establish whether there are any protein alterations in the intact areas of psoriatic skin. Fourier self-deconvolution (FSD) of the amide-I band was followed by curve-fitting to generate the underlying components. Integration of band areas provided an estimate of the secondary structure. The results indicated decreases in all amide-I band components, the peak at 1660 cm^{-1} revealing the most dramatic change. This peak is characteristic of the turn structure in the protein chain. The decrease is marked in the case of the β-sheet structure at 1630 cm^{-1} too. This ATR-FTIR imaging is a rapid and simple noninvasive method, promotes a better understanding of the disease, and would be helpful in following the treatment.

1. Introduction

Psoriasis, one of the most common chronic inflammatory skin diseases, with a frequency of approximately 1–2% of the population in the developed world, is characterized by regular exacerbations of cutaneous symptoms and frequent articular involvement. The prototypic psoriatic skin lesions are sharply demarcated erythematous plaques covered by silvery-white scaling, most often seen on the elbows, knees, scalp, umbilicus and lumbar area. The diagnosis is usually made on clinical grounds, though rarely a skin biopsy is necessary. The disease has a polygenic inheritance, and the expression of the symptoms is greatly influenced by environmental factors, such as stress or streptococcal infections [1,2].

Histologically, the disease is characterized by keratinocyte hyperproliferation, lymphocyte and granulocyte infiltration of the epidermis and dermis, and vasodilation of the dermal blood vessels. Hyperproliferation of the keratinocytes results in highly perturbed functions of the stratum corneum (SC). The SC, the uppermost layer of the epidermis, consists of keratin-rich anucleate nonviable cells (corneocytes) embedded in an intercellular matrix of lipids [3]. It is well known that multiple lipid bilayers play an important role in the permeability of the skin, and psoriatic skin is more permeable than healthy skin [2]. A number of studies have demonstrated that psoriatic skin exhibits alterations in lipid metabolism [4,5], whereas the changes in the proteins and their conformations in the SC of psoriatic skin have not been well studied to date.

One of the most common applications of Fourier transform infrared (FTIR) spectroscopy in protein studies is the analysis of secondary structure. FTIR spectroscopy involves the measurement of the wavelength and intensity of the absorption of IR radiation by a sample. The amide-I band region (1700–1600 cm^{-1}) is the spectral region most sensitive to the secondary structural components of the proteins; this is due very largely (approximately 80%) to the C═O stretch vibrations of the peptide linkages. Fourier self-deconvolution (FSD), a band-narrowing method, has not only enriched the qualitative interpretation of IR spectra, but has also provided a basis for the semiquantitative estimation of the secondary structure of proteins [6,7].

Attenuated total reflection FTIR (ATR-FTIR) spectroscopy is a tool that is often used to characterize the lipids, proteins and water content of the SC [8]. The sample is placed on an IR-transparent crystal, the IR

* Corresponding author at: Department of Pharmaceutical Technology, University of Szeged, Eötvös str. 6, H-6720 Szeged, Hungary. Tel.: +36 62 545 573; fax: +36 62 545 571.
E-mail address: csanyi@pharm.u-szeged.hu (E. Csányi).

http://dx.doi.org/10.1016/j.microc.2014.07.003
0026-265X/

beam is directed onto the crystal with high refractive index and the internal reflectance creates an evanescent wave which penetrates into the sample. Unlike the case of the KBr pellet method, this method does not require sample preparation. We made use of the application of an adhesive tape to obtain the spectrum of human SC in vivo [9].

The aim of the present paper is to give an account of the primary results of an in vivo study of intact psoriatic skin, using the components of the amide-I band to determine the changes in the secondary structure of the proteins by combining tape stripping and ATR-FTIR spectroscopy.

2. Materials and methods

2.1. Experiments

Psoriatic SC samples were obtained from 6 untreated psoriatic patients (3 males and 3 females) aged between 32 and 64. Normal SC samples were collected from 20 healthy volunteers (10 males and 10 females) aged between 21 and 42 with no history of dermatological disease. The study was approved by the local ethics committee (Government Office of Csongrád County Policy Administration Services of Public Health, PSO-SPEKT-001). All volunteers were asked not to apply any moisturizer or cosmetic product for at least 24 h before the process. The forearm skin of each volunteer was stripped with adhesive cellophane tape; this was repeated up to 25 strips. In the case of the psoriatic patients, the samples were taken from the unharmed skin of the forearm. Every first tape with one strip was discarded because of the possibility of surface contamination. Every second adhesive tape with three strips was analyzed, because this gave the most intensive IR spectrum.

2.2. FTIR spectroscopy and curve-fitting analysis

ATR-FTIR spectra were recorded with an Avatar 330 FT-IR spectrometer (Thermo Nicolet, USA) equipped with a horizontal ATR crystal (ZnSe, 45°), between 4000 and 400 cm^{-1}, at an optical resolution of 4 cm^{-1}. 128 scans were co-added and all spectral manipulations were performed by using Thermo Scientific's GRAMS/AI Suite software. The components of the amide-I band and their relative intensities were estimated semiquantitatively in the 1695–1600 cm^{-1} region of the FTIR spectra by a curve-fitting algorithm using Gaussian–Lorenzian mixing functions. The best fits were found by an iterative process minimizing the standard error.

2.3. Statistical analysis

The results of curve-fitting were evaluated and analyzed statistically by Student's t-test. The data given are the averages of the results of 13 parallel (3 psoriatic and 10 healthy) experiments ± SD ($p < 0.05^*$, $p < 0.01^{**}$).

3. Results and discussion

The amide-I band appears clearly in the ATR-FTIR spectrum of the skin as a consequence of the coupling of the transition dipole moments of the amide groups within the protein backbone. Various protein secondary structures have their own characteristic amide-I bands. However, because of the strong overlap between the characteristic bands, the amide-I bands of the recorded infrared spectra are too complex to permit the direct determination of the components with various secondary structures [10].

Band-narrowing procedures such as FSD and curve-fitting greatly enhance the potential of this band as a meaningful structural probe. Such mathematical processes increase the degree of separation by narrowing the half-bandwidths of the individual components for easier visualization without seriously distorting the spectrum. The main disadvantage of this procedure is its tendency to magnify both the signal and the noise in the spectrum. This causes a dramatic increase in the noise level, which necessitates coupling the FSD with a smoothing function [6,11,12].

FSD of the corresponding ranges of the recorded spectra were used to determine the approximate frequencies of the components of the amide-I bands indicating the presence of protein chain sections with various secondary structures [10,13]. Seven bands were fitted to all the spectra and their areas were compared (Fig. 1). The ratios of the integrated band areas provide an estimate of the proportions of the parts with various secondary protein structures.

A protein molecule is formed from a chain of amino acids. The secondary structure of a protein is determined by the set of dihedral angles (φ, ψ) which define the spatial orientation of the peptide backbone, and the presence of specific hydrogen-bonds. Regular secondary structures include α-helices and β-sheets. An ideal α-helix has 3.6 residues per turn, and is built up from a contiguous amino acid segment via backbone–backbone hydrogen-bond formation between amino acids in positions i and i + 4. The residues taking part in an α-helix have φ angles around −60° and ψ angles around −45°.

β-Sheets are created when atoms of β-strands are hydrogen-bonded. β-Sheets may consist of parallel strands, antiparallel strands or a mixture of parallel and antiparallel strands. In parallel β-sheets the strands run in one direction, whereas in antiparallel sheets they run in alternating directions. The dihedral angles of the β-sheet are φ ~ −130° and ψ ~ −120°, forming an extended structure with some right-handed twist.

Turns allow a protein to fold back on itself and are stabilized by a hydrogen-bond that holds the ends together. They are classified according to the number of residues involved in the hydrogen-bonded structure. Unordered structure is generally defined as a conformation that is not helix, sheet or turn [13].

In the SC, greater flexibility is achieved through loose packing of the keratin filaments and a lower number of disulfide crosslinks. It was observed that the overall intensities of the amide-I bands were lower for the psoriatic SC than for the healthy SC (Fig. 2), but the peak at 1660 cm^{-1} exhibited the most pronounced alteration, as shown in Fig. 3. The proteins in the SC are mainly in α-helical conformation [14]. The peak at 1650 cm^{-1} indicates the presence of an α-helix (Fig. 3), which always has the largest area. We focused on the peak at 1660 cm^{-1}, characteristic of the turns in the protein chain [13]. The intensity of this peak decreases almost to zero in psoriatic patients, indicating the drop in concentration in the turn protein regions (Table 1). We have given the results for men and women separately, because of the differences in skin between the genders [15].

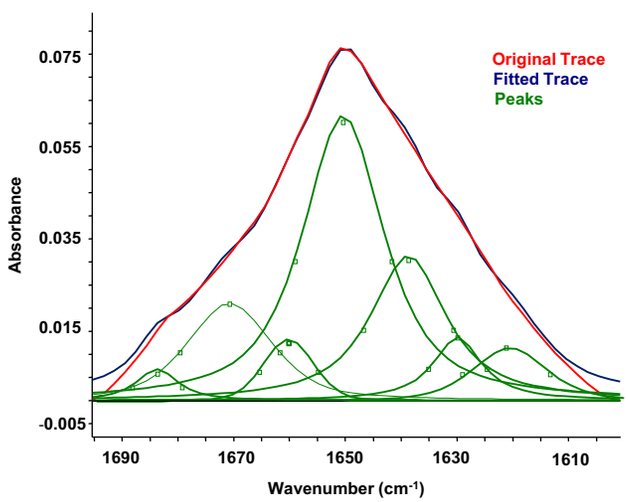

Fig. 1. The original FTIR spectra of the SC and the deconvolved and curve-fitted components.

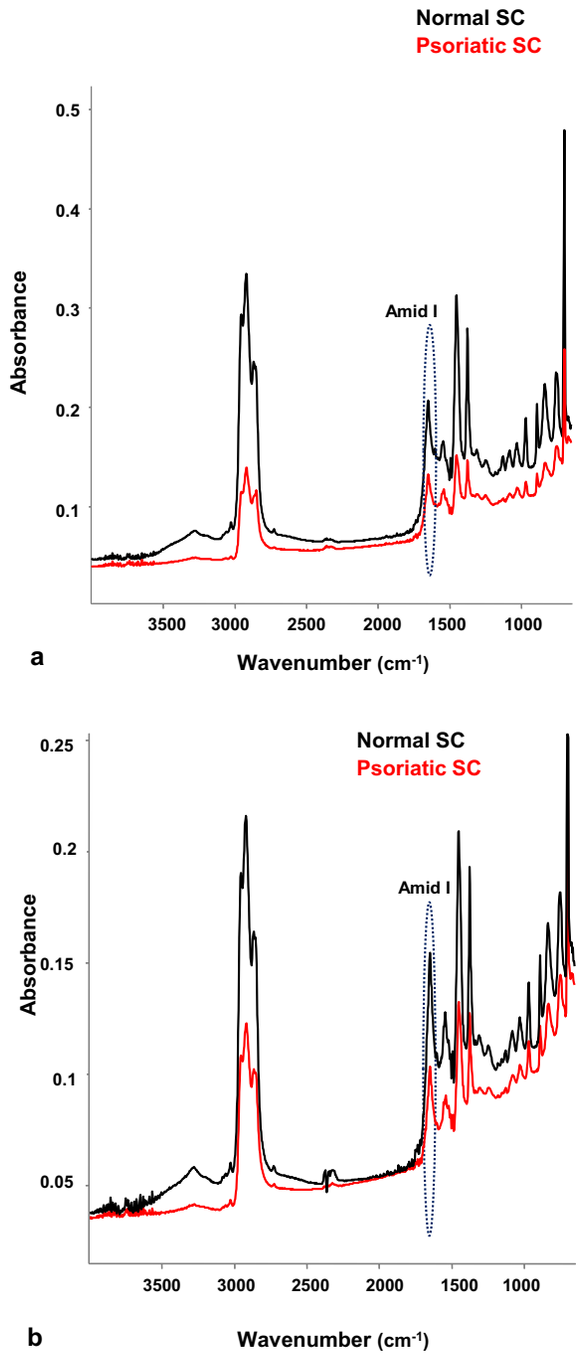

Fig. 2. Intensities differences between normal SC and psoriatic SC spectrums. a: Man; b: woman.

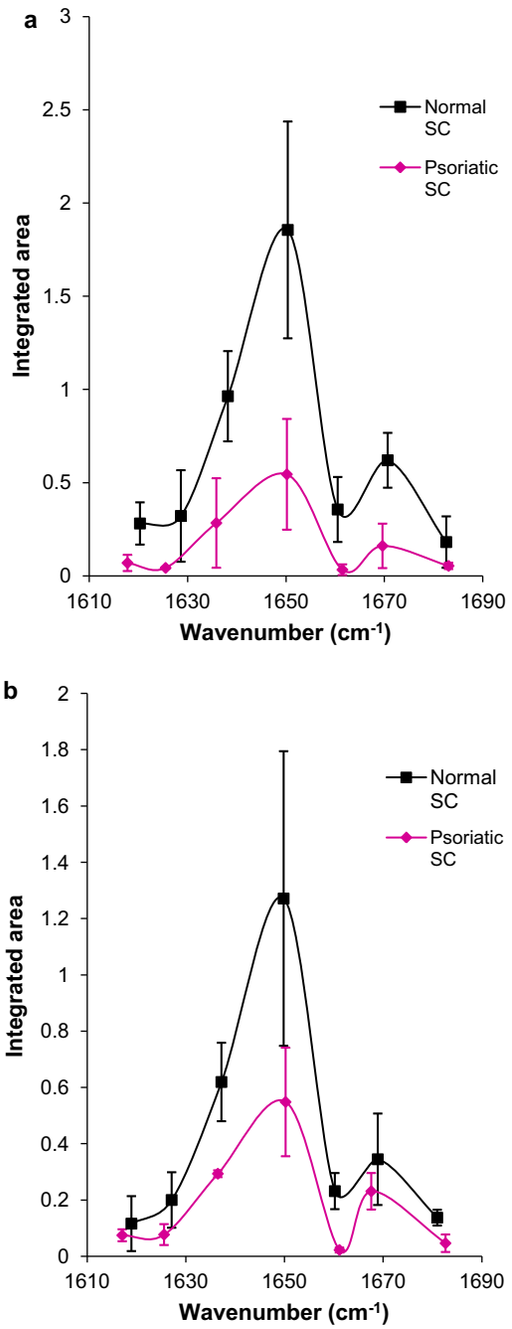

Fig. 3. Area of the fitted components of the amide-I band in the cases of normal and psoriatic SC. a: men; b: women.

Fig. 4 compares the areas of the peak at 1660 cm^{-1} for the healthy control group and the psoriatic patients. As a result of the presence of psoriasis, the intensity of this band is significantly lower for both males ($p < 0.05^{*}$) and females ($p < 0.01^{**}$). The areas of all the amide-I band components are less in the psoriatic group, but the decrease is especially marked in the cases of the bands at 1630 and at 1660 cm^{-1} (Fig. 3). The former is in the middle of the region characteristic of the β-sheet structure, and the latter reflects the turn structure. The fall in the intensity of the latter suggests the loss of those parts of the protein structure even in the unharmed psoriatic SC which provide the protein with flexibility.

4. Conclusions

The protein structure is changed on the unaffected area in the psoriatic skin disease. The combination of tape stripping and ATR-FTIR spectroscopy could serve as an appropriate, rapid, simple noninvasive method for the study of psoriasis and for follow-up of the efficiency of treatment. From a pharmaceutical technology aspect, these results suggest the development of a targeted dermal system which ensures convenient treatment to unaffected areas of the psoriatic skin. However, further investigations with higher numbers of patients are needed in order to refine the method and to gain deeper insight into the nature of psoriasis itself.

Table 1
Decreased integrated area of amide-I protein structures in psoriatic skin.

Conformation	β-sheet		α-helix	Turns		β-sheet	Turn
Wavenumber [cm^{-1}]	1620	1640	1650	1670	1680	1630	1660
Healthy men mean integrated area (±SD)	0.28 (0.11)	0.96 (0.24)	1.85 (0.58)	0.62 (0.15)	0.18 (0.14)	0.32 (0.25)	0.36 (0.17)
Psoriatic men mean integrated area (±SD)	0.07 (0.04)	0.28 (0.24)	0.54 (0.30)	0.16 (0.12)	0.05 (0.02)	0.04 (0.005)	0.03 (0.03)
Integrated area percentage (%) of psoriatic over healthy	**24.6**	**29.4**	**29.3**	**25.9**	**29.3**	**13.2**	**9.2**
Healthy women mean integrated area (±SD)	0.12 (0.10)	0.62 (0.14)	1.27 (0.52)	0.34 (0.16)	0.14 (0.03)	0.20 (0.10)	0.23 (0.06)
Psoriatic women mean integrated area (±SD)	0.07 (0.02)	0.29 (0.01)	0.55 (0.19)	0.23 (0.06)	0.05 (0.03)	0.08 (0.04)	0.02 (0.01)
Integrated area percentage (%) of psoriatic over healthy	**64.4**	**47.4**	**43.1**	**67**	**33.9**	**3.9**	**9.7**

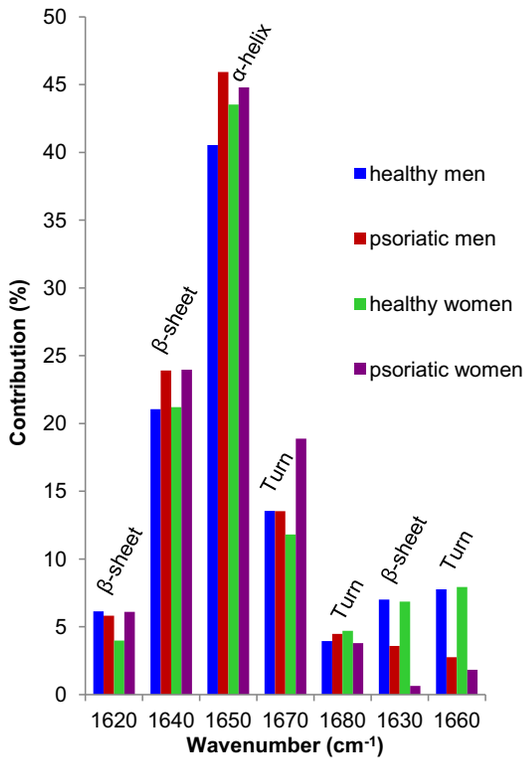

Fig. 4. Percentage contributions of the components of the amide-I band for psoriatic and healthy patients of both genders.

Acknowledgements

This project was supported by the 'European Union and co-financed by the European Social Fund: TÁMOP-4.2.2.A-11/1/KONV-2012-0035'.

References

[1] M.P. Schon, W.H. Boehncke, Psoriasis, N. Engl. J. Med. 352 (2005) 1899–1912.
[2] G. Bernard, M. Auger, J. Soucy, R. Pouliot, Physical characterization of the stratum corneum of an in vitro psoriatic skin model by ATR-FTIR and Raman spectroscopies, Biochim. Biophys. Acta 1770 (2007) 1317–1323.
[3] M. Denda, New strategies to improve skin barrier homeostasis, Adv. Drug Deliv. Rev. 54 (Suppl. 1) (2002) S123–S130.
[4] S. Motta, S. Sesana, M. Monti, A. Giuliani, R. Caputo, Interlamellar lipid differences between normal and psoriatic stratum corneum, Acta Derm. Venereol. Suppl. (Stockh.) 186 (1994) 131–132.
[5] M. Holtje, T. Forster, B. Brandt, T. Engels, W. von Rybinski, H.D. Holtje, Molecular dynamics simulations of stratum corneum lipid models: fatty acids and cholesterol, Biochim. Biophys. Acta 1511 (2001) 156–167.
[6] J. Kong, S. Yu, Fourier transform infrared spectroscopic analysis of protein secondary structures, Acta Biochim. Biophys. Sin. 39 (2007) 549–559.
[7] J. Hadgraft, M.E. Lane, Skin permeation: spectroscopic methods, in: H.A.E. Benson, A.C. Watkinson (Eds.), Transdermal and Topical Drug Delivery, John Wiley & Sons, Inc., Hoboken, NJ, 2011, pp. 155–166.
[8] M. Dias, A. Naik, R.H. Guy, J. Hadgraft, M.E. Lane, In vivo infrared spectroscopy studies of alkanol effects on human skin, Eur. J. Pharm. Biopharm. 69 (2008) 1171–1175.
[9] D. Bommannan, R.O. Potts, R.H. Guy, Examination of stratum corneum barrier function in vivo by infrared spectroscopy, J. Investig. Dermatol. 95 (1990) 403–408.
[10] A. Barth, Infrared spectroscopy of proteins, Biochim. Biophys. Acta 1767 (2007) 1073–1101.
[11] O.P. Lamba, D. Borchman, S.K. Sinha, J. Shah, V. Renugopalakrishnan, M.C. Yappert, Estimation of the secondary structure and conformation of bovine lens crystallins by infrared spectroscopy: quantitative analysis and resolution by Fourier self-deconvolution and curve fit, Biochim. Biophys. Acta 1163 (1993) 113–123.
[12] J.I. Al-Mustafa, FTIR investigation of the conformational properties of the cyanide bound human hemoglobin, Vib. Spectrosc. 30 (2002) 139–146.
[13] J.T. Pelton, L.R. McLean, Spectroscopic methods for analysis of protein secondary structure, Anal. Biochem. 277 (2000) 167–176.
[14] M. Gniadecka, O. Faurskov Nielsen, D.H. Christensen, H.C. Wulf, Structure of water, proteins, and lipids in intact human skin, hair, and nail, J. Investig. Dermatol. 110 (1998) 393–398.
[15] E. Tur, Physiology of the skin — differences between women and men, Clin. Dermatol. 15 (1997) 5–16.

II.

Pro-apoptotic Effect of Soy Total Extract Incorporated in Lyotropic Liquid Crystals Formulation

CORINA DANCIU[1#], MARIUS BIRIS[1#], BOGLÁRKA BALÁZS[2], ERZSÉBET CSÁNYI[2], IOANA ZINUCA PAVEL[1], GEORGETA POP[3], CODRUTA SOICA[1], LAVINIA CEUTA[1], LUCIAN NITA[3], CLAUDIU MORGOVAN[4*], DANA STOIAN[1]

[1]University of Medicine and Pharmacy "Victor Babes", 2 Eftimie Murgu Sq., 300041, Timisoara, Romania

[2] University of Szeged, 6 Eotvos u., H-6720, Szeged, Hungary, Department of Pharmaceutical Technology

[3] University of Agricultural Sciences and Veterinary Medicine, Department of Plant Culture, 119 Aradului Str., Timisoara, Romania

[4] "Vasile Goldis" Univesity of Arad, 94-96 Revolutiei Blv., 310025, Arad, Romania

The paper aims to test the pro apoptotic capacity of soy total extract on the B164A5 mouse melanoma cells alone and after incorporation in the modern formulation lyotropic liquid crystals. DAPI dye and Annexin-FITC-7AAD double staining show that soy extract present both early and late apoptotic properties against B164A5 murine melanoma cell line. Furthermore , incorporation of soy extract in the modern formulation does not affect in a negative manner this property. As explained in the paper the benefits of such an approach, this preliminary study represent an obvious proof that incorporation of soy extract in this new formulation is a good option for furtherer in vivo studies on animal model of melanoma.

Keywords: soy extract, lyotropic liquid crystals, murine melanoma, apoptosis

Among the modern formulations used in the pharmaceutical field for local administration of different active agents, lyotropic liquid crystals (LLC) have gained increased attention due to their special physico-chemical properties [1,2] . As a brief description of the formulation-LLC are formed by surfactants having two different parts: a non polar, seldom hydrocarbon tail and a polar, seldom ionic, head [3]. LLC have the properties somewhere in between a conventional liquid and a solid crystal [4]. They have the ability to exhibit phase transitions depending on the temperature and on the concentration of the liquid crystals in the employed solvent which is frequently water [5]. The thermodynamic stability of these formulations and the intense similarity of these systems to those in living organism makes LLC a great excipient for the local administration of different active agents [6,7].

Pure natural compounds or plant total extract represent a wellspring of remedies for a variety of pathologies. During the past decades a spectacular number of remedies from nature turned in classical therapy, well accepted by an increasing number of patients. An intensively and controversy studied extract is represented by soy extract, respectively its activate isoflavones genistein and daidzein. Recent studies show that soy total extract induce apoptosis in prostate cancer cells [8]. Furthermore it shows anti menopause effects[9] . It has been show that soy extract is more potent than genistein on an animal model of breast cancer on tumor growth inhibition [10]. It has been reported its antiproliferative activity in a mouse model of skin cancer [11].Soy isoflavones have been studied for their ant diabetic and hypolipidemic effects [12]. The group of Catania *et al*., have published that in case of ovariectomized rats orally administered soy extract improves the endothelial dysfunction [13] . Soy germ extract have been proofed pro apoptotic properties *in vitro* in case of colon cancer [14] .

The paper represents a preliminary study of the soy based formulation for furtherer *in vivo* investigations on animal models of melanoma . It aims to test the pro apoptotic capacity of soy extract employing the B164A5 mouse melanoma cells alone and after incorporation in the modern lyotropic liquid crystals formulation.

Experimental part

Materials and methods

Extraction

Soy seeds were kindly provided from University of Agricultural Sciences and Veterinary Medicine, Timisoara, Romania, Department of Plant Culture. As previously described hydroalcoholic extracts were performed. Dry soybeans were put into powder. A hydroalcoholic solvent containing 70% ethanol was prepared. 10% vegetal product extracts were ultrasonicated for 10 min in the ultrasonic bath . Afterwards the solvent was evaporated and the powder was used for furtherer experiments [15].

Lamellar lyotropic liquid crystalline soy extract based formulation

Soy extract, the active agent was incorporated in the lamellar lyotropic liquid crystal formulation in a concentration of 10%. The carrier was the mixture of a non-ionic surfactant, Cremophor RH40 (Polyoxyl 40 Hydrogenated Castor Oil USP/NF). It was obtained from BASF (67056, Ludwigshafen, Germany). The water phase of the systems was purified water (Ph.Eur.6.), while the oil phase was isopropyl myristate (Merck Kft. 1121, Budapest, Hungary). The oil-surfactant mixture (oil:surfactant ratio = 2:1) was homogenized with a magnetic stirrer at room temperature. Then 10% of water was added to this mixture in small amounts while stirring. The 10 % soy extract was incorporated in the oil-surfactant mixture with a magnetic stirrer.

DAPI (4, 6-Diamidino-2-phenylindole) staining

B16 cells were seeded at a concentration of $5x10^4$ in a chamber slide system formed of 8 well glass slides in culture medium. After 24h cells were incubated in medium containing 10%FCS and 200μg/mL of soy extract, respectively 200μg/mL of soy extract corresponding to

* *email: claudiumorgovan@yahoo.com* # *equal contribution*

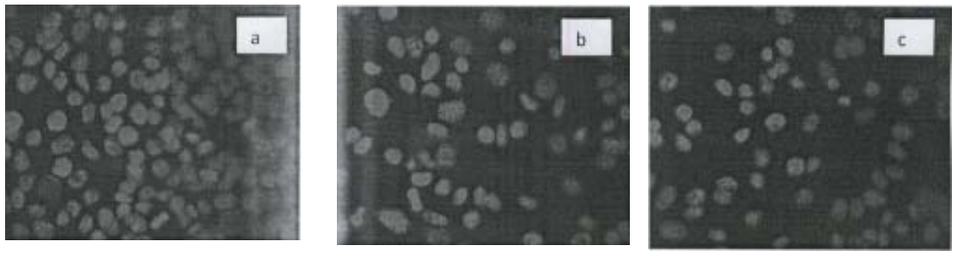

Fig. 1. DAPI staining after 72h incubaton of B164A5 cells with a) Medium; b) 200 μg/mL of soy extract c) 200 μg/mL of soy extract corresponding to the 10% LLC formulation

the 10% lamellar lyotropic liquid crystalline formulation. The total volume added in chamber was 400 μL. Cells were incubated for 72 h and afterwards the medium was removed. Cells were washed with PBS and afterwards 400μL of staining solution were added in each well. The staining solution consisted of a mixture of methanol and DAPI (Roche) as follows: 1 mL methanol: 2 μL DAPI (from a stock solution of 1mg/mL). Cells were incubated for 5 minutes with this staining solution and afterwards washed with PBS and analyzed by fluorescence microscopy.

Annexin-FITC-7AAD double staining

Cells were cultivated in a 6 well plates at a density of 80% using normal medium. After 24h medium containing 10% FCS and and 200 μg/mL of soy extract, respectively 200 μg/mL of soy extract corresponding to the 10% lamellar lyotropic liquid crystalline formulation were added. After 48h cells were detached using trypsin, washed with ice cold PBS and resuspended in 500 μLAnnexin binding buffer (1.19 g HEPES NaOH *p*H =7.4; 4.09 g NaCl; 0.138 g $CaCl_2$ in 50 mL distillated water and diluted 1:10) at a concentration of $1x10^6$ cells/mL. Cells were centrifugated 5 min at 1200 rpm, the supernatant was discarded and the cells were resuspended in 70 μL of Annexin binding buffer. 5 μL Annexin V-FITC (ImmunoTools) and 5 μL 7AAD (ImmunoTools) were added and cells were incubated 15 min on ice and in the dark. Samples were measured by FACS on FL1 and FL3 fluorescence channels using a BD Canto II FACS DIVA device. Flow Jo soft (7.6.3) was used for data analysis.

Statistics

One Way ANOVA followed by Bonferroni post test were used to determine the statistical difference between various experimental and control groups.*, ** and *** indicate $p<0.05$, $p<0.01$ and $p<0.001$ compared to control group.

Results and discussions

The balance between proliferation and apoptosis has a vital role in many human diseases including cancer [16]. Among years different approaches have been conducted in order to fight cancer and one important strategy points towards finding pro-apoptotic agents [17]. DAPI staining is frequently used as a preliminary assay to test the pro-apoptotic capacity of different active agents [18] . After a period of incubation of 72h with 200μg/mL of soy extract, respectively 200μg/mL of soy extract corresponding to the 10% lamellar lyotropic liquid crystalline formulation, cells stained with DAPI displayed the typical characteristics of cells undergoing apoptosis (fig. 1). The blue stained nucleus allows to notice the morphological hallmarks of apoptosis: nuclear fragmentation, chromatin condensation, nuclear condensation as a sign of loss of cell membrane integrity, reduction of cellular volume, rounding up of the cell. It can not be detected a significant difference regarding the morphological signs of apoptosis between soy extract respectively the soy extract corresponding to the 10% lamellar lyotropic liquid crystalline based formulation. This aspect represent a good news for furtherer *in vivo* investigations, meaning that the formulation does not affect the biological activity of soy extract, but it helps, as explained in the introduction to its delivery. In addition it can be observed that after the 72 h of incubation both the extract respectively the extract incorporated in the formulation present also anti-proliferative effect, as it can be noticed by the decreased number of cells presented in a specific field. DAPI staining was previously used in order to test the pro-apoptotic activity of genistein, the most active isoflavone in soy extract, on human uterine leiomyoma, human prostate carcinoma PC-3 cells, Ewing's sarcoma CHP-100 cells, breast cancer MCF-7 cells [19-21].a

In order to be able to get more data about the apoptotic process, the double staining Annexin-FITC-7AAD was performed. This assay allows to get information about early apoptotic, late apoptotic and necrotic cells after incubation to different active agents [22] . Results show (fig. 2), that after a period of incubation of 72 h both the soy extract alone, respectively incorporated in the LLC formulation present early and late apoptotic properties. Average value corresponding to three different experiment show 3.38±2.89 early apoptotic cells in case of incubation with 200 μg/mL of soy extract and 2.60±0.84 early apoptotic cells in case of incubation with 200 μg/mL of soy extract incorporated in the LLC formulation. The tested active agents succeeded to induce more intense the phenomena of late apoptosis, as it can be depicted from figure 2, namely

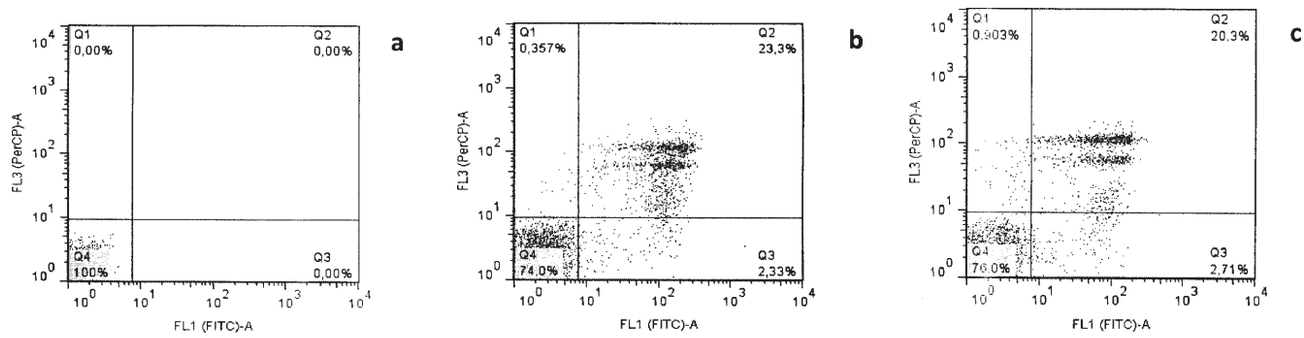

Fig. 2. Annexin-FITC-7AAD double staining after 72h incubation of B164A5 cells with: a) Medium; b) 200μg/mL of soy extract; c) 200μg/mL of soy extract corresponding to the 10% LLC soy extract based formulation

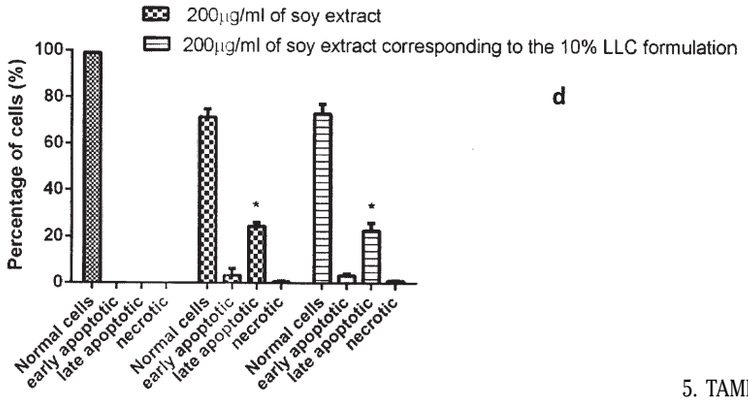

Fig. 2d cont. Average value corresponding to three different experiments

24.52±1.69 late apoptotic cells in case of incubation with 200µg/mL of soy extract and 22.66±3,34 late apoptotic cells in case of incubation with 200µg/mL of soy extract incorporated in the LLC formulation. A decreased number of necrotic cells could be also detected, namely 0.613 ±0.36 necrotic cells in case of incubation with 200 µg/mL of soy extract and 0.987±0.11 late apoptotic cells in case of incubation with 200µg/mL of soy extract incorporated in the LLC formulation. The pro-apoptotic capacity of soy extract was also described in case of prostate cancer cells, human AGS gastric cancer cells [8,23]. Soy isoflavones, the most active phytocompounds, as we previously discussed showed pro-apoptotic effect in case of breast cancer cells, murine and human bladder cancer cells, HT-29 colon cancer cells, human prostatic cancer cell line LNCaP, human hepatoma cell lines HepG2, Hep3B, Huh7, PLC, and HA22T [14.24.27].Furthermore, a recent study shows that the biotransformed soy extract fermented by *Aspergillus awamor* induces apoptosis in case of A375 human melanoma cell line [28]. Correlating to the data existing in the literature this study brings in to light the pro-apoptotic activity of soy extract on the murine melanoma B164A5 cell line.

Conclusions

Results show that soy extract present apoptotic properties against B164A5 murine melanoma cell line. Furthermore , incorporation of soy extract in the modern formulation lamellar lyotropic liquid crystals does not affect in a negative manner this property. As explained in the introduction the benefits of such an approach, this preliminary study represents an obvious proof that incorporation of soy extract in this new formulation is a good option for furtherer *in vivo* studies on animal model of melanoma

Acknowledgments: This study was published under the frame of European Social Found, Human Resources Development Operational Programme 2007-2013, project no. POSDRU/159/1.5/S/136893 obtained by postdoc. Danciu Corina

References

1. CHEN, Y., MA, P., GUI, S., Cubic and Hexagonal Liquid Crystals as Drug Delivery Systems, BioMed. Res.Int.,2014,:e815981, doi.org/10.1155/2014/815981.
2. BAGUENARD, C., GUYMON, C.A,. Self-Assembled Supramolecular Architectures. Lyotropic Liquid Crystals, Wiley, Angew. Chem. Int., GARTI, N., SOMASUNDARAN, P., MEZZENGA, R, New Jersey, 2012, p. 97.
3. STEGMEYER, H., Liquid Crystals, Springer, HILTROP, K., New York, 1994, p.143.
4. CHANDRASEKHAR, S., Discotic liquid crystals. A brief review, Liquid Crystals ,14, nr.1, 1993, p.3.
5. TAMBADE, T.A., ALOORKAR, N.H., DABANE, N.S., OSMANI, R.M., KALE, B.B., INDALKAR, Y.R., Formulation and evaluation of novel gel containing liquid crystals of naproxen, Am. J.of Adv. Drug Delivery, 2, nr.3, 2014, p.364.
6. MAKAI, M., CSÁNYI, E., DÉKÁNY, I., NÉMETH, Z., ER S, I., Structural properties of nonionic surfactant/glycerol/paraffin lyotropic liquid crystals, Colloid Polym Sci.,281, nr.9,2003, p.839.
7. MAKAI, M., CSÁNYI, E., NÉMETH, Z., PÁLINKÁS, J., ER S, I., Structure and drug release of lamellar liquid crystals containing glycerol, Int. J of Pharmaceutics, 256, nr.1-2 ,2003, p.95.
8. HSU,A., BRAY, T.M., HELFERICH, W.G., DOERGE, D.R., HO, E., Differential effects of whole soy extract and soy isoflavones on apoptosis in prostate cancer cells, Exp. Biol. Med.,235, nr.1, 2010, p.90.
9. SCAMBIA, G., MANGO, D., SIGNORILE, P.G., ANSELMI ANGELI, R.A., PALENA, C., GALLO ,D., et al. Clinical effects of a standardized soy extract in postmenopausal women: a pilot study, Menopause, 7, nr.2, p.105.
10. KIM, H.A., JEONG, K.S., KIM, Y.K., Soy extract is more potent than genistein on tumor growth inhibition,Anticancer Res.,28, nr.5A, 2008, p.2837.
11. TIULEA ,C., PEEV, C., BREZOVAN, D., DEHELEAN, C., MOTOC, A., A comparison regarding antiproliferative action between soy total extract and genistein. Rom J Morphol Embryol., 52, nr.3, 2011, p.1065
12 .MEZEI, O., BANZ, W.J., STEGER, R.W., PELUSO, M.R., WINTERS, T.A., SHAY, N,. Soy Isoflavones Exert Antidiabetic and Hypolipidemic Effects through the PPAR Pathways in Obese Zucker Rats and Murine RAW 264.7 Cells., J Nutr.,133, nr.5, 2003, p.1238.
13. CATANIA, M.A., CRUPI, A., FIRENZUOLI, F., PARISI, A., STURIALE, A., SQUADRITO, F., et al. Oral Administration of a Soy Extract Improves Endothelial Dysfunction in Ovariectomized Rats, Planta Med., 68, nr.12, 2002, p.1142
14. KIM, G.N., SONG, J.H., KIM, E.S., CHOI, H.T., JANG, H.D., Isoflavone content and apoptotic effect in HT-29 cancer cells of a soy germ extract, Food Chem., 130, nr.2, 2012, p.404.
15. TIULEA, C., PEEV, C., FEFLEA, S., VLASE, L., DEHELEAN, C., POP, G., A screening for the most representative classes of compounds from two varieties of soy, JAPT, 17, nr.1, 2011, p.15.
16. WONG, R.S., Apoptosis in cancer: from pathogenesis to treatment, J. of Exp.& Clin. Cancer Res., 30, nr.1, 2011, p.87.
17. GRAZIA, G., PENNA, I., PEROTTI, V., ANICHINI, A., TASSI, E., Towards combinatorial targeted therapy in melanoma: From pre-clinical evidence to clinical application , Int J Oncol., 45, nr.3, 2014, p.929.
18. KEPP, O., GALLUZZI, L., LIPINSKI, M., YUAN, J., KROEMER, G., Cell death assays for drug discovery, Nat Rev Drug Discov., 10, nr.3, 2011, p.221.
19. MOORE, A.B., CASTRO, L., YU, L., ZHENG, X., DI, X., SIFRE, M.I., et al. Stimulatory and inhibitory effects of genistein on human uterine leiomyoma cell proliferation are influenced by the concentration, Hum Reprod, 22, nr.10, 2007, p.2623.
20. CHOI ,Y.H., LEE, S.J., KIM, M., ZHANG, L., LEE, W.H., PARK, K.Y., Genistein Induced Inginition of Cell Proliferation and Programmed Cell Death in the Human Cancer Cell Lines, J. Korean Cancer Assoc., 30, nr.4, 1998, p.800.

21. CHOI, E., JUNG, J., KIM, G.H., Genistein inhibits the proliferation and differentiation of MCF-7 and 3T3-L1 cells via the regulation of ERá expression and induction of apoptosis, Exp.Ther. Med.,8,nr.2, 2014, p.454.
22. IYER, S., CHAPLIN, D.J., ROSENTHAL, D.S., BOULARES, A.H., LI, L.Y., SMULSON M.E., Induction of Apoptosis in Proliferating Human Endothelial Cells by the Tumor-specific Antiangiogenesis Agent Combretastatin A-4,Cancer Res, 58, nr.20, 1998, p.4510 .
23. ZOU, Y., CHANG, S.K.C., Effect of Black Soybean Extract on the Suppression of the Proliferation of Human AGS Gastric Cancer Cells via the Induction of Apoptosis., J Agric Food Chem., 59, nr.9, 2011, p..4597.
24. MESSINA, M., Soy, soy phytoestrogens (isoflavones), and breast cancer, Am J Clin Nutr., 70, nr.4, 1999, p.574.
25. ZHOU, J.R., MUKHERJEE, P., GUGGER, E.T., TANAKA, T., BLACKBURN, G.L., CLINTON, S.K., Inhibition of Murine Bladder Tumorigenesis by Soy Isoflavones via Alterations in the Cell Cycle, Apoptosis, and Angiogenesis, Cancer Res., 58, nr.22, 1998, p.5231.
26. ONOZAWA, M., FUKUDA, K., OHTANI, M., AKAZA, H., SUGIMURA, T., WAKABAYASHI, K., Effects of Soybean Isoflavones on Cell Growth and Apoptosis of the Human Prostatic Cancer Cell Line LNCaP, Jpn. J. Clin. Oncol., 28, nr.6, 1998, p.360.
27. SU, S.J., CHOW, N.H., KUNG, M.L., HUNG, T.C., CHANG, K.L., Effects of Soy Isoflavones on Apoptosis Induction and G2-M Arrest in Human Hepatoma Cells Involvement of Caspase-3 Activation, Bcl-2 and Bcl-XL Downregulation, and Cdc2 Kinase Activity. Nutr. Cancer, 45, nr.1, 2003, p.113.
28. VILELA, F.M.P., SYED, D.N., CHAMCHEU, J.C., CALVO-CASTRO, L.A., FORTES, V.S., FONSECA, M.J.V., et al. Biotransformed Soybean Extract (BSE) Inhibits Melanoma Cell Growth and Viability In Vitro: Involvement of Nuclear Factor-Kappa B Signaling, PLoS ONE, 9, nr.7, 2014, e103248.

Manuscript received: 18.12.2014

III.

Int. J. Mol. Sci. **2015**, *16*, 15425-15441; doi:10.3390/ijms160715425

OPEN ACCESS
International Journal of
Molecular Sciences
ISSN 1422-0067
www.mdpi.com/journal/ijms

Article

The Effect of Electroporation of a Lyotroic Liquid Crystal Genistein-Based Formulation in the Recovery of Murine Melanoma Lesions

Corina Danciu [1,*], Szilvia Berkó [2], Gábor Varju [3], Boglárka Balázs [2], Lajos Kemény [4], István Balázs Németh [4], Andreea Cioca [5], Alexandra Petruș [6], Cristina Dehelean [7], Citu Ioan Cosmin [8], Elena Amaricai [9,*] and Claudia Crina Toma [10]

1 Department of Pharmacognosy, "Victor Babes" University of Medicine and Pharmacy, 300041 Timisoara, Romania
2 Department of Pharmaceutical Technology, University of Szeged, Szeged 6720, Hungary; E-Mails: berko@pharm.u-szeged.hu (S.B.); balazs.boglarka@pharm.u-szeged.hu (B.B.)
3 Dr. Derm Clinic of Anti-Aging Dermatology, Aesthetic Laser and Plastic Surgery, Budapest 1026, Hungary; E-Mail: g.varju@drderm.net
4 Department of Dermatology and Allergology, University of Szeged, Szeged 6720, Hungary; E-Mails: kl@mail.derma.szote.u-szeged.hu (L.K.); nemeth.istvan.balazs@med.u-szeged.hu (I.B.N.)
5 Department of Pathology, "Iuliu Hatieganu" University of Medicine and Pharmacy, 400006 Cluj-Napoca, Romania; E-Mail: cioca_andre@yahoo.com
6 Department of Anatomy, Physiology and Pathophysiology, "Victor Babes" University of Medicine and Pharmacy, 300041 Timisoara, Romania; E-Mail: alexandra.petrus@umft.ro
7 Department of Toxicology, "Victor Babes" University of Medicine and Pharmacy, 300041 Timisoara, Romania; E-Mail: cadehelean@umft.ro
8 Department of Obstetrics and Gynecology, "Victor Babes" University of Medicine and Pharmacy, 300041 Timisoara, Romania; E-Mail: citu.ioan@umft.ro
9 Department of Rehabilitation, Physical Medicine and Rheumatology, "Victor Babes" University of Medicine and Pharmacy, 300041 Timisoara, Romania
10 Department of Pharmacognosy, Western University "Vasile Goldis", 310025 Arad, Romania; E-Mail: claudiatoma2004@yahoo.com

* Authors to whom correspondence should be addressed; E-Mails: corina.danciu@umft.ro (C.D.); ama.elena@gmail.com (E.A.); Tel.: +40-744-648-855 (C.D.); +40-749-278-434 (E.A.).

Academic Editor: Andrzej Slominski

Received: 5 March 2015 / Accepted: 25 June 2015 / Published: 8 July 2015

Abstract: A lamellar lyotropic liquid crystal genistein-based formulation (LLC-Gen) was prepared in order to increase the aqueous solubility of the lipophilic phytocompound genistein. The formulation was applied locally, in a murine model of melanoma, with or without electroporation. The results demonstrated that, when the formulation was applied by electroporation, the tumors appeared later. During the 21 days of the experiment, the LLC-Gen formulation decreased the tumor volume, the amount of melanin and the degree of erythema, but when electroporation was applied, all these parameters indicated a better prognosis even (lower tumor volume, amount of melanin and degree of erythema). Although hematoxylin–eosin (HE) staining confirmed the above events, application of the LLC-Gen formulation by electroporation did not lead to a significant effect in terms of the serum concentrations of the protein S100B and serum neuron specific enolase (NSE), or the tissue expression of the platelet-derived growth factor receptor β (PDGFRβ) antibody.

Keywords: genistein; lyotropic liquid crystals; electroporation; murine melanoma

1. Introduction

The most recent statistics regarding new melanoma cases in Europe show that an average of 47.2 males and 53.1 females per 100,000 investigated subjects were diagnosed with melanoma in 2012 [1]. The incidence varies within the countries of the European Union, with very high rates registered in Switzerland, Denmark, and Norway as compared with Greece, Bulgaria, Cyprus and Romania [2,3]. Melanin pigmentation in mammalian skin is under complex regulatory control by several pathways triggered by receptor-dependent and -independent mechanisms, hormonal, auto-, para-, or intracrine manner [4]. As the incidence of melanoma is increasing worldwide, researchers are investing considerable amounts of time and money in the search for an effective treatment for this dangerous disease [5–7]. However there is no reliable therapy for metastatic melanoma despite the progress made in the field [8].

Natural compounds, and especially plant secondary metabolites, have been studied for centuries for their complex therapeutic benefits [9]. Different types of cancer have revealed positive responses to certain natural compounds both *in vitro* and *in vivo*. Genistein (Gen) is a naturally occurring compound in the class of isoflavonoids. It is well known for its estrogeno-mimetic properties [10]. It has been intensively studied in cases of breast and prostate cancer [11,12]. Its efficacy has been shown in malignant melanoma. In an earlier study we observed that Gen decreases the tumor size, the metastasis potential and the level of melanization in a B16 mouse model of melanoma. However, the recovery of the skin lesions was impaired [13]. Those data led us to propose another approach to promote the recovery of murine melanoma lesions: electroporation of a lyotropic liquid crystal Gen-based formulation (LLC-Gen).

Lyotropic liquid crystal systems (LLC) have recently received increased attention in both the cosmetic and pharmaceutical fields [14]. They flow like liquids (hence the name liquid crystals) and in

part maintain the ordered structure of crystalline solids [15]. The advantageous qualities of such formulations include their amphiphilic nature, the similarity to colloidal systems existing in living organisms, the various structures of liquid crystal states, and their thermodynamic stability [16]. Gen is a lipophilic compound that is practically insoluble in water, which can be a real problem in terms of formulation and bioavailability. LLCs display good solubilizing effects, sustained release and enhanced bioavailability of other lipophilic drugs [17].

We decided to attempt a new approach by applying this new LLC-Gen formulation locally with or without electroporation, a process characterized by structural changes in the cell membrane barrier and resulting reversible increase in transmembrane transport; practically, aqueous pores are created in lipid bilayers. These transitory changes, possible due to the application of high-voltage pulses, can be used to load different molecules into the cells [18,19]. Primarily designed for gene transfer, electroporation is nowadays used for a wide range of structures, such as antibodies, oligonucleotides, DNA, ions, drugs, *etc.* [20].

Thus, the aims of this study were to investigate whether lamellar LLC systems form a good base for Gen incorporation, and to analyze the effects of electroporation with such a formulation in a murine model of melanoma.

2. Results and Discussion

2.1. Polarization Microscopic Examinations

In the development of the dermal delivery, we prepared a LLC formulation that is able to suspend Gen at a concentration of 3%.

Figure 1 presents a polarized microscopic picture of the developed LLC structure, revealing a lamellar LLC pattern with a characteristic ribbon structure in polarized light.

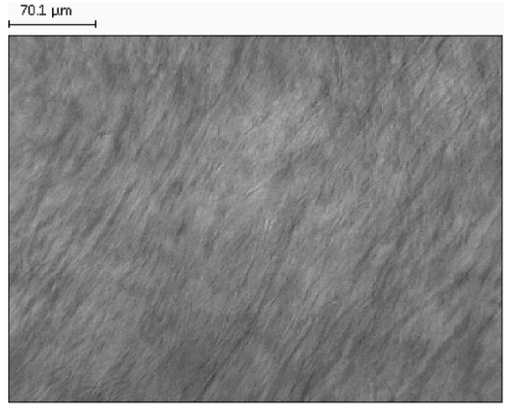

Figure 1. Polarizing microscopic examination of blank lyotropic liquid crystal systems (LLC) at a magnification of 20×.

2.2. Rheological Investigations

The characteristics of the LLC system include the frequency-dependent storage and loss moduli. In the investigated frequency range, the blank LLC system is more elastic than viscous. The solubilization of Gen in the LLC system led to a consistency increase (Figure 2).

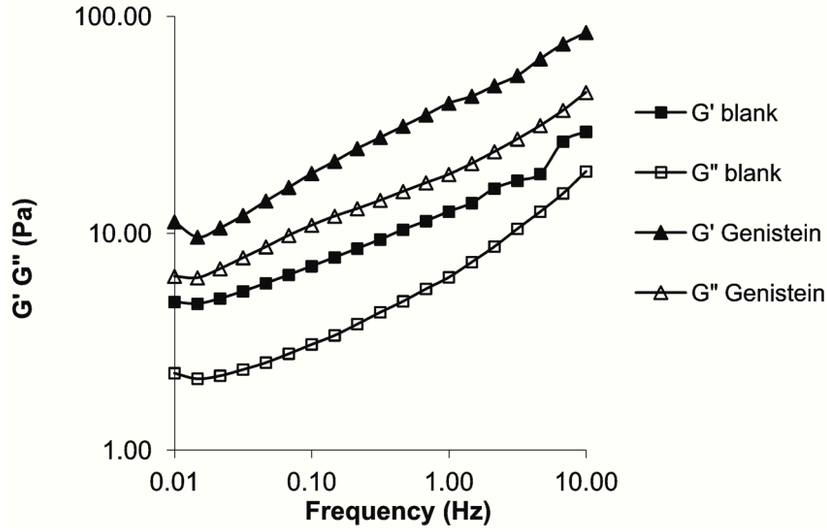

Figure 2. Rheological characterization of the blank and Genistein (Gen)-containing LLC formulations.

Melanoma was induced and the formulation was applied as indicated in the Experimental Section. In each of the inoculated mice, the volume of the tumor was observed to be increased, to an extent directly proportional to the number of days of the examination. Tumors appeared on day eight post-inoculation in both the treated and the untreated groups, with the exception of the mice in group F; in these mice, which were inoculated with B164A5 cells and treated with LLCs containing 3% Gen and electroporated for 6 min at high-voltage, the tumors appeared on day 10 post-inoculation. The mean tumor volume in group F was 83.33 ± 28.86 mm^3, in contrast with 466.66 ± 208.16 mm^3 in group B, 589.78 ± 204.67 mm^3 in group C, 309.00 ± 207.81 mm^3 in group D and 603.23 ± 264.57 mm^3 in group E. Comparison of the curves corresponding to the different treatment approaches reveals that the LLC-Gen formulation decreased the tumor volume, but following electroporation of this formulation, the results were even better. On day 21 of the experiment, the tumor volumes were 1001.58 ± 409.26 mm^3 in group B, 1000.86 ± 404.96 mm^3 in group C, 866.66 ± 256.58 mm^3 in group D, 999.87 ± 408.95 mm^3 in group E and 751.00 ± 151.03 mm^3 in group F. Significant results ($p < 0.05$) between the different experimental groups were found as shown in Figure 3.

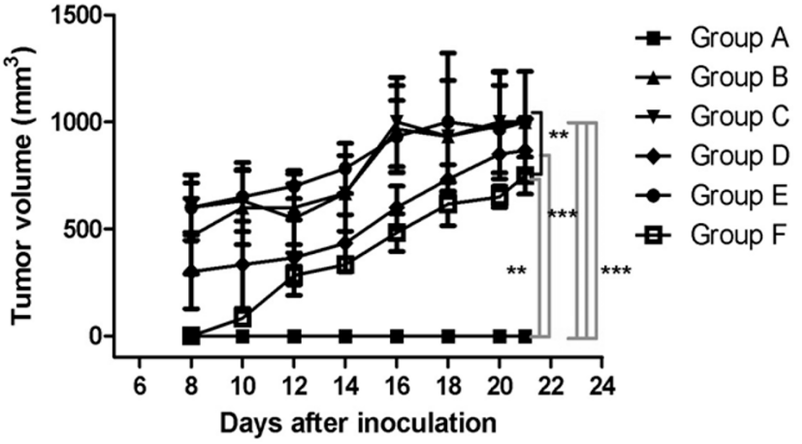

Figure 3. Tumor volumes (mm^3) in the different experimental groups on day 21 of the experiment. ** $p < 0.01$, *** $p < 0.001$.

During the 21 days of the experiment, noninvasive measurements of relative melanin pigmentation and the degree of erythema were performed every two days with the Courage-Khazaka Mexameter® MX 18 Multiprobe Adapter System (MPA5). Curves corresponding to relative melanin pigmentation were plotted and differences relative to the blank group A were recorded starting from day five post-inoculation. The normal amount of melanin in the skin of the C57BL6J mouse varies in the interval 635–670 arbitrary units (A.U.). On day five post-inoculation, the interval increased to 695–720 A.U. Differences between the experimental groups in the amount of relative melanin pigmentation were observed on day 9: 645 ± 14 A.U. in group A, 789 ± 60 A.U. in group B, 788 ± 19 A.U. in group C, 752 ± 5 A.U. in group D, 782 ± 12 A.U. in group E and 735 ± 28 A.U. in group F. The curves presented in Figure 4 show that application of the LLC-Gen formulation to the skin resulted in a slight decrease in the amount of melanin, but when the formulation was applied by electroporation the level of pathological melanin was reduced significantly. On day 21 of the experiment, the results were 650 ± 13 A.U. in group A, 901 ± 21 A.U. in group B, 909 ± 17 A.U. in group C, 851 ± 28 A.U. in group D, 879 ± 45 A.U. in group E and 826 ± 36 A.U. in group F. Significant differences ($p < 0.05$) between the different experimental groups were found as shown in Figure 4.

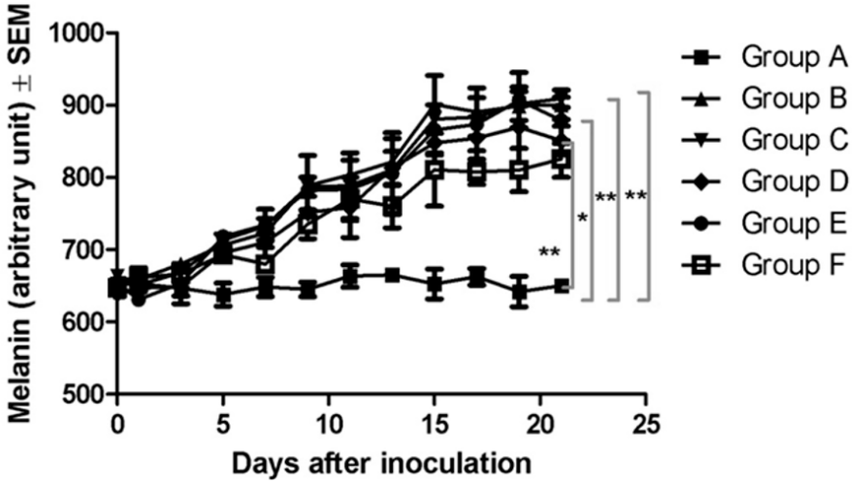

Figure 4. Melanin amounts (in arbitrary units (A.U.) as determined by the manufactured device) in the different experimental groups on day 21 of the experiment. * $p < 0.05$, ** $p < 0.01$.

The MX18 device was also employed to determine the degree of erythema after the appearance of the tumors and to observe any changes that occurred after treatment. The normal values for the skin of the C57BL6J mouse are in the range 50–60 A.U. Increased levels, corresponding to erythema, were observed from day nine post-inoculation. The recorded levels on day nine were 58 ± 2 A.U. in group A, 218 ± 26 A.U. in group B, 210 ± 16 A.U. in group C, 192 ± 28 A.U. in group D, 214 ± 21 A.U. in group E and 161 ± 23 A.U. in group F. The LLC-Gen formulation proved to diminish the degree of erythema slightly, but when electroporation was applied the LLC-Gen formulation acted more effectively. On day 21 of the experiment, the levels were 59 ± 3 A.U. in group A, 228 ± 14 A.U. in group B, 215 ± 4 A.U. in group C, 183 ± 14 A.U. in group D, 228 ± 3 A.U. in group E and 152 ± 9 A.U. in group F. Significant results ($p < 0.05$) between the different experimental groups were found as shown in Figure 5.

On day 21 of the experiment, blood was collected from the mice in all groups and the serum concentrations of the protein S100B (μg/L) (a highly specific melanoma marker) and of neuron specific enolase (NSE) (ng/L) were determined. The mean concentrations of S100B in the different experimental groups were 0.55 ± 0.35 μg/L in group A, 0.96 ± 0.18 μg/L in group B, 0.86 ± 0.56 μg/L in group C, 0.510 ± 0.36 μg/L in group D, 0.690 ± 0.28 μg/L in group E and 0.54 ± 0.28 μg/L in group F. Higher values than the control were observed in the groups inoculated with melanoma cells. Although the mean values were slightly lower when electroporation was applied, the LLC-Gen formulation did not have a significant effect on the serum S100B concentration (Figure 6). The mean concentrations of NSE in the different experimental groups were 4.0 ± 1.4 ng/L in group A, 9.2 ± 3.0 ng/L in group B, 9.0 ± 5.1 ng/L in group C, 7.9 ± 5.6 ng/L in group D, 9.8 ± 8.3 ng/L in group E and 6.0 ± 2.8 ng/L in group F. Again, levels higher than the control were observed in the groups inoculated with melanoma cells. Although the mean NSE levels were slightly lower when electroporation was applied, the LLC-Gen formulation did not have a significant effect in reducing this marker either (Figure 7).

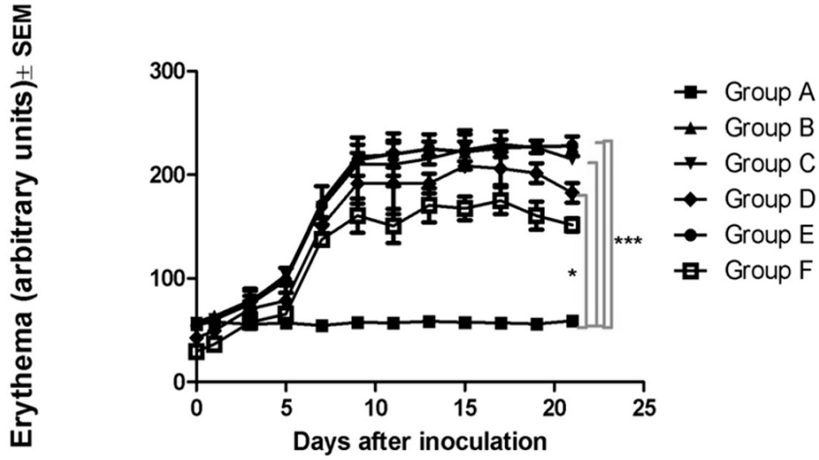

Figure 5. Erythema (in A.U. as determined by the manufactured device) in the different experimental groups on day 21 of the experiment. * $p < 0.05$, *** $p < 0.001$.

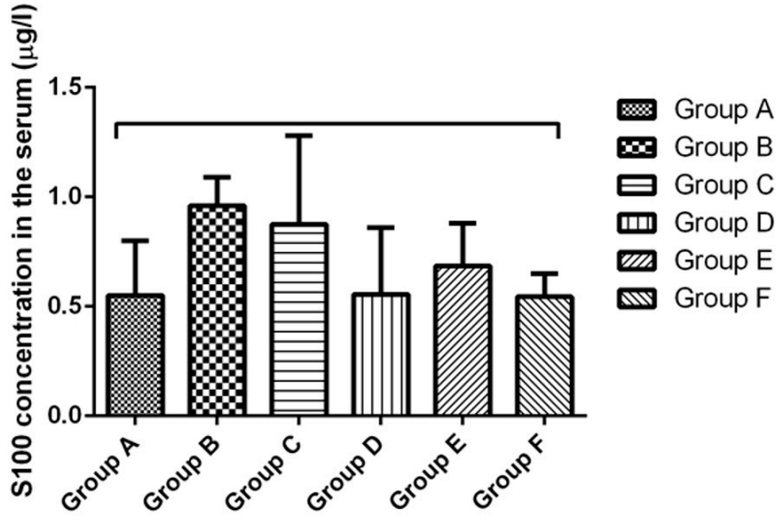

Figure 6. Serum concentrations of the protein S100B (μg/L) in the different experimental groups on day 21 of the experiment.

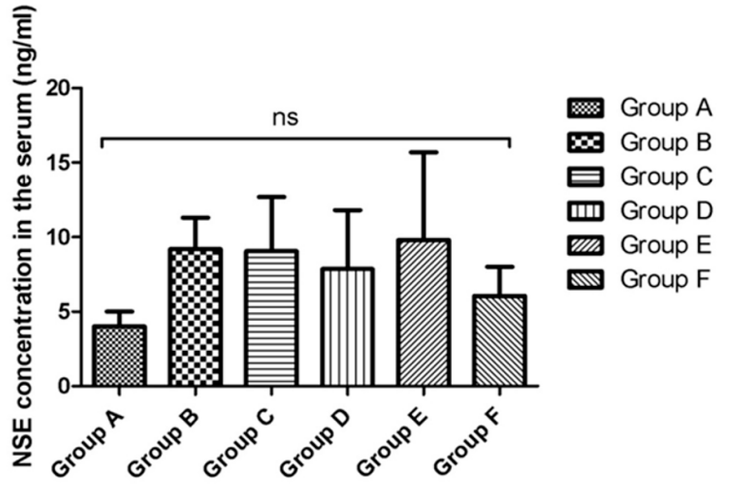

Figure 7. Serum neuron specific enolase (NSE) concentrations (ng/mL) in the different experimental groups on day 21 of the experiment. "ns" indicates not-significant.

2.3. Histological and Immunohistochemical Results

Conventional hematoxylin–eosin (HE) analysis revealed similar features in groups B and C, with moderate to intense pigmentation in almost all the tumor cells (Figure 8a,b). In group D, weak pigmentation was observed in isolated cells (Figure 8c). Group E was characterized by moderate pigmentation with intense pigmentation in a few nests of tumor melanocytes (Figure 8d). Group F exhibited similarities with group D, with a general feature of a lower level of pigmentation and with melanin present in a few tumor cells (Figure 8e).

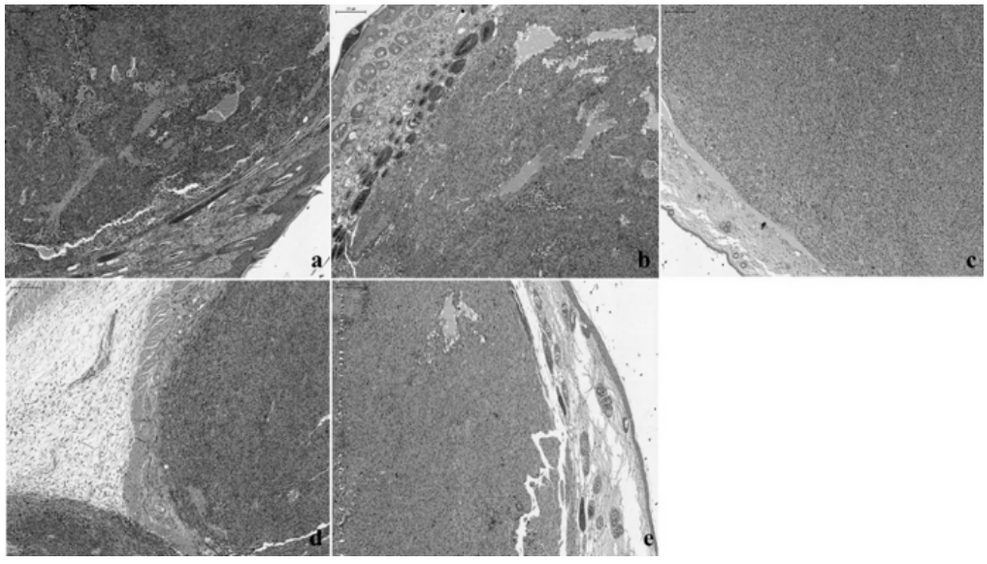

Figure 8. Hematoxylin–eosin (HE) staining in the different groups with skin melanoma: (**a**,**b**): groups B and C with moderate to intense pigmentation in almost all the tumor cells; (**c**): group D, exhibiting melanoma with weak and isolated pigment; (**d**): group E, displaying moderate pigmentation, with intense pigmentation in a few nests of tumor melanocytes; (**e**): group F, with the presence of melanin in isolated cells. Magnification: 40×; scale bar: 200 μm.

In the case of platelet-derived growth factor receptor β (PDGFRβ) immunostaining only a mild intratumoral reaction was seen in the peritumoral stromal myofibroblasts (Figure 9a,b) and in the tumor cells (Figure 9c), independently of the nature of the groups.

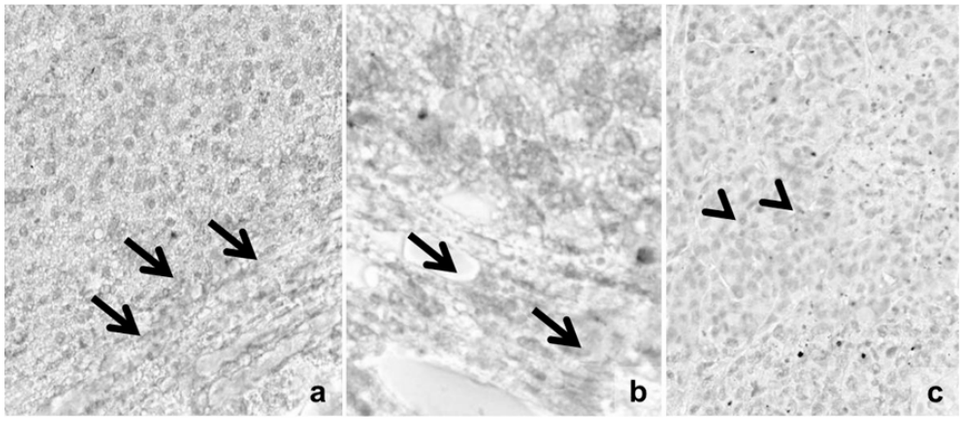

Figure 9. Representative pictures of platelet-derived growth factor receptor β (PDGFRβ)-immunostaining. Only a mild intratumoral reaction is seen in the peritumoral stromal myofibroblasts (**a**,**b**) and in the tumor cells (**c**), independently of the nature of the groups. Arrows and arrowheads highlight peritumoral stromal cells and intratumoral positive tumor cells, respectively. Dacarbazine red reaction; optical scanning microscopy—OM 200×.

2.4. Discussion

Polarization microscopy can be used for the examination and identification of the LLC system. The behavior of light in crystalline materials depends on its direction relative to the crystal structure. Unlike isotropic materials which are invisible between the crossed polarizers of a polarization microscope, a thin sample of LLC in the same experimental arrangement yields a typical picture (called texture) which shows the effective positional birefringence of the system [21].

Oscillating rheological measurements offer a convenient possibility for identification of the lamellar phase in dermal and transdermal drug delivery systems [22]. The viscoelastic properties are indicated by the changes in the elastic storage modulus (G′), and the viscous loss modulus (G″), as a function of frequency. The G′, which defines the energy stored per unit volume, is proportional to the elastic property of the sample, whereas the G″ is the energy dissipated per unit volume, proportional to the viscous component of the sample [23,24]. It is clear from Figure 2 that the blank LLC composition demonstrates more elastic than viscous behavior. The incorporation of Gen led to increases in G′ and G″, with maintenance of LLC state.

Gen has previously been described as a phytocompound active on melanoma, both on different cell lines *in vitro* and on various murine models *in vivo* [25–28]. An half maximal inhibitory concentration (IC_{50}) of 12.5 μM has been reported after seven days of incubation in the case of the B164A5 cell line for the induction of angiogenesis and the inhibition of solid tumors when the cell line was implanted in C57BL6J mice, at a rate of 30%–50% (depending on the mode of administration) [13,29,30]. The present study involves a new approach toward the recovery of murine melanoma lesions: electroporation of an LLC-Gen formulation. This approach combines a new local formulation and a new mode of

administration for Gen. To the best of our knowledge, the effect of the local administration of a Gen-based formulation on murine melanoma has not been reported previously. We chose this combination because LLCs have been intensively studied as carrier systems for lipophilic drugs with a view to increasing the dermal penetration [14,31,32], and because electroporation increases the cutaneous penetration of various active agents [33–35]. We used polarizing microscopy and rheological investigations to confirm that this system was a lamellar LLC.

Our first important observation was that the tumors appeared two days later in the mice treated with LLC with 3% Gen and electroporated for six minutes at high-voltage than in the untreated or the normally treated mice. The second important observation was that the locally applied formulation decreased the tumor volume to an extent proportional to the number of days of treatment, and when electroporation was applied, the effect was increased.

Experimental data suggest that the degree of skin pigmentation correlates directly with the amount of melanin [36]. However, the measurement of skin pigmentation is not a perfectly reliable method to determine the exact melanin content but it indicates the relative melanin pigmentation, as a prediction value [4,37]. The decrease in skin pigmentation can reflect with certain limitation the decrease of melanin content reflecting the inhibition of melanogenesis, as a secondary effect. Substantial evidence indicates that the inhibition of melanogenesis has a therapeutic effect [38–41]. The presence of melanin pigment or the presence of an active melanogenesis can alter the sensitivity and behavior of melanoma cells to chemoimmunotherapy [38,39], thus the inhibition of melanogenesis can represent a therapeutic target. Melanin measurement with the Mexameter MX18 in physiological or pathological cases, with or without treatment is a noninvasive method currently used in skin research [42–45]. The level of melanin in the mice treated with LLCs with 3% Gen and electroporated for 6 min at high-voltage was significantly decreased. The same held for the extent of erythema, a skin disorder that occurs with any skin lesion [13]. Melanoma is one of the most severe skin lesions [46].

After the noninvasive measurements, blood was collected in order to determine the concentrations in the different experimental groups of two melanoma markers: S100B and NSE. S100B is a 21-kDa protein that plays a role in preserving the cytoskeletal integrity, migration, cell cycle regulation and apoptosis [47]. Elevated S100B serum levels have been found in advanced stages of melanoma and have been associated with tumor progression and a shorter survival [48]. In contrast with S100B, NSE has been reported to be elevated in the early stages of melanoma [49]. Our results revealed decreased serum concentrations of both selected markers in mice treated with LLCs with 3% Gen and electroporated for 6 min at high-voltage as compared with the untreated mice, but the results were not statistically significant ($p > 0.05$).

The PDGFRs are members of a family of tyrosine kinase receptors found on the surface of cells. They regulate important processes such as cell differentiation, proliferation, growth and development [50]. There are two forms, encoded by different genes, PDGFRα and PDGFRβ [51]. PDGFRβ is normally present in cells of mesenchymal origin, e.g., vascular endothelial cells, fibroblasts, bone marrow cells and monocytes [52]. However, its expression is upregulated in the event of imbalances such as atherosclerosis, fibrosis and cancer [50]. B16 murine melanoma cells express PDGFRβ in the tumor microenvironment and the tumor stroma [53,54]. We therefore checked its expression after local Gen treatment with or without electroporation. The results showed that there was no marked difference in expression profile between the groups. Recent studies have shown that, in the case of the vascular smooth

muscle, isoflavone inhibits PDGF-stimulated proteoglycan synthesis without blocking PDGFRβ phosphorylation [55]. Additionally, Gen did not affect early signal transduction through PDGFRβ in primary cultured rat aortic smooth muscle cells [56]. We can now report that Gen did not affect the expression of PDGFR and PDGFRβ in B16 murine melanoma.

3. Experimental Section

3.1. Materials

Gen was from Extrasynthèse (Genay, France; purity > 95%), and the mouse adherent melanoma cell line B164A5 was purchased from the European Collection of Cell Cultures (ECACC) (Salisbury, UK). The cells were grown in Dulbecco's Modified Eagle's Medium (DMEM) supplemented with 10% heat-inactivated fetal calf serum (FCS), 1% non-essential amino acids and 1% penicillin-streptomycin in a humidified atmosphere containing 5% CO_2 at 37 °C. All cell culture media and supplements were from Life Technologies (Paisley, UK). In the preparation for injection, cells were trypsinized, counted with the aid of trypan blue, washed with PBS, resuspended at 1×10^6 cells/0.1 mL in saline solution and injected immediately, as described below.

3.2. Lamellar Lyotropic Liquid Crystal Genistein (LLC-Gen) Formulation

The lamellar LLC formulation was developed because this crystal structure demonstrates the greatest similarity to the lipid bilayer of the skin [57]. Three percent of Gen was incorporated as active agent. The carrier was a mixture of a non-ionic surfactant, Cremophor RH40 (Polyoxyl 40 Hydrogenated Castor Oil USP/NF), obtained from BASF (Ludwigshafen, Germany). It is tolerated well by tissues and has low toxicity, and its HLB (hydrophilic-lipophilic balance) value is 14–16. The aqueous phase of the systems was purified water (European Pharmacopoeia 6th Edition), while the oil phase was isopropyl myristate (Merck, Budapest, Hungary).

A Gen-free LLC was prepared by the following procedure. The oil-surfactant mixture (oil:surfactant ratio = 2:1) was homogenized with a magnetic stirrer at room temperature. Ten percent of water was then added in small amounts to this mixture during stirring. A similar composition was prepared by using Gen, and the 3% of Gen was incorporated in the oil-surfactant mixture with a magnetic stirrer.

3.3. Electroporation Parameters

The Mezoforte Duo Mez 120905-D was provided by the Derm Clinic of Anti-Aging Dermatology, Aesthetic Laser and Plastic Surgery (Budapest, Hungary). The device operates on the basis of a pulsed electromagnetic field. The polypropylene-covered treating handpiece contains a 25 mm diameter plate electrode. Modulation was achieved with 1800 V high-voltage pulses with a voltage pulse duration of 5 ms followed by a 20 ms break. The treatment time was 6 min.

3.4. Polarization Microscopic Examinations

The structures of the samples were examined with a polarization microscope (LEICA Q500 MC Image Analyzer System, Leica Microsystems GmbH, Wetzlar, Germany) at room temperature. The magnification was 20×.

3.5. Rheological Investigations

The rheological profiles of the samples were studied with a PaarPhysica MCR101 rheometer (Anton Paar GmbH, Graz, Austria). The measuring device was of plate-plate type (diameter 25 mm, gap distance 0.2 mm). The measurements were carried out at 25 °C. The linear viscoelastic range was determined in the first step by examining the complex modulus as a function of the shear stress at a given frequency (1 Hz). On the basis of these experiments, the shear stress was set at 1 Pa during the dynamic testing as this value was always within the linear viscoelastic range. The storage and loss moduli values were examined as a function of frequency (0.01–10 Hz).

3.6. Animal Studies

Animal studies were conducted on 7–8 week old C57BL/6J female mice with an average weight of 20–25 g, purchased from Charles River (Sulzfeld, Germany). The working protocol strictly followed all the National Institute of Animal Health (NIAH) regulations: animals were maintained under standard conditions throughout the experiments: a 12 h light-dark cycle, food and water *ad libitum*, temperature 24 °C and humidity >55%. The experiments were conducted in accordance with the rules of the Ethical Committee of University of Medicine and Pharmacy "Victor Babes" Timisoara, Romania no. 27.11.2014_ref.1.2015. The number of mice involved in the study was 30, divided equally into 6 groups of 5 animals as follows:

Group A: blank group;

Group B: mice inoculated with B164A5 cells and otherwise not treated;

Group C: mice inoculated with B164A5 cells and treated with LLCs without Gen;

Group D: mice inoculated with B164A5 cells and treated with LLCs with 3% Gen;

Group E: mice inoculated with B164A5 cells and treated with LLCs without Gen and electroporated at high-voltage for 6 min with a Mezoforte Duo Mez 120905-D;

Group F: mice inoculated with B164A5 cells and treated with LLCs with 3% Gen and electroporated at high-voltage for 6 min with a Mezoforte Duo Mez 120905-D.

On day 0 of the experiment, the mice in groups B–F received a subcutaneous (s.c.) inoculation of 0.1 mL containing 1×10^6 cells/mouse into the depilated lateral abdomen. For the mice in groups C–F treatment with 2 mL of a 3% Gen-LLC formulation was administered from day 2 post-inoculation, using 6 min of high-voltage electroporation (Mezoforte Duo Mez 120905-D) or the classical application as described above. The mice were inspected daily for the development of tumors or other changes. Tumor growth was measured daily in millimeters, using calipers, and the tumor volume was estimated by the formula: length × width^2/2. On day 21 post-inoculation, after the last measurements had been made, the mice were anesthetized with gaseous isoflurane. Blood was collected from the cava vein, and the

concentrations of the melanoma-specific markers S100B and NSE (neuron specific enolase) were investigated. The mice were subsequently euthanized by cervical dislocation. Tumors were collected, measured and weighed, and histological and immunohistochemical analyses were performed.

3.7. Noninvasive Skin Measurements

All the measurements on the skin of the mice were carried out with a Multiprobe Adapter System (MPA5) from Courage-Khazaka, Köln, Germany: the measurements of pigmentation and erythema with the Mexameter® MX 18 from Courage-Khazaka, Köln, Germany furnish quantitative information relating to the relative melanin pigmentation and erythema (hemoglobin) subject to modifications by tumor evolution with or without treatment.

The measurements were made on four regions of the skin located near the tumor, and the mean and standard deviation were calculated. The amounts of melanin and erythema were measured at the baseline (day 0) and then every two days until day 21 of the experiment. The measurement areas were 5 mm in diameter.

3.8. Determination of Neuron Specific Enolase (NSE) and S100 Calcium Binding Protein B (S100B) in the Blood

The mice were anesthetized with isoflurane, and blood was collected from the posterior vena cava and by cardiac puncture and inserted into a serum separator tub. Samples were allowed to clot overnight at 4 °C before centrifugation at approximately 1000× *g* for 20 min. The enzyme-linked immunosorbent assay kits for S100 calcium binding protein B (S100B) and neuron specific enolase (NSE) were from Cloud Clone Corp. (Houston, TX, USA). The manufacturer's protocol was used to determine the S100B and NSE concentrations in the mouse serum. All kit components and samples were brought to room temperature (18–25 °C) before use.

3.9. Histology

For histological analysis, tissue samples (skin) were fixed in 4% buffered formaldehyde solution and embedded into paraffin. For standardized evaluation, each sample was organized into a tissue microarray (TMA) block. Sections of 4 um from the TMA blocks were deparaffinized, stained with hematoxylin-eosin (HE) by a Leica Autostainer, Medist, Bucharest, Romania and analyzed microscopically. Samples were visualized and archived by computerized scanning microscopy (3D Histech Ltd., Budapest, Hungary).

3.10. Immunohistochemistry

Sections of 4 μm from the TMA blocks were used for immunohistochemistry. Rabbit antibody of PDGFRβ (polyclonal; Sigma-Aldrich Co., St. Louis, MI, USA) was applied in a dilution of 1:2000. Antigen retrieval was performed according to the datasheets of the antibody. Visualization was carried out with an autostainer with the Leica Bond kit. Sections were counterstained with conventional hematoxylin and gently coverslipped. Evaluation was based on the brown colorimetric discoloration of the

samples. For intensity assessment, optical densitometry was performed with Image Pro Plus software, Media Cybernetics, Rockville, MD, USA.

3.11. Statistics

Results are presented as means ± SD. One-way ANOVA followed by the Bonferroni test was used to determine the statistical differences between the various experimental and control groups; *, ** and *** indicate $p < 0.05$, $p < 0.01$ and $p < 0.001$. "ns" indicates not-significant.

4. Conclusions

We conclude that LLCs serve as a good formulation for the local delivery of genistein. Further studies will be conducted with higher concentrations of this active agent. Electroporation proved to be a good method for the delivery of the new formulation because it delayed the appearance of the tumors, and decreased the tumor volume, the amount of melanin and the degree of erythema. HE staining confirmed the above events, but this approach did not have a significant effect in terms of the serum concentrations of S100B and NSE, or the tissue expression of the PDGFRβ antibody.

Acknowledgments

We wish to thank the Derm Clinic of Anti-Aging Dermatology, Aesthetic Laser and Plastic Surgery for providing the Mezoforte Duo Mez 120905-D device. This study was financed by the European Social Fund, Human Resources Development Operational Programme 2007–2013, project No. POSDRU/159/1.5/S/136893, awarded to Corina Danciu.

Author Contributions

Corina Danciu, Cristina Dehelean and Lajos Kemény conceived and designed the experiments, Boglárka Balázs, Alexandra Petruş, István Balázs Németh and Citu Ioan Cosmin performed the experiments; Szilvia Berkó and Andreea Cioca analyzed the data; Gábor Varju and Elena Amaricai contributed to the reagents/materials/analysis tools; and Corina Danciu and Claudia Crina Toma wrote the paper.

Conflicts of Interest

The authors declare no conflict of interest.

References

1. Ferlay, J.; Steliarova-Foucher, E.; Lortet-Tieulent, J.; Rosso, S.; Coebergh, J.W.W.; Comber, H.; Forman, D.; Bray, F. Cancer incidence and mortality patterns in Europe: Estimates for 40 countries in 2012. *Eur. J. Cancer* **2013**, *49*, 1374–1403.
2. Forsea, A.M.; del Marmol, V.; de Vries, E.; Bailey, E.E.; Geller, A.C. Melanoma incidence and mortality in Europe: New estimates, persistent disparities. *Br. J. Dermatol.* **2012**, *167*, 1124–1130.

3. Ferlay, J.; Shin, H.; Bray, F.; Forman, D.; Mathers, C.; Parkin D.M. Estimates of worldwide burden of cancer in 2008: GLOBOCAN 2008. *Int. J. Cancer* **2010**, *127*, 2893–2917.
4. Slominski, A; Tobin, D.J.; Shibahara, S.; Wortsman, J. Melanin pigmentation in mammalian skin and its hormonal regulation. *Physiol. Rev.* **2004**, *84*, 1155–1228.
5. Erdei, E.; Torres, S.M. A new understanding in the epidemiology of melanoma. *Expert Rev. Anticancer Ther.* **2010**, *10*, 1811–1823.
6. Godar, D.E. Worldwide increasing incidences of cutaneous malignant melanoma. *J. Skin Cancer* **2011**, *2011*, 858425.
7. De Giorgi, V.; Gori, A.; Grazzini, M.; Rossari, S.; Oranges, T.; Longo, A.S.; Lotti, T.; Gandini, S. Epidemiology of melanoma: Is it still epidemic? What is the role of the sun, sunbeds, Vit D, betablocks, and others? *Dermatol. Ther.* **2012**, *25*, 392–396.
8. Slominski, A.T. Carlson, J.A. Melanoma resistance: A bright future for academicians and a challenge for patient advocates. *Mayo Clin. Proc.* **2014**, *89*, 429–433.
9. Ji, H.F.; Li, X.J.; Zhang, H.Y. Natural products and drug discovery. Can thousands of years of ancient medical knowledge lead us to new and powerful drug combinations in the fight against cancer and dementia? *EMBO Rep.* **2009**, *10*, 194–200.
10. Dweck, A.C. Isoflavones, phytohormones and phytosterols. *J. Appl. Cosmetol.* **2006**, *24*, 17–32.
11. Lamartiniere, C.A. Protection against breast cancer with genistein: A component of soy. *Am. J. Clin. Nutr.* **2000**, *71*, 1705–1707.
12. Perabo, F.G.E.; von Löw, E.C.; Ellinger, J.; von Rücker, A.; Müller, S.C.; Bastian, P.J. Soy isoflavonegenistein in prevention and treatment of prostate cancer. *Prostate Cancer Prostatic Dis.* **2007**, *11*, 6–12.
13. Danciu, C.; Borcan, F.; Bojin, F.; Zupko, I.; Dehelean, C. Effect of the isoflavonegenistein on tumor size, metastasis potential and melanization in a B16 mouse model of murine melanoma. *Nat. Prod. Commun.* **2013**, *8*, 343–346.
14. Guo, C.; Wang, J.; Cao, F.; Lee, R.J.; Zhai, G. Lyotropic liquid crystal systems in drug delivery. *Drug Discov. Today* **2010**, *15*, 1032–1040.
15. Tadwee, I.; Shahi, S.; Ramteke, V.; Syed, I. Liquid crystals pharmaceutical application: A review. *Int. J. Pharm. Res. Sci.* **2012**, *1*, 6–11.
16. Makai, M.; Csányi, E.; Németh, Z.; Pálinkás, J.; Erős, I. Structure and drug release of lamellar liquid crystals containing glycerol. *Int. J. Pharm.* **2003**, *256*, 95–107.
17. Boyd, B.J.; Whittaker, D.V.; Khoo, S.M.; Davey, G. Lyotropic liquid crystalline phases formed from glycerate surfactants as sustained release drug delivery systems. *Int. J. Pharm.* **2006**, *309*, 218–226.
18. Denet, A.R.; Vanbever, R.; Préat, V. Skin electroporation for transdermal and topical delivery. *Adv. Drug Deliv. Rev.* **2004**, *56*, 659–674.
19. Prausnitz, M.R.; Bose, V.G.; Langer, R.; Weaver, J.C. Electroporation of mammalian skin: A mechanism to enhance transdermal drug delivery. *Proc. Natl. Acad. Sci. USA* **1993**, *90*, 10504–10508.
20. Gehl, J. Electroporation: Theory and methods, perspectives for drug delivery, gene therapy and research. *Acta Physiol. Scand.* **2003**, *177*, 437–447.

21. Stegemeyer, H. *LyotropeFlüssigkristalle: Grundlagen, Entwicklung, Anwendung*; Springer DE: Darmstadt, Germany, 1999; p. 200.
22. Németh, Z.; Halász, L.; Pálinkás, J.; Bóta, A.; Horányi, T. Rheological behaviour of a lamellar liquid crystalline surfactant–water system. *Colloids Surf. A* **1998**, *145*, 107–119.
23. Laba, D. *Rheological Properties of Cosmetics and Toiletries*; CRC Press: New York, NY, USA, 1993.
24. Schramm, G.A. *A Practical Approach to Rheology and Rheometry*; Haake: Karlsruhe, Germany, 1994.
25. Ji, C.; Yang, Y.L.; He, L.; Gu, B.; Xia, J.P.; Sun, W.L.; Su, Z.L.; Chen, B.; Bi, Z.G. Increasing ceramides sensitizes genistein-induced melanoma cell apoptosis and growth inhibition. *Biochem. Biophys. Res. Commun.* **2012**, *421*, 462–467.
26. Sun, Q.; Cong, R.; Yan, H.; Gu, H.; Zeng, Y.; Liu, N.; Chen, J.; Wang, B. Genistein inhibits growth of human uveal melanoma cells and affects microRNA-27a and target gene expression. *Oncol. Rep.* **2009**, *22*, 563–567.
27. Wang, H.; Zhu, Y.; Li, C.; Xie, L.; Chen, G.; Nie, Y. Effects of genistein on cell cycle and apoptosis of two murine melanoma cell lines. *Tsinghua Sci. Technol.* **2007**, *12*, 372–380.
28. Cong, R.; Sun, Q.; Yang, L.; Gu, H.; Zeng, Y.; Wang, B. Effect of genistein on vasculogenic mimicry formation by human uveal melanoma cells. *J. Exp. Clin. Cancer Res.* **2009**, *28*, 124, doi:10.1186/1756-9966-28-124.
29. Record, I.R.; Broadbent, J.L.; King, R.A.; Dreosti, I.E.; Head, R.J.; Tonkin, A.L. Genistein inhibits growth of B16 melanoma cells *in vivo* and *in vitro* and promotes differentiation *in vitro*. *Int. J. Cancer* **1997**, *72*, 860–864.
30. Farina, H.G.; Pomies, M.; Alonso, D.F.; Gomez, D.E. Antitumor and antiangiogenic activity of soy isoflavonegenistein in mouse models of melanoma and breast cancer. *Oncol. Rep.* **2006**, *16*, 885–891.
31. Chorilli, M.; Prestes, P.S.; Rigon, R.B.; Leonardi, G.R.; Chiavacci, L.A.; Sarmento, V.H.V.; Oliveira, A.G.; Scarpa, M.V. Structural characterization and *in vivo* evaluation of retinylpalmitate in non-ionic lamellar liquid crystalline system. *Colloids Surf. B Biointerfaces* **2011**, *85*, 182–188.
32. Attama, A.A.; Momoh, M.A.; Builders, P.F. Lipid nanoparticulate drug delivery systems: A revolution in dosage form design and development. In *Recent Advances in Novel Drug Carrier Systems*; Sezer, A.D., Ed.; InTech: Rijeka, Croatia, 2012.
33. Nino, M.; Calabrò, G.; Santoianni, P. Topical delivery of active principles: The field of dermatological research. *Dermatol. Online J.* **2010**, *16*, 4.
34. Essa, E.A.; Bonner, M.C.; Barry, B.W. Electroporation and ultradeformable liposomes; human skin barrier repair by phospholipid. *J. Control. Release* **2003**, *92*, 163–172.
35. Escobar-Chávez, J.J. *Current Technologies to Increase the Transdermal Delivery of Drugs*; Bentham Science Publishers: Valencia, Spain, 2010.
36. Yamashita, T.; Kuwahara, T.; González, S.; Takahashi, M. Non-invasive visualization of melanin and melanocytes by reflectance-mode confocal microscopy. *J. Investig. Dermatol.* **2005**, *124*, 235–240.
37. Slominski, A.; Zmijewski, M.A.; Pawelek, J. L-tyrosine and L-dihydroxyphenylalanine as hormone-like regulators of melanocyte functions. *Pigment Cell Melanoma Res.* **2012**, *25*, 14–27.
38. Slominski, A.; Blazej, Z.; Slominski, R. Inhibitors of melanogenesis increase toxicity of cyclophosphamide and lymphocytes agains melanoma cells. *Int. J. Cancer* **2009**, *124*, 1470–1477.

39. Anna, A.; Brożyna, A.; Jóźwicki, W.; Carlson, A.; Slominski, A. Melanogenesis affects overall and disease-free survival in patients with stage III and IV melanoma. *Hum. Pathol.* **2013**, *44*, 2071–2074.
40. Slominski, A.; Kim, T.K.; Brożyna, A.A.; Janjetovic, Z.; Brooks, D.L.; Schwab, L.P.; Skobowiat, C.; Jóźwicki, W.; Seagroves, T.N. The role of melanogenesis in regulation of melanoma behavior: Melanogenesis leads to stimulation of HIF-1α expression and HIF-dependent attendant pathways. *Arch. Biochem. Biophys.* **2014**, *563*, 79–93.
41. Slominski, R.; Zmijewski, M.; Slominsk, A. The role of melanin pigment in melanoma. *Exp. Dermatol.* **2015**, *24*, 258–259.
42. Hoshino, T.; Matsuda, M.; Yamashita, Y.; Takehara, M.; Fukuya, M.; Mineda, K.; Maji, D.; Ihn, H.; Adachi, H.; Sobue, G.; *et al.* Suppression of melanin production by expression of HSP70. *J. Biol. Chem.* **2010**, *285*, 13254–13263.
43. Matts, P.J.; Dykes, P.J.; Marks, R. The distribution of melanin in skin determined *in vivo*. *Br. J. Dermatol.* **2007**, *156*, 620–628.
44. Park, E.S.; Na, J.I.; Kim, S.O.; Huh, C.H.; Youn, S.W.; Park, K.C. Application of a pigment measuring device—Mexameter—For the differential diagnosis of vitiligo and nevus depigmentosus. *Skin Res. Technol.* **2006**, *12*, 298–302.
45. Baquié, M.; Kasraee, B. Discrimination between cutaneous pigmentation and erythema: Comparison of the skin colorimeters Dermacatch and Mexameter. *Skin Res. Technol.* **2013**, *20*, 218–227.
46. Garbe, C.; Eigentler, T.K.; Keilholz, U.; Hauschild, A.; Kirkwood, J.M. Systematic review of medical treatment in melanoma: Current status and future prospects. *Oncologist* **2011**, *16*, 5–24.
47. Kruijff, S.; Bastiaannet, E.; Kobold, A.C. S-100B concentrations predict disease-free survival in stage III melanoma patients. *Ann. Surg. Oncol.* **2009**, *16*, 3455–3462.
48. Weinstein, D.; Leininger, J.; Hamby, C.; Safai, B. Diagnostic and prognostic biomarkers in melanoma. *J. Clin. Aesthet. Dermatol.* **2014**, *7*, 13–24.
49. Tofani, A.; Cioffi, RP.; Sciuto, R.; Rea, S.; Festa, A.; di Filippo, F.; Cavaliere, R.; Maini, C.L. S-100 and NSE as serum markers in melanoma. *Acta Oncol.* **1997**, *36*, 761–764.
50. Andrae, J.; Gallini, R.; Betsholtz, C. Role of platelet-derived growth factors in physiology and medicine. *Genes Dev.* **2008**, *22*, 1276–1312.
51. Demoulin, J.B.; Montano-Almendras, C.P. Platelet-derived growth factors and their receptors in normal and malignant hematopoiesis. *Am. J. Blood Res.* **2012**, *2*, 44–56.
52. Board, R.; Jayson, G.C. Platelet-derived growth factor receptor (PDGFR): A target for anticancer therapeutics. *Drug Resist. Updates* **2005**, *8*, 75–83.
53. Furuhashi, M.; Sjöblom, T.; Abramsson, A.; Ellingsen, J.; Micke, P.; Li, H.; Bergsten-Folestad, E.; Eriksson, U.; Heuchel, R.; Betsholtz, C.; *et al.* Platelet-derived growth factor production by B16 melanoma cells leads to increased pericyte abundance in tumors and an associated increase in tumor growth rate. *Cancer Res.* **2004**, *64*, 2725–2733.
54. Raica, M.; Cimpean, A.M. Platelet-derived growth factor (PDGF)/PDGF receptors (PDGFR) axis as target for antitumor and antiangiogenic therapy. *Pharmaceuticals* **2010**, *3*, 572–599.

55. Little, P.J.; Getachew, R.; Rezaei, H.B.; Sanchez-Guerrero, E.; Khachigian, L.M.; Wang, H.; Liao, S.; Zheng, W.; Ballinger, M.L.; Osman, N. Genistein inhibits PDGF-stimulated proteoglycan synthesis in vascular smooth muscle without blocking PDGFβ receptor phosphorylation. *Arch. Biochem. Biophys.* **2012**, *525*, 25–31.
56. Yu, J.Y.; Lee, J.; Lim, Y.; Kim, T.J.; Jin, Y.R.; Sheen, Y.Y.; Yun, Y.P. Genistein inhibits rat aortic smooth muscle cell proliferation through the induction of p27kip1. *J. Pharmacol. Sci.* **2008**, *107*, 90–98.
57. Vicentini, F.; Casagrande, R.; Georgetti, S.R.; Bentley, V.; Fonseca, M. Influence of vehicle on antioxidant activity of quercetin: A liquid crystalline formulation. *Lat. Am. J. Pharm.* **2007**, *26*, 805–810

IV.

TS110388 – 28.7.15 dk/stm köthen

Boglárka Balázs[1,2], Eszter Csizmazia[2], Szilvia Berkó[1], Mária Budai-Szűcs[1], Piroska Szabó-Révész[1] and Erzsébet Csányi[1]

New Approach of Sucrose Myristate as a Promising Penetration Enhancer in Dermal Preparations

The aim of this work was to compare the penetration enhancer effect of newly developed sucrose myristate with the generally used sucrose laurate. Hydrogel formulations containing sucrose esters (SEs) were prepared and the model drug was Ibuprofen (IBU), which has oral side effects, so applying it in a transdermal system could be useful. We evaluated the effect of SE hydrogel formulations on the skin by the noninvasive *in vivo* test and examined their concentration dependent influence on the penetration of IBU through synthetic membrane (*in vitro*) by the Franz cell method. The results indicated that sucrose myristate incorporated into hydrogel moistures the skin well and lastingly and showed a better drug penetration enhancing effect at a much lower concentration compared to sucrose laurate. Our results revealed that sucrose myristate could be a promising and effective penetration enhancer in the pharmaceutical field.

Key words: Sucrose esters, penetration enhancers, dermal dosage form, skin hydration, in vitro drug diffusion

Saccharosemyristinsäureester als ein vielversprechender Penetrationsverstärker in dermalen Zubereitungen – Ein neuer Ansatz. Ziel dieser Arbeit ist, den penetrationsverstärkenden Effekt eines kürzlich entwickelten Saccharosemyristinsäureesters mit dem des üblicherweise eingesetzten Saccharoselaurinsäuresters zu vergleichen. Hydrogelfomulierungen mit den Saccharoseestern (ESs) wurden präpariert. Ibuprofen (IBU) wurde als Modellwirkstoff eingesetzt. Wegen seiner oralen Nebenwirkungen könnte sein Einsatz in transdermalen Systemen sinnvoll sein. Wir bestimmten den Einfluss von SE-haltigen Hydrogelen auf die Haut mittels nichtinvasiven *in-vivo*-Tests und untersuchten ihren konzentrationsabhängigen Einfluss auf die Penetration von IBU durch eine synthetische Membrane mittels der Franz-Zellen-Methode. Die Ergebnisse zeigten, dass der in die Hydrogele befindliche Saccharosemyristinsäureester die Haut gut und langanhaltend befeuchtet und eine bessere Wirkstoffpenetration bei sehr geringerer Konzentration im Vergleich zum Saccharoselaurinsäurester hat. Unsere Resultate machten deutlich, dass der Saccharosemyristinsäureester ein vielversprechender und effektiver Penetrationsverstärker auf dem pharmazeutischen Gebiet sein kann.

Stichwörter: Saccharoseester, Penetrationsverstärker, dermale Verabreichungsform, Hautfeuchtigkeit, in-vitro-Wirkstoffdiffusion

1 Introduction

Sucrose esters (SEs) are non-ionic surfactants consisting of a sugar substituent, sucrose as the hydrophilic group and fatty acid as the lipophilic group [1]. These natural compounds show many advantages such as excellent biodegradability, biocompatibility and no toxicity [2, 3]. Furthermore, their HLB value ranges from 1 to 16 [4]. SEs are widely used in the food and cosmetic industries and they have recently received increased attention in the pharmaceutical field [5].

As penetration enhancers, SEs belong to a new generation of surfactants as promising agents in transdermal therapeutic systems (TTS) to control drug release and enhance penetration [6]. Generally, ionic surfactants are more potent enhancers than their non-ionic counterparts, but these agents can damage the barrier of the skin. SEs cause less dermatological damage while they act by altering the ordered structure of the intercellular region of the stratum corneum (SC). The drug release effect of SEs depends on their HLB value and the C atom number of the fatty acid chain [7]. The most potent SEs enhancers are with shorter fatty acid chain length and higher HLB value [7, 8]. In the case of TTS patch formulation, sucrose laurate (C = 12, HLB = 16) was found to be the best penetration enhancer [7]. However, the enhancing efficacy of a surfactant is dependent not only on its structure, but also on the physicochemical properties of the drug, and the nature of the vehicle may also play an important role in the surfactant–skin interaction [9].

Sucrose myristate is a monoester of myristic acid and sucrose. It has many applications in the cosmetics and personal care industry as surfactant, emulsifying, skin-conditioning agent and emollient [10]. It has food and cosmetic grade with a HLB value of 16 and a linear alkyl chain of 14 carbon atoms. These structural parameters make sucrose myristate an attractive candidate to serve as a possible absorption enhancer in dermal drug delivery systems.

In this study we prepared hydrogel formulations containing SEs. The penetration of a drug into the deeper layers can be enhanced through a well-hydrated skin, too. During moisturizing, the intercellular space between the corneocytes increases due to the swelling of SC. Furthermore, in many dermatological disorders a significant improvement can be achieved with a well-moisturizing vehicle even in the absence of any active compounds [11]. Our model drug was Ibuprofen – used for the treatment of musculoskeletal disorders – because the transdermal delivery of non-steroidal anti-inflammatory drugs (NSAIDs) offers several advantages over the conventional dosage forms.

The primary aim of this work was to investigate the effect of two SEs (sucrose laurate and sucrose myristate) in human

[1] University of Szeged, Department of Pharmaceutical Technology, Szeged, Hungary
[2] Gedeon Richter Plc., Budapest, Hungary

TS110388 – 28.7.15 dk/stm köthen

skin *in vivo* and to evaluate their concentration dependent enhancing effect on the *in vitro* drug liberation of Ibuprofen from hydrogel based topical formulation.

2 Materials and Methods

2.1 Materials

Sucrose laurate (D-1216) and sucrose myristate (C-1416) were a generous gift from Mitsubishi-Kagaku Foods Corporation (Tokyo, Japan). Ibuprofen (IBU) was purchased from Sigma-Aldrich (St Louis, United States). Carbopol 971P was supplied by Lubrizol Corporation/Azelis (Budapest, Hungary). Polyethylene glycol 400 (PEG 400) and Trolamine was from Hungaropharma Ltd (Budapest, Hungary).

2.2 Sample preparations

API free hydrogel (Blank gel) was prepared by the following procedure. PEG 400 (20 wt.%) solution was added to Carbopol 971P hydrogel. The pH value was adjusted by adding Trolamine (7 wt.%). A penetration enhancer free IBU gel was prepared by the same method, 5 wt.% IBU was dissolved in PEG 400. In order to compare the effect of different SEs, we formulated 2.64 wt.% SE containing compositions using sucrose laurate (IBU-D1216 2.64 wt.% gel) or sucrose myristate (IBU-C1416 2.64 wt.% gel). The 2.64 wt.% was chosen because this was the maximum SE concentration containing hydrogel which did not require centrifugation process to remove the bubbles. Different SE concentration gels were also prepared by a similar method (IBU-D1216 1; 2; 4; 6; 8,; 10 wt.% gel, IBU-C1416 0.25; 0.5; 1; 2; 4; 6; 10 wt.% gel) to investigate the *in vitro* diffusion influenced by the penetration enhancer contents.

2.3 Skin hydration measurements

Skin hydration was measured by Corneometer® CM 825 (Courage and Khazaka Electronic GmbH, Cologne, Germany). Seven healthy female volunteers of ages between 23 and 60 years with no history of dermatological diseases or allergy participated in the experiment (approved by the local ethics committee: Regional and Institutional Human Medical Biological Research Ethics Committee at the University of Szeged) after giving their written consent. All volunteers were asked not to apply any moisturizer or cosmetic product for at least 24 h before the process. Measurements were performed under standardized conditions (room temperature of 21–23 °C, and 40–50% RH). Time was allowed for the patients to adapt to room conditions. 0.3 g of the samples (Blank gel and API free 2.64 wt.% SE containing formulations) was applied on the dorsal hand (3 × 3 cm area) of all the subjects. The electrical capacitance of the SC, indicating the hydration level of the SC was determined before and after the sample application at 30, 90 and 150 min. The measured values were compared with the values detected on the non-treated skin. The changes in moisturizing level were expressed in percentage [12–14].

2.4 Drug diffusion investigations

Membrane diffusion studies were carried out with vertical Franz-diffusion cell system (Hanson Research, Chatsworth, CA, USA). The surface area for diffusion was 1.767 cm^2. A stirring rate of 450 rpm was used. The donor phase was 0.30 g of sample, which was placed on cellulose acetate membranes (Porafil, Machenerey-Nagel, Germany and Pall Life Sciences, USA) itself (*in vitro*). PBS (pH = 7.4) was used as an acceptor phase [15]. The receptor medium temperature was maintained at 37 ± 0.5 °C throughout the experiments to strengthen the physiological skin temperature (32 ± 0.5 °C) on the membrane in the Franz cell [16–18]. The experiments were performed for 24 h [19]. Samples of 0.8 mL were taken from the acceptor phase by the autosampler (Hanson Research, Chatsworth, CA, USA) and replaced with fresh receiving medium. The absorbance of the IBU content was measured by UV spectrophotometer (Unicam Heλios α Thermospectronic UV-spectrophotometer v4.55, UK) at a wavelength of λ = 263 nm [20]. Five parallel measurements were done with plotting the penetration amount of IBU over a time period. Results were expressed as the mean ± SD.

2.5 Dissolution analysis

Permeation parameters were obtained from the cumulative amount of IBU permeated per cm^2 versus time plots (Q). The steady state flux (J) was obtained from the slope of the linear regression versus $t^{1/2}$, respectively. The permeability coefficient (Kp) was calculated according to Fick's first law of diffusion, based on the steady state flux and the applied drug concentration (Cd) of the donor phase [21]:

$$Kp = J/Cd \quad (1)$$

The effectiveness of penetration enhancers was determined by comparing the Kp in the presence and absence of the enhancer. This was defined as the enhancer index (EI), which was calculated using the Kp of the hydrogels with enhancer (Kp_e) and the Kp of the enhancer free IBU-gel (Kp_{ef}) [19]:

$$EI = Kp_e/Kp_{ef} \quad (2)$$

2.6 Statistical analysis

Two-way ANOVA was performed to see any significant difference in the diffused and permeated amount of IBU (Q) between the control (IBU gel) and test preparations using GraphPad Prism software (Graph-Pad Software Inc., CA, USA). Differences were regarded as significant with $p < 0.05$*, $p < 0.01$*, $p < 0.001$***.

3 Results and Discussion

3.1 *In vivo* skin test

As discussed earlier, increased tissue hydration appears to increase skin penetration. This is the most widely used and safest method to increase the transdermal delivery of both hydrophilic and lipophilic compounds. The ideal semisolid dermal drug delivery system should moisture the skin well to enhance the drug penetration.

Figure 1 shows that every sample increased the hydrated state of the skin and ensured a good, lasting moisturizing effect. The greatest increase in skin water content was obtained with 2.64 wt.% sucrose myristate gel, exhibiting a 3-fold increase after 30 min, 1.6-fold increase after 90 min and 1.3-fold increase after 150 min. The application of the 2.64 wt.% sucrose myristate gel results in significantly higher skin hydration compared to the Blank gel after 30, 90 and 150 min ($p < 0.001$***). The Blank gel and the 2.64 wt.% sucrose laurate gel showed a similar hydration state after 30 min, but after 90 min the 2.64 wt.% sucrose laurate gel achieved a greater and more enduring moisturizing effect

TS110388 – 28.7.15 dk/stm köthen

than the Blank gel. However, the results were not statistically significant compared to the SE free hydrogel.

It was proved earlier that sucrose laurate acts as an effective and non-irritating hydration and penetration enhancer for IBU through the skin [6]. Based on our results, it can be concluded that the SEs incorporated into the hydrogel vehicle interact synergistically to modify the skin barrier, but statistically sucrose myristate achieved a higher skin water-holding capacity increase. The SEs have the same HLB value (HLB = 16), but using the 14 C-atom-long fatty acid chains, sucrose myristate in a hydrogel formulation is probably able to integrate into the SC lipid bilayer more efficiently than sucrose laurate (C = 12).

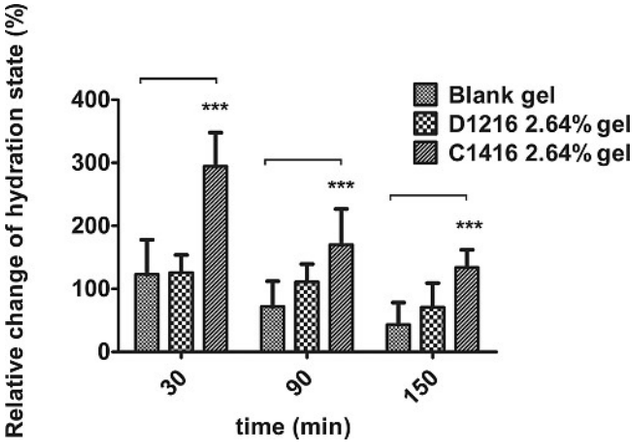

Figure 1 Skin water hydration measurement after single application of three Ibuprofen free topical formulations: penetration enhancer free hydrogel (Blank gel), 2.64 % sucrose laurate gel (D1216 2.64 % gel) and 2.64 % sucrose myristate gel (C1416 2.64 % gel) given as average values ± SD over all 7 volunteers. The differences between Blank gel and C1416 2.64 % gel for each test measurement time are significant using two-way ANOVA ($p < 0.001$***)

3.2 *In vitro* drug release

First, in order to investigate how the SEs influenced the diffusion of IBU *in vitro*, we tested the 2.64 wt.% SE content formulations. Figure 2. presents the cumulative amount per unit area of IBU diffused through synthetic membrane from the different formulations against time. Without penetration enhancers, the drug liberation was about 6687.58 ± 823.86 in 24 h. Both 2.64 wt.% SE containing hydrogels increased IBU diffusion, but in this concentration great differences were not observed between the different SEs. Although sucrose laurate containing hydrogel caused slightly slower drug release than the IBU gel in the first hours, the cumulative drug amount in 24 h was greater than in case of the IBU gel. The diffused drug amounts were not statistically significant in this case. However, using sucrose myristate, the amount of the liberated drug was similar to the IBU gel in the first 3 h, but after the 9th hour the difference between the IBU amount diffused from IBU gel and IBU-C1416 2.64 wt.% gel was statistically significant ($p < 0.05$*).

After this, to examine the effect of penetration enhancer concentrations on *in vitro* drug diffusion, we carried out *in vitro* tests with both SE gels in different concentrations. The steady state fluxes (J) – representing the absorption rate per unit area – and the enhancer indexes (EI) suggest that sucrose laurate has a concentration dependent enhancing effect (Table 1). It can be seen that from 2 wt.% sucrose lau-

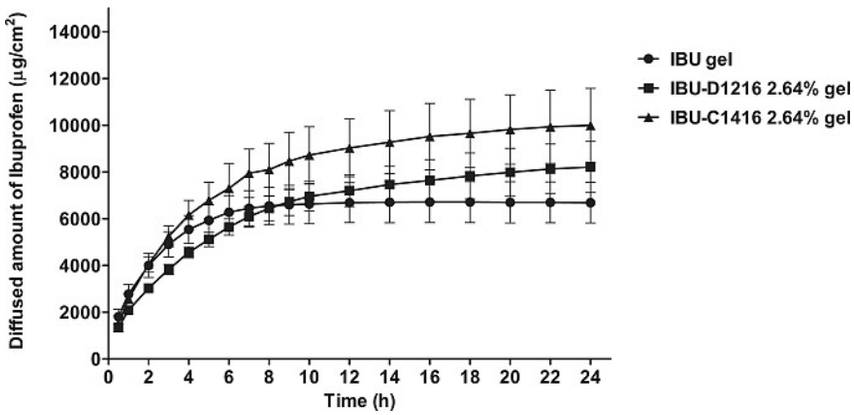

Figure 2 The cumulative diffused amount of Ibuprofen through synthetic membrane given as average values ± SD (n = 5 for each formulation). Diffused amounts are compared to penetration enhancer free IBU gel and with 2.64 % sucrose laurate gel (IBU-D1216 2.64 % gel) as well as with a 2.64 % sucrose myristate gel (IBU-C1416 2.64 % gel)

Formulation	Q (µg cm^{-2})	J (µg cm^{-2} h^{-1})	Kp · 10^{-3} (cm h^{-1})	Enhancer Index (E1)
IBU-gel	6687.59 ± 869.12	971.73	19.43	1.00
IBU D1216 1 % gel	2443.09 ± 452.22	117.05	2.34	0.12
IBU D1216 2 % gel	7002.61 ± 1674.47	1248.60	24.97	1.28
IBU D1216 2.64 % gel	8213.55 ± 1092.08	1629.60	32.59	1.68
IBU D1216 4 % gel	8331.24 ± 478.75	1619.40	32.39	1.67
IBU D1216 6 % gel	10824.16 ± 1130.68	2282.30	45.65	2.35
IBU D1216 8 % gel	10317.58 ± 1736.76	2233.70	44.67	2.29
IBU D1216 10 % gel	7542.37 ± 930.57	1575.60	31.51	1.62

Table 1 Diffusion parameters of Ibuprofen from different sucrose laurate containing hydrogels after 24 h (J: steady state flux; Kp: permeability coefficient)

TS110388 – 28.7.15 dk/stm köthen

rate content the EI values and the diffused amount of IBU after 24 hour were better than in case of the penetration enhancer free hydrogel. We got a maximum curve and the best penetration of IBU was strengthened by the 6 wt.% sucrose laurate gel (Fig. 3.). This gel showed the highest IBU diffusion profile and after the 10th hour the results were significant. Then 8 wt.% and 10 wt.% sucrose laurate containing hydrogels showed lower penetration parameters than 6 wt.% sucrose laurate gel.

When examining sucrose myristate, the same tendency was observed, we found a maximum curve again, but this curve reached the maximum at much lower SE concentration. The diffusion profile of IBU from the 0.5% sucrose myristate containing gel was the highest and after the 3rd hour this formulation showed the earliest significantly increased diffused IBU amount ($p < 0.05$*) compared to the IBU gel (Fig. 4.). This gel reached the best IBU diffusion profile and enhanced the IBU diffusion 1.5 fold when comparing the EI value of 6% sucrose laurate gel. Based on the enhancer indexes it could be established, too, that sucrose myristate up to 4% is a more effective diffusion increaser for IBU than sucrose laurate through synthetic membrane (Table 2).

4 Conclusion

Our results indicate that sucrose myristate is a promising agent in hydrogel formulation for Ibuprofen to enhance the penetration. The *in vivo* results demonstrated that the incorporation of sucrose esters – especially sucrose myristate – into hydrogel extends and increases the hydration phenomenon. Sucrose myristate significantly improved the moisturizing effect of blank hydrogel vehicle. Furthermore, it could be established that the sucrose ester concentration influenced the *in vitro* absorption process notably. It could be concluded from our study that both tested SEs have a concentration dependent enhancing effect and it is not worth using the tested SEs above a certain concentration. While sucrose laurate is an effective penetration enhancer in 6% concentration, sucrose myristate presented a better enhancing effect at a much lower concentration. In case of sucrose myristate, this effect maximized at 0.5%. On the one hand, this phenomenon has not negligible economic aspects, and the other hand, it also facilitates hydrogel preparation. These results suggest that food and cosmetic grade sucrose myristate will be useful as a penetration enhancer in the pharmaceutical field. Furthermore, our results present that it is always important to determine the minimum and maximum effective concentration of the penetration enhancer because it could be influenced by the physicochemical properties of the drug and the vehicle, too.

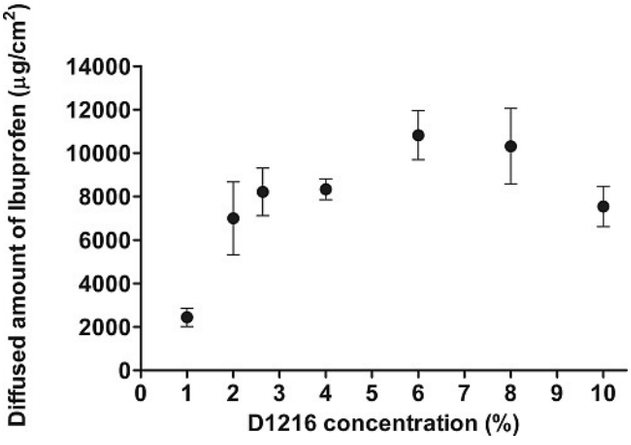

Figure 3 The diffused amount of Ibuprofen from different sucrose laurate containing hydrogels after 24 h (average value ± SD, n = 5)

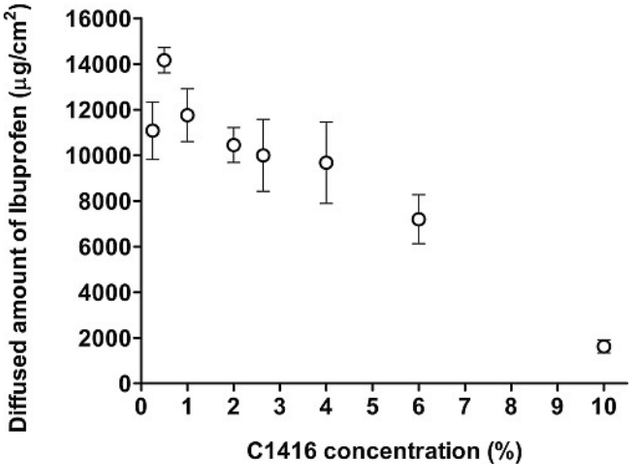

Figure 4 The diffused amount of Ibuprofen from different sucrose myristate containing hydrogels after 24 h (average value ± SD, n = 5)

Formulation	Q (µg cm^{-2})	J (µg cm^{-2} h^{-1})	Kp · 10^{-3} (cm h^{-1})	Enhancer Index (EI)
IBU-gel	6687.59 ± 869.12	971.73	19.43	1.00
IBU C1416 0.25% gel	11075.59 ± 1251.89	2166.20	43.32	2.76
IBU C1416 0.5% gel	14166.39 ± 549.12	2792.30	55.85	3.56
IBU C1416 1% gel	11753.84 ± 1152.88	2192.80	43.86	2.79
IBU C1416 2% gel	10449.58 ± 766.22	2109.20	42.18	2.69
IBU C1416 2.64% gel	9999.87 ± 1581.83	1932.80	38.66	2.46
IBU C1416 4% gel	9675.14 ± 1784.70	1927.90	38.56	2.46
IBU C1416 6% gel	7198.69 ± 1070.05	1387.00	27.54	1.77
IBU C1416 10% gel	1619.33 ± 282.15	312.24	6.24	0.39

Table 2 Diffusion parameters of Ibuprofen from different sucrose myristate containing hydrogels after 24 h (J: steady state flux; Kp: permeability coefficient)

TS110388 – 28.7.15 dk/stm köthen

Acknowledgements

The authors are grateful to Mitsubishi-Kagaku Foods Corporation (Tokyo, Japan) for providing samples of sugar-esters and Lubrizol Corporation/Azelis (Budapest, Hungary) for providing Carbopol samples.

References

1. Mitsubishi-Kagaku Foods Corporation, 1982. Ryoto Sugar Ester Technical Information. Nonionic surfactant/Sucrose fatty acid ester/Food additive. http://www.mfc.co.jp/english.
2. *Youan, B. C., Hussain, A.* and *Nguyen, N. T.*: Evaluation of sucrose esters as alternative surfactants in micro-encapsulation of proteins by the solvent evaporation method, AAPS. Pharmsci. *5* (2003) 1 – 9. DOI:10.1208/ps050222
3. *Kanikkannan, N.* and *Singh, M.*: Skin permeation enhancement effect and skin irritation of saturated fatty alcohol, Int. J. Pharm. *248* (2002) 219 – 228. DOI:10.1016/S0378-5173(02)00454-4
4. *Ganem-Quintanar, A., Quintanar-Guerrero, D., Falson-Rieg, F.* and *Buri, P.*: Ex vivo oral mucosal permeation of lidocaine hydrochloride with sucrose fatty acid esters as absorption enhancers, Int. J. Pharm. *173* (1998) 203 – 210. DOI:10.1016/S0378-5173(98)00226-9
5. *Szuts, A.* and *Szabo-Revesz, P.*: Sucrose esters as natural surfactants in drug delivery systems – a mini-review, Int. J. Pharm. *433* (2012) 1 – 9. DOI:10.1016/j.ijpharm.2012.04.076
6. *Csizmazia, E., Erős, G., Berkesi, O., Berkó, Sz., Szabó-Révész* and *P., Csányi, E.*: Penetration enhancer effect of sucrose laurate and Transcutol on ibuprofen, J. Drug Del. Sci. Tech. *21* (2011) 411 – 415. DOI:10.1016/S1773-2247(11)50066-8
7. *Csóka, G., Marton, S., Zelko, R., Otomo, N.* and *Antal, I.*: Application of sucrose fatty acid esters in transdermal therapeutic systems, Int. J. Pharm. *65* (2007) 233 – 237. DOI:10.1016/j.ejpb.2006.07.009
8. *El-Laithy, H. M.*: Novel transdermal delivery of Timolol maleate using sugar esters: preclinical and clinical studies, Eur. J. Pharm. Biopharm. *72* (2009) 239 – 245. DOI:10.1016/j.ejpb.2008.12.003
9. *Cázares-Delgadillo, J., Naik, A., Kalia, Y. N., Quintanar-Guerrero, D.* and *Ganem-Quintanar, A.*: Skin permeation enhancement by sucrose esters: A pH-dependent phenomenon, Int. J. Pharm. *297* (2005) 204 – 212. DOI:1016/j.ijpharm.2005.03.020
10. http://www.ec.europa.eu.
11. *Benson, H. A. E.*: Transdermal drug delivery: penetration enhancement techniques, Curr. Drug Deliv. *2* (2005) 23 – 33. DOI:10.2174/1567201052772915
12. *Betz, G., Aeppli, A., Menshutina, N.* and *Leuenberger, H.*: In vivo comparison of various liposome formulations for cosmetic application, Int. J. Pharm. *296* (2005) 44 – 54. DOI:10.1016/j.ijpharm.2005.02.032
13. *Nicander, I.* and *Ollmar, S.*: Clinically normal atopic skin vs. non-atopic skin as seen through electrical impedance, Skin Res. Technol. *10* (2004) 178 – 183. DOI:10.1111/j.1600-0846.2004.00065.x
14. *Savic, S., Tamburic, S., Savic, M., Cekic, N., Milic, J.* and *Vuleta, G.*: Vehicle-controlled effect of urea on normal and SLS-irritated skin, Int. J. Pharm. *271* (2004) 269 – 280;. DOI:10.1016/j.ijpharm.2003.11.033
15. *Potthast, H., Dressman, J. B., Junginger, H. E., Midha, K. K., Oeser, H., Shah, V. P., Vogelpoel, H.* and *Barends, D. M.:* Biowaiver monographs for immediate release solid oral dosage forms: ibuprofen, J. Pharm. Sci. *94* (2005) 2121 – 2131. DOI:10.1002/jps.20444
16. *Brain, K. R., Green, D. M., Lalko, J.* and *Api, A. M.*: In vitro human skin penetration of the fragrance material geranyl nitrile, Toxicol. in Vitro *21* (2007) 133 – 138. DOI:10.1016/j.tiv.2006.08.005
17. *Schaefer, U. F., Hansen, S., Schneider, M., Contreras, J. L.* and *Lehr, C-M.*: Models for skin absorption and skin toxicity testing, in: *Ehrhardt, C., Kim, K.-J.* (Eds.), Drug Absorption Studies In situ, In vitro and In Silico Models, Springer, New York (2008) 1. DOI:10.1007/978-0-387-74901-3
18. *Mura, S., Manconi, M., Sinico, Ch., Valenti, D.* and *Fadda, A. M.*: Penetration enhancer-containing vesicles (PEVs) as carriers for cutaneous delivery of minoxidil, Int. J. Pharm. *380* (2009) 72 – 79. DOI:10.1016/j.ijpharm.2009.06.040
19. *Vaddi, H. K., Ho, P. C., Chan, Y. W.* and *Chan, S. Y.*: Terpens in ethanol:haloperidol permeation and partition through human skin and stratum corneum changes, J. Control. Release *81* (2002) 121 – 133. DOI:10.1016/S0168-3659(02)00057-3
20. *Resch, M., Resch, B., Csizmazia, E., Imre, L., Németh, J., Révész, P.* and *Csányi, E.*: Permeability of human amniotic membrane to ofloxacin in vitro, Invest. Ophthalmol. Vis. Sci. *51* (2010) 1024 – 1027. DOI:10.1089/jop.2011.0007
21. *Wagner, H., Kostka, K.-H., Lehr, C.-M.* and *Schaefer, U. F.*: Interrelation of permeation and penetration parameters obtained from in vitro experiments with human skin and skin equivalents, J. Control. Release *75* (2001) 283 – 295. DOI:10.1016/S0168-3659(01)00396-0

Received: 00. 00. 1900
Revised: 00. 00. 1900

Bibliography

DOI 10.3139/113.110388
Tenside Surf. Det.
52 (2015) 5; page 1 – 5

ISSN 0932-3414

Correspondence address

Mrs. Dr. Erzsébet Csányi
Department of Pharmaceutical Technology, University of Szeged
Eötvös str. 6
H-6720 Szeged
Hungary
Tel.: +36 62 54 55 73
Fax: +36 62 54 55 71
E-Mail: csanyi@pharm.u-szeged.hu

The authors of this paper

Boglárka Balázs was born in September 1988. She has graduated as pharmacist at University of Szeged, Faculty of Pharmacy in 2012. She is 3rd year Ph.D. student at University of Szeged, Doctoral School of Pharmaceutical Sciences. Her research fields are investigation of skin diseases with spectroscopy methods (ATR-FTIR, NIR and RAMAN), development of dermal and transdermal systems and electrically-assisted transdermal delivery.

Dr. *Eszter Csizmazia* was born in September 1984. She completed her post graduation at University of Szeged, Faculty of Pharmacy in 2008. She obtained her Ph.D. in 2011 at University of Szeged. At present she is working as Developer at Gedeon Richter Plc. Her research activities are investigation of the drug permeation through various biological membranes and development of dermal and transdermal systems.

Dr. *Szilvia Berkó* was born in September 1973, studied for her pharmacist diploma at Medical University of Szeged. She did her Ph.D. in 2003, from University of Szeged, Doctoral School of Pharmaceutical Sciences. At present she is working as Assistant Lecturer at Department of Pharmaceutical Technology, University of Szeged. Her research activities are formulation rectal dosage forms, development of semisolid dosage forms and modification of skin penetration of different drugs.

Dr. *Mária Budai-Szűcs* was born in June 1981. She completed her post graduation in 2005 from University of Szeged, Faculty of Pharmacy. She did her Ph.D. in 2008, from University of Szeged, Doctoral School of Pharmaceutical Sciences. At present she is working as Assistant Lecturer at Department of Pharmaceutical Technology, University of Szeged. Her research focuses on stimuli responsive polymer drug deliveries, and focal drug deliveries.

Dr. *Piroska Szabó-Révész* was born in August 1951. She completed her post graduation at Medical University of Szeged in 1975. After obtaining her University Doctorate, she worked for as Assistant Lecturer at Department of Pharmaceutical Technology, Medical University of Szeged. Since 2005 she is working as Professor & Head of the Department of Pharmaceutical Technology. She obtained her D.Sc. in 2006. Her research activities are preparation, optimization and characterization of nanoparticular (e.g. nanocrystalline) systems with the aim of improvement of dissolution rate and permeability of water insoluble active pharmaceutical ingredients.

Dr. *Erzsébet Csányi* was born in February 1957. She studied for her pharmacist diploma at Medical University of Szeged. After she obtained her post graduation in 1980 she joined Medical University of Szeged as Teaching Assistant in the Department of Pharmaceutical Technology. She obtained her University Doctorate in 1982 and did her Ph.D. in 2005. Since 2005 she is working as Associate Professor at Department of Pharmaceutical Technology, University of Szeged. Her research fields are development of dermal and transdermal systems, their rheological and biopharmaceutical investigation, enhancement of the solubility of poorly soluble drugs with solubilization, with the use of microemulsion and lyotropic liquid crystalline systems and *in vitro* and *ex vivo* drug penetration examination.

V.

Biomedical Optics EXPRESS

ATR-FTIR and Raman spectroscopic investigation of the electroporation-mediated transdermal delivery of a nanocarrier system containing an antitumour drug

Boglárka Balázs,[1,2] Péter Sipos,[1] Corina Danciu,[3] Stefana Avram,[4] Codruta Soica,[5] Cristina Dehelean,[6] Gábor Varju,[7] Gábor Erős,[8,9] Mária Budai-Szűcs,[1] Szilvia Berkó,[1] and Erzsébet Csányi[1,*]

[1]*Department of Pharmaceutical Technology, University of Szeged, Szeged, H-6720, Hungary*
[2]*Gedeon Richter Plc., Budapest, H-1103, Hungary*
[3]*Department of Pharmacognosy, "Victor Babes" University of Medicine and Pharmacy, Timisoara, 300041, Romania*
[4]*Discipline of Pharmacology, "Victor Babes" University of Medicine and Pharmacy, Timisoara, 300041, Romania*
[5]*Discipline of Pharmaceutical Chemistry, "Victor Babes" University of Medicine and Pharmacy, Timisoara, 300041, Romania*
[6]*Department of Toxicology, "Victor Babes" University of Medicine and Pharmacy, Timisoara, 300041, Romania*
[7]*Dr. Derm Clinic of Anti-Aging Dermatology, Aesthetic Laser and Plastic Surgery, Budapest, H-1026, Hungary*
[8]*Department of Dermatology and Allergology, University of Szeged, Szeged, H-6720, Hungary*
[9]*Department of Oral Biology and Experimental Dental Research, University of Szeged, Szeged, H-6720, Hungary*
**csanyi@pharm.u-szeged.hu*

Abstract: The aim of the present work was the optimization of the transdermal delivery of a lyotropic liquid crystal genistein-based formulation (LLC-GEN). LLC was chosen as medium in view of the poor solubility of GEN in water. Membrane diffusion and penetration studies were carried out with a Franz diffusion cell, through a synthetic membrane *in vitro*, a chick chorioallantoic membrane *ex ovo*, and *ex vivo* excised human epidermis. Thereafter, LLC-GEN was combined with electroporation (EP) to enhance the transdermal drug delivery. The synergistic effect of EP was verified by *in vivo* ATR-FTIR and *ex vivo* Raman spectroscopy on hairless mouse skin.

OCIS codes: (170.3880) Medical and biological imaging; (300.6540) Spectroscopy, ultraviolet; (120.7280) Vibration analysis; (300.6340) Spectroscopy, infrared; (300.6300) Spectroscopy, Fourier transforms; (170.5660) Raman spectroscopy.

References and links

1. M. R. Prausnitz, P. M. Elias, T. J. Franz, M. Schmuth, J.-C. Tsai, G. K. Menon, W. M. Holleran, and K. R. Feingold, "Skin barrier and transdermal drug delivery," in: *Dermatology*, J. L. Bolognia, J. L. Jorizzo, J. V. Schaffer, ed. (Elsevier Health Sciences, 2012)
2. G. A. Hofmann, "Instrumentation and Electrodes for In Vivo Electroporation", in: *Electrochemotherapy, Electrogenetherapy, and Transdermal Drug Delivery*, M. J. Jaroszeski, R. Heller, R. Gilbert, ed. (Humana Press, 2000)
3. A. R. Denet, R. Vanbever, and V. Préat, "Skin electroporation for transdermal and topical delivery," Adv. Drug Deliv. Rev. **56**(5), 659–674 (2004).
4. R. Vanbever and V. Préat, "In vivo efficacy and safety of skin electroporation," Adv. Drug Deliv. Rev. **35**(1), 77–88 (1999).
5. C. Lombry, N. Dujardin, and V. Préat, "Transdermal delivery of macromolecules using skin electroporation," Pharm. Res. **17**(1), 32–37 (2000).
6. L. M. Mir and S. Orlowski, "Mechanisms of electrochemotherapy," Adv. Drug Deliv. Rev. **35**(1), 107–118 (1999).
7. A. C. Dweck, "Isoflavones, phytohormones and phytosterols," J. Appl. Cosmetol. **24**, 17–32 (2006).
8. B. Pawlikowska-Pawlega, L. E. Misiak, B. Zarzyka, R. Paduch, A. Gawron, and W. I. Gruszecki, "Localization and interaction of genistein with model membranes formed with dipalmitoylphosphatidylcholine (DPPC)," Biochim. Biophys. Acta **1818**(7), 1785–1793 (2012).

#253195 Received 2 Nov 2015; revised 18 Nov 2015; accepted 18 Nov 2015; published 8 Dec 2015

9. C. Danciu, F. Borcan, F. Bojin, I. Zupko, and C. Dehelean, "Effect of the isoflavone genistein on tumor size, metastasis potential and melanization in a B16 mouse model of murine melanoma," Nat. Prod. Commun. **8**(3), 343–346 (2013).
10. J.-G. Wu, J. Ge, Y.-P. Zhang, Y. Yu, and X.-Y. Zhang, "Solubility of Genistein in Water, Methanol, Ethanol, Propan-2-ol, 1-Butanol, and Ethyl Acetate from (280 to 333) K," J. Chem. Eng. Data **55**(11), 5286–5288 (2010).
11. C. Danciu, M. Biriş, B. Balázs, E. Csányi, I. Z. Pavel, G. Pop, C. Soica, L. Ceuta, L. Nita, C. Morgovan, and D. Stoian, "Pro-apoptotic effect of soy total extract incorporated in lyotropic liquid crystals formulation," Rev. Chim-Bucharest **66**(7), 1038–1041 (2015).
12. C. Danciu, S. Berkó, G. Varju, B. Balázs, L. Kemény, I. B. Németh, A. Cioca, A. Petruş, C. Dehelean, C. I. Cosmin, E. Amaricai, and C. C. Toma, "The effect of electroporation of a lyotroic liquid crystal Genistein-based formulation in the recovery of murine melanoma lesions," Int. J. Mol. Sci. **16**(7), 15425–154418 (2015).
13. M. Makai, E. Csányi, Z. Németh, J. Pálinkás, and I. Erős, "Structure and drug release of lamellar liquid crystals containing glycerol," Int. J. Pharm. **256**(1-2), 95–107 (2003).
14. B. J. Boyd, D. V. Whittaker, S. M. Khoo, and G. Davey, "Lyotropic liquid crystalline phases formed from glycerate surfactants as sustained release drug delivery systems," Int. J. Pharm. **309**(1-2), 218–226 (2006).
15. A. Vargas, M. Zeisser-Labouèbe, N. Lange, R. Gurny, and F. Delie, "The chick embryo and its chorioallantoic membrane (CAM) for the in vivo evaluation of drug delivery systems," Adv. Drug Deliv. Rev. **59**(11), 1162–1176 (2007).
16. M. Dias, A. Naik, R. H. Guy, J. Hadgraft, and M. E. Lane, "In vivo infrared spectroscopy studies of alkanol effects on human skin," Eur. J. Pharm. Biopharm. **69**(3), 1171–1175 (2008).
17. E. Csizmazia, G. Eros, O. Berkesi, S. Berkó, P. Szabó-Révész, and E. Csányi, "Ibuprofen penetration enhance by sucrose ester examined by ATR-FTIR in vivo," Pharm. Dev. Technol. **17**(1), 125–128 (2012).
18. D. Bommannan, R. O. Potts, and R. H. Guy, "Examination of stratum corneum barrier function in vivo by infrared spectroscopy," J. Invest. Dermatol. **95**(4), 403–408 (1990).
19. N. Surendra Babu and T. Abute Lelisho, "Computational studies of solvent effects on structure and Vibrational Spectra of isofavonoid 5,7-Dihydroxy-3-(4-hydroxyphenyl)chromen-4-one(Genistein) by ab intio HF and DFT methods," Adv. Appl. Sci. Res. **3**(6), 3916–3934 (2012).
20. G. Bernard, M. Auger, J. Soucy, and R. Pouliot, "Physical characterization of the stratum corneum of an in vitro psoriatic skin model by ATR-FTIR and Raman spectroscopies," Biochim. Biophys. Acta **1770**(9), 1317–1323 (2007).
21. V. Crupi, D. Majolino, A. Paciaroni, B. Rossi, R. Stancanelli, V. Venuti, and G. Viliani, "The effect of hydrogen bond on the vibrational dynamics of genistein free and complexed with β-cyclodextrins," J. Raman Spectrosc. **41**(7), 764–770 (2010).
22. R. Sekine, E. G. Robertson, and D. McNaughton, "Raman, infrared and computational analysis of genistein and its methoxy derivatives," Vib. Spectrosc. **57**(2), 306–314 (2011).
23. M. Leroy, J.-F. Labbé, M. Ouellet, J. Jean, T. Lefèvre, G. Laroche, M. Auger, and R. Pouliot, "A comparative study between human skin substitutes and normal human skin using Raman microspectroscopy," Acta Biomater. **10**(6), 2703–2711 (2014).
24. G. Zhang, D. J. Moore, K. B. Sloan, C. R. Flach, and R. Mendelsohn, "Imaging the prodrug-to-drug transformation of a 5-fluorouracil derivative in skin by confocal Raman microscopy," J. Invest. Dermatol. **127**(5), 1205–1209 (2007).
25. C. R. Flach and D. J. Moore, "Infrared and Raman imaging spectroscopy of ex vivo skin," Int. J. Cosmet. Sci. **35**(2), 125–135 (2013).
26. A. M. Kligman and E. Christophers, "Preparation of isolated sheets of human stratum corneum," Arch. Dermatol. **88**(6), 702–705 (1963).
27. K. R. Brain, D. M. Green, J. Lalko, and A. M. Api, "In-vitro human skin penetration of the fragrance material geranyl nitrile," Toxicol. In Vitro **21**(1), 133–138 (2007).
28. I. Schroeder, P. Franke, U. F. Schaefer, and C.-M. Lehr, "Delivery of ethinylestradiol from film forming polymeric solutions across human epidermis in vitro and in vivo in pigs," J. Control. Release **118**(2), 196–203 (2007).
29. R. Vanbever and V. Préat, "Factors affecting transdermal delivery of metoprolol by electroporation," Bioelectrochem. Bioenerg. **38**(1), 223–228 (1995).
30. M. R. Prausnitz, V. G. Bose, R. Langer, and J. C. Weaver, "Electroporation of mammalian skin: a mechanism to enhance transdermal drug delivery," Proc. Natl. Acad. Sci. U.S.A. **90**(22), 10504–10508 (1993).
31. R. Vanbever, E. LeBoulengé, and V. Préat, "Transdermal delivery of fentanyl by electroporation. I. Influence of electrical factors," Pharm. Res. **13**(4), 559–565 (1996).

1. Introduction

The transport of molecules through the skin is made difficult by the presence of the stratum corneum (SC). The epidermis is an intricate and highly inhomogeneous structure built up from different layers, but the SC (the outermost layer of the skin consisting of dead flattened cells) causes its barrier function, such as the electrical properties [1, 2]. Transdermal drug delivery has a number of advantages over conventional delivery methods such as oral administration and injection (e.g. elimination of the first-pass metabolism, the minimization

#253195 Received 2 Nov 2015; revised 18 Nov 2015; accepted 18 Nov 2015; published 8 Dec 2015

of pain, and the possibility of the sustained release of drugs). However, for the delivery of large molecules through the skin, the use of chemical or physical methods is unavoidable [1].

Electroporation (EP) involves the application of short (microsecond to millisecond) pulses of high voltage (HV) to achieve a transitory structural perturbation of the lipid bilayer membranes. Its main advantages are that it is easy and rapid, and is able to open different kinds of lipid bilayer membranes: artificial (liposomes), cellular (bacterial, yeast, plant and mammalian cells) or even more complex structures (e.g. SC) [3]. Through the use of skin EP, the transdermal delivery of small dyes, drugs, oligonucleotides, DNA plasmids, antigens, hydrophilic molecules, neutral or highly charged compounds, and macromolecules with molecular weights up to 40 kDa can be enhanced by several orders of magnitude [4, 5].

Currently the most broadly developing area of EP is electrochemotherapy, which is an effective way to treat cutaneous and subcutaneous tumours: HV pulses are applied to permeabilize tumour cells to an impermeable cytotoxic drug, which is administered by injection either into a vein or directly into a tumour [6].

Genistein (GEN; 4,5,7-trihydroxyisoflavone), one of the most abundant isoflavones in soybeans, is also called a phytoestrogen because of its structural similarity to the human hormone 17β-oestradiol [7]. GEN, a potent tyrosine kinase inhibitor, has been extensively used in the prevention and treatment of many diseases and disorders, including cancer, cardiovascular diseases, osteoporosis and postmenopausal symptoms [8]. Danciu et al. demonstrated the beneficial effects of GEN as regards tumour size, metastasis potential and melanization in a B16 mouse model of murine melanoma [9]. However, GEN is only poorly soluble in water and this can be a serious problem in terms of formulation [10].

A topically applied GEN-based lyotropic liquid crystal (LLC) formulation was earlier developed and combined with EP to treat murine melanoma lesions [11, 12]. The results showed that this strategy is promising for the recovery of skin lesions of murine melanoma type. LLCs are novel nanosystems usually formed from water and one or two surfactants, possibly with cosurfactants and oils. The main advantages of these systems include their similarity with colloidal systems existing in living organisms, their thermodynamic stability, and the situations that they can be stored for long periods of time without phase separation, they exhibit good penetration and they can facilitate the progressive diffusion of biologically active substances into the skin or systemic circulation. Besides their good solubilizing effects, they are able to incorporate and control the release of drugs of varying size and polar characteristics as they contain lipophilic, hydrophilic and amphiphilic domains [13, 14].

In the present work, the diffusion and penetration of GEN and LLC-GEN through different membranes were first investigated by conventional treatment without EP, and also with the mediation of EP. Measurements were made with a Franz diffusion cell system through a synthetic membrane *in vitro*, chick chorioallantoic membrane (CAM) *ex ovo* and excised human epidermis *ex vivo*. CAM has been introduced as a new and useful biological membrane model for preclinical permeability studies of pharmaceutical substances [15].

Vibrational spectroscopies were used to investigate the effects of EP on animal skin. Infrared (IR) and Raman spectroscopy have recently received increased attention in both the cosmetic and pharmaceutical fields. These methods offer attractive possibilities for the study of EP-mediated drug delivery.

Attenuated total reflection Fourier transform IR spectroscopy (ATR-FTIR) is a suitable tool with which to study the structure of the SC at the molecular level, to characterize its lipids, proteins and water content [16], and to analyse the penetration of drugs into the skin and the biochemical modifications induced by the penetration [17]. ATR-FTIR is essentially a non-destructive sampling technique which combined with tape-stripping serves as a rapid, simple, non-invasive method for studies of the skin. Through sequential tape-stripping, SC layers can be obtained from the deeper regions. The ATR device allows a spectrum to be acquired from a surface of a sample without preparation [18]. FTIR spectrometric studies on GEN have been investigated and reported earlier [19].

Raman spectroscopy is also widely used to study biological samples and to study the skin [20]. It has been utilized to determine the structures of GEN-cyclodextrin inclusion complexes

#253195 Received 2 Nov 2015; revised 18 Nov 2015; accepted 18 Nov 2015; published 8 Dec 2015

[21], GEN and other 5-hydroxyisoflavones [22]. The assignment of the Raman spectrum of native skin was reported by Pouliot [23]. Confocal Raman images have been investigated as chemical maps of *ex vivo* pigskin [24] and *ex vivo* human abdominal skin [25].

Following an investigation of the transdermal delivery of our newly developed LLC-GEN formulation through different membranes without EP, LLC-GEN was combined with EP to examine the efficiency of this combination by means of *in vivo* ATR-FTIR and *ex vivo* Raman spectroscopy. With vibrational spectroscopic monitoring, various treatment times and voltages were applied to evaluate the effects of EP on the skin.

2. Materials and methods

2.1. Materials

GEN was purchased from Extrasynthèse (Genay, France; purity >95%), and the non-ionic surfactant Cremophor RH 40 (CRH40; Polyoxyl 40 Hydrogenated Castor Oil USP/NF) from BASF (Ludwigshafen, Germany). The aqueous phase of the systems was purified water (Ph.Eur.6.), and the oil phase was isopropyl myristate (IPM; Merck Kft., Budapest, Hungary). The average particle size of GEN is 12.04 ± 7.74 μm (n = 564).

2.2. Sample preparation

Samples produced with a 2:1 by the oil-surfactant mixture were homogenized with a magnetic stirrer at room temperature, and 10 wt.% of water was then added in small amounts under stirring. For the drug-containing samples, 3 wt.% of GEN as active agent was partly dissolved (1 wt.%) in the oil-surfactant mixture with the aid of a magnetic stirrer.

2.3. Drug diffusion and penetration investigations

2.3.1. Preparation of CAM

Fertilized chicken eggs (*Gallus gallus domesticus*) were prepared for the experiment by cleaning with ethanol, and then placed horizontally in an incubator at 37 °C, with constant humidity. On the third day of incubation, 3–4 mL of albumen was extracted from the most pointed part of the egg, so that the developing CAM could be detached from the inner shell in order to work directly on the membrane. On day 4 of incubation, a window was cut in the surface of the egg, it was resealed with adhesive tape and incubation was continued until the day of the experiment. CAMs were collected in buffered formalin and used for *ex ovo* studies.

2.3.2. Preparation of heat-separated epidermis

With the approval of the Ethical Committee of the University of Szeged, Albert Szent-Györgyi Clinical Centre (Human Investigation Review Board licence number: 83/2008.), excised human skin was obtained from a Caucasian female patient who underwent abdominal plastic surgery. This was. The subcutaneous fatty tissue was separated from the outer skin layers after excision and the skin was stored at −20 °C. For the penetration experiment, after the skin had thawed, the epidermis was separated from the underlying dermis by a heat-separation technique [26]. Individual portions were immersed in water at 60 °C for 90 s. After removal of the skin from the water, it was placed SC side up on a filter paper, and the epidermis (comprising the SC and the viable epidermis) was gently removed from the underlying dermis with the use of forceps and was discarded. The epidermal membrane was floated onto the surface of PBS (phosphate buffer solution, pH = 7.4) for at least 20 min and then placed on a supporting cellulose acetate membrane (Porafil, Machenerey-Nagel, Düren, Germany, and Pall Life Sciences, Washington, NY, USA; pore diameter 0.45 μm) [27, 28].

2.3.3. Franz diffusion cell method

Membrane diffusion and permeability studies of GEN were carried out with a vertical Franz diffusion cell system (Hanson Research, Chatsworth, CA, USA) in a six-unit assembly (effective permeation area 1.33 cm^2) for 24 h (*in vitro* or *ex ovo*) or 48 h (human epidermis) at

#253195 Received 2 Nov 2015; revised 18 Nov 2015; accepted 18 Nov 2015; published 8 Dec 2015

37 °C. The donor phase was 0.30 g of sample, which was placed on a cellulose acetate membrane (Porafil, Machenerey-Nagel, Düren, Germany, and Pall Life Sciences, Washington, NY, USA) itself (*in vitro*), or in the case of *ex ovo* and *ex vivo* measurements the CAM and the epidermis were supported with a Porafil membrane filter. The acceptor compartment consisted of 10 wt.% ethanol containing PBS (pH 7.4), which was stirred at 450 rpm throughout the experiment. Samples of 0.8 mL were taken from the acceptor phase by the autosampler (Hanson Research, Chatsworth, CA, USA) and replaced with an equal volume of fresh receiving medium. The absorbance of the GEN content was measured at 261 nm with a Unicam Heλios α Thermospectronic UV-spectrophotometer v4.55 (Unicam, Thermo Fisher Scientific Inc., Waltham, MA, USA). Five parallel measurements were carried out and the amount of GEN penetrating during a time period was plotted. The results were expressed as means ± SEM.

2.3.4. Penetration analysis

Penetration parameters were obtained from the cumulative amount of GEN penetrated per cm^2 versus time plots (Q). The transdermal flux (J) was calculated from the slope of the concentration versus time profile in the receiver compartment, and expressed in $\mu g\ cm^{-2}\ h^{-1}$. For the linear regression analysis, the linear range of the incubation period from 1 to 6 h was selected, and was used to calculate the flux data of the compounds.

2.4. EP parameters

A Mezoforte Duo Mez 120905-D instrument (Dr Derm Equipment Ltd., Budapest, Hungary) was used to generate the electric pulses for the skin EP. The operation of this device is based on a pulsed electromagnetic field generated by an amplitude-modulated sine wave radiofrequency current. The polypropylene-covered treatment headpiece contains a plate electrode 25 mm in diameter indirectly contact with the treated surface. Modulation involves HV pulses 5 ms in duration, followed by a 20 ms break. GEN transport by means of skin EP can be influenced by using 700 V or 900 V with different treatment times (1 or 2 min).

2.5. Animal experiments

12-week-old male SKH-1 hairless mice were housed in plastic cages in a thermoneutral environment with a 12 h light-dark cycle and had access to standard laboratory chow and water *ad libitum*. All interventions were in full accordance with the NIH guidelines and the protocols were approved in advance by the Ethical Committee for the Protection of Animals in Scientific Research at the University of Szeged (licence number: V./145/2013). Prior to the intervention, the animals were anaesthetized with a mixture of ketamine (90 mg (kg bodyweight)$^{-1}$) and xylazine (25 mg (kg bodyweight)$^{-1}$) administered intraperitoneally. At the end of the experiments, the mice were euthanized with an overdose of ketamine (300 mg kg^{-1}).

The mice involved in the study were divided into 5 groups as follows:

Group A: mice treated with dermally applied LLC-GEN for 2 min (conventional treatment)

Group B: mice treated with LLC-GEN and EP at 700 V for 1 min

Group C: mice treated with LLC-GEN and EP at 900 V for 1 min

Group D: mice treated with LLC-GEN and EP at 700 V for 2 min

Group E: mice treated with LLC-GEN and EP at 900 V for 2 min

For ATR-FTIR measurements, 5 mice were randomly assigned to each experimental condition. Corneocytes were collected from the uppermost layer of their dorsal skin with the use of adhesive tape (D Squames, CuDerm Corporation, Dallas, TX, USA) immediately after treatment. The treated and the untreated dorsal skin of each mouse was stripped with adhesive tape; this procedure was repeated up to 18 strips, an IR spectrum being recorded after every third tape strip. Every first tape with one strip was discarded because of the possibility of surface contamination.

#253195 Received 2 Nov 2015; revised 18 Nov 2015; accepted 18 Nov 2015; published 8 Dec 2015

For Raman measurements, 2 mice were randomly assigned to each of groups A, C and E. At the end of the observation period of these groups, the animals were sacrificed (as described above) and full-thickness skin samples were excised from the treated areas. The samples were embedded in Cryomatrix resin (Thermo Fisher Scientific Inc., Waltham, MA, USA) and cryosections of 6 μm were made.

2.6. ATR-FTIR measurements

ATR-FTIR spectra were recorded with an Avatar 330 FT-IR spectrometer (Thermo Fisher Scientific Inc., Waltham, MA, USA) equipped with a horizontal ATR crystal (ZnSe, 45°), between 4000 and 400 cm^{-1}, at an optical resolution of 4 cm^{-1}. 128 scans were co-added and all spectral manipulations were performed with the Thermo Scientific's GRAMS/AI Suite software. In order to obtain a reference spectrum of the API, a KBr pellet containing 0.5 mg of GEN was prepared and used. The spectra of the preparations were also recorded. The spectra of five parallel samples, gained from five different animals, were recorded. Each average layer spectrum of the treated SC was corrected with the corresponding average layer spectrum of the untreated SC. No ATR correction was performed.

2.7. Raman measurements

Raman spectra were acquired with a Dispersive Raman Microscope (Thermo Fisher Scientific Inc., Waltham, MA, USA) equipped with a CCD camera and a diode laser operating at 780 nm. The spectra of the CRH40, IPM and GEN were collected with an exposure time of 6 s, with 48 scanning and cosmic ray and fluorescence corrections. Raman measurements were carried out with a laser power of 12 mW at a slit width of 25 μm. The localization of GEN in the skin samples was investigated by confocal Raman mapping. For mapping, the microtomed skin samples as depth sections were rotated by 90° and placed on an aluminium surface with the SC towards the top of the plate. Thus, a 1000 μm length of the sample specimen corresponds to a 1000 μm depth into the skin. The mapping was achieved in a point-by-point mode, using a step size of 10 μm perpendicular and parallel to the SC. Raman maps of skin with dimensions 30-40 μm parallel and 900-1300 μm perpendicular to the SC surface were generated one-by-one. The spectrum acquisition time was 3 s per spectrum, and 24 spectra were accumulated and averaged at each measured point, these parameters ensuring an acceptable signal-to-noise ratio. The mapping was carried out with a laser power of 24 mW at a slit width of 25 μm. The vibrational chemical images were studied by a multivariate curve resolution – alternating least squares chemometric method; the purpose was to identify GEN in the Raman spectra.

2.8. Statistical analysis

Two-way ANOVA was used to identify any significant differences in the total penetrated amount of GEN between the conventional treatment and the combined EP treatments by using GraphPad Prism software (Graph-Pad Software Inc., La Jolla, CA, USA). Differences were regarded as significant if $p < 0.05$* and $p < 0.001$***.

3. Results and discussion

3.1. Drug diffusion and penetration

The membrane diffusion investigations indicated that good drug release and diffusion was attained through the synthetic membrane *in vitro,* 713.26 ± 90.73 μg cm^{-2} being liberated in 24 h (Fig. 1(a)). Somewhat less drug was observed after 24 h (491.26 ± 15.55 μg cm^{-2}) in the case of *ex ovo* penetration (Fig. 1(b)). In the e*x vivo* investigations which revealed not only the amount of drug that diffused through the skin, but also the interaction with the skin and the incidental reservoir function of the SC, only a small amount of drug penetrated through the human epidermis (8.93 ± 1.81 μg cm^{-2} after 24 h and 15.68 ± 3.09 μg cm^{-2} after 48 h), but the penetration profile was similar to that for *ex ovo* penetration and sustained drug release was achieved (Fig. 1(c)). The transdermal flux (J) (reflecting the absorption rate per unit area)

#253195 Received 2 Nov 2015; revised 18 Nov 2015; accepted 18 Nov 2015; published 8 Dec 2015

showed that the drug penetration was slowed down by the application of the biological membrane, and that LLC-GEN alone was not sufficient to reach an appropriate plasma concentration.

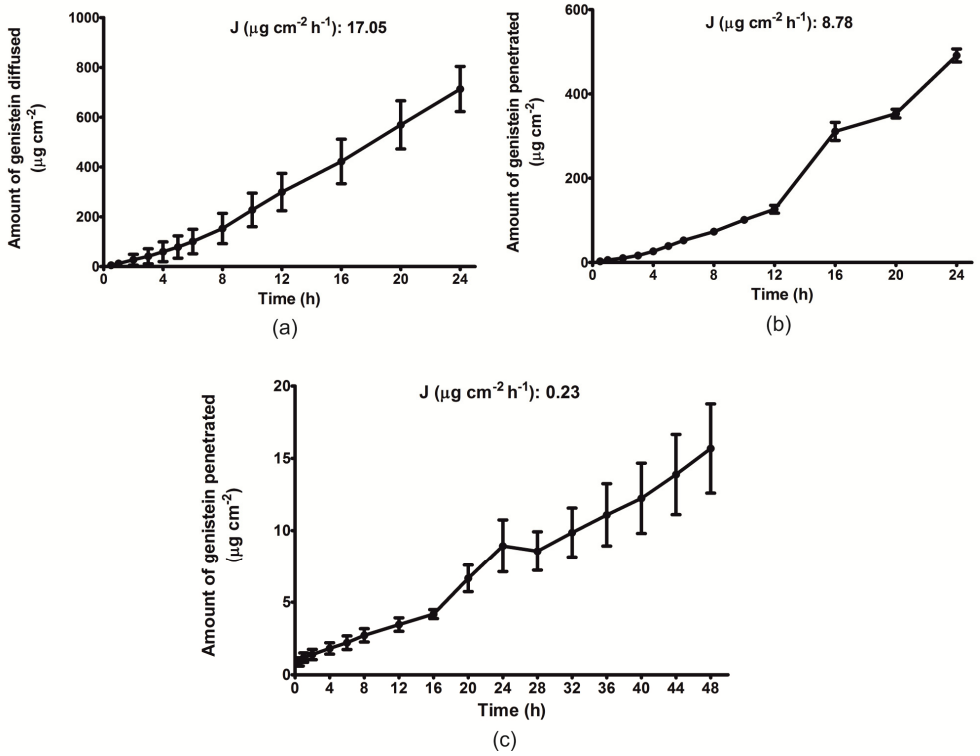

Fig. 1. Amount of GEN diffused *in vitro* (a), or penetrated *ex ovo* (b) or *ex vivo* (c).

3.2. ATR-FTIR spectroscopy

The penetration profile of GEN within the different layers of the SC was established with a combination of tape stripping and ATR-FTIR spectroscopy. The most characteristic peaks in the ATR-FTIR spectrum of GEN were assigned to the C1 = C2 stretch at 1652 cm^{-1}, and the C = O stretch, O7-H22 bend, and ring A C-C stretch at 1518 cm^{-1} (Fig. 2) [19].

Table 1 presents the relative absorbances in the SC layers at 1652 cm^{-1} and 1518 cm^{-1}, which correspond to the amounts of GEN that penetrated into the SC after conventional and EP treatments (Fig. 3). The drug delivery and the onset time for transport depend on the electrical parameters of the pulses and the physicochemical properties of the drug [3]. It was found that EP treatment at 700 V for 1 min EP treatment did not enhance the GEN transdermal delivery relative to the conventional treatment. This may be explained by the high viscosity of the drug carrier, which decreases the efficacy of EP on the skin [29]. Slightly deeper GEN penetration was ensured by EP treatment at 900 V for 1 min, but the total amount of GEN did not exceed that for conventional treatment with LLC-GEN. However, EP treatment at 700 V for 2 min resulted in a deeper penetration of a 2-fold amount of the drug than without EP treatment (revealed at both characteristic bonds of GEN). The best penetration profile of GEN was obtained on EP treatment at 900 V for 2 min, when the total amount of the drug was 3-fold greater as compared with conventional treatment at both assigned bonds ($p < 0.001$*** and $p < 0.05$*), but the GEN distribution was not consistent. The presence of GEN was not seen in the 5th and 6th tape strips, whereas the drug appeared again in the 7th strips. This phenomenon could be explained by the electrical breakdown of

#253195 Received 2 Nov 2015; revised 18 Nov 2015; accepted 18 Nov 2015; published 8 Dec 2015

the SC layers. Furthermore the amount of drug that penetrated increased with increasing voltage of the pulses [30, 31].

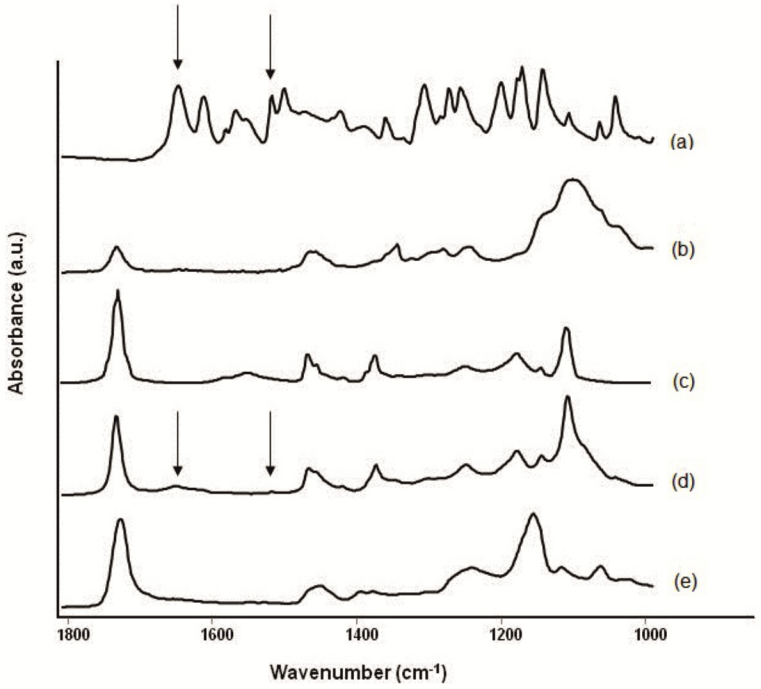

Fig. 2. ATR-FTIR spectra of pure GEN (a), Cremophor RH 40 (b), isopropyl myristate (c), LLC-GEN composition (d) and non-treated SC (e).

Table 1. Intensities of GEN in the different layers of the treated SC (average value ± SD, n = 3) (CT = conventional treatment).

	Treated with LLC-GEN (CT, 2 min)		**Treated with LLC-GEN + EP (700 V, 1 min)**		**Treated with LLC-GEN + EP (900 V, 1 min)**		**Treated with LLC-GEN + EP (700 V, 2 min)**		**Treated with LLC-GEN + EP (900 V, 2 min)**	
No. of tape strips	**Absorbance at**		**Absorbance at**		**Absorbance at**		**Absorbance at**		**Absorbance at**	
	1652 cm^{-1} GEN	**1518 cm^{-1} GEN**	**1652 cm^{-1} GEN**	**1518 cm^{-1} GEN**	**1652 cm^{-1} GEN**	**1518 cm^{-1} GEN**	**1652 cm^{-1} GEN**	**1518 cm^{-1} GEN**	**1652 cm^{-1} GEN**	**1518 cm^{-1} GEN**
1	0.06 ± 0.03	0.05 ± 0.02	0.05 ± 0.05	0.04 ± 0.04	0.04 ± 0.01	0.03 ± 0.00	0.15 ± 0.02	0.12 ± 0.02	0.22 ± 0.10	0.18 ± 0.08
2	0.03 ± 0.01	0.03 ± 0.01	0.02 ± 0.02	0.02 ± 0.01	0.01 ± 0.01	0.01 ± 0.01	0.04 ± 0.02	0.04 ± 0.02	0.08 ± 0.06	0.07 ± 0.05
3	0.03 ± 0.02	0.02 ± 0.01	-	-	0.03 ± 0.00	0,03 ± 0.00	0.06 ± 0.00	0.05 ± 0.00	0.06 ± 0.00	0.05 ± 0.00
4	-	-	-	-	0.03 ± 0.00	0.02 ± 0.00	0.02 ± 0.00	0.02 ± 0.00	0.03 ± 0.01	0.03 ± 0.01
5	-	-	-	-	-	-	0.01 ± 0.00	0.01 ± 0.00	-	-
6	-	-	-	-	-	-	-	-	-	-
7	-	-	-	-	-	-	-	-	0.02 ± 0.02	0.02 ± 0.01
8	-	-	-	-	-	-	-	-	-	-

#253195 Received 2 Nov 2015; revised 18 Nov 2015; accepted 18 Nov 2015; published 8 Dec 2015

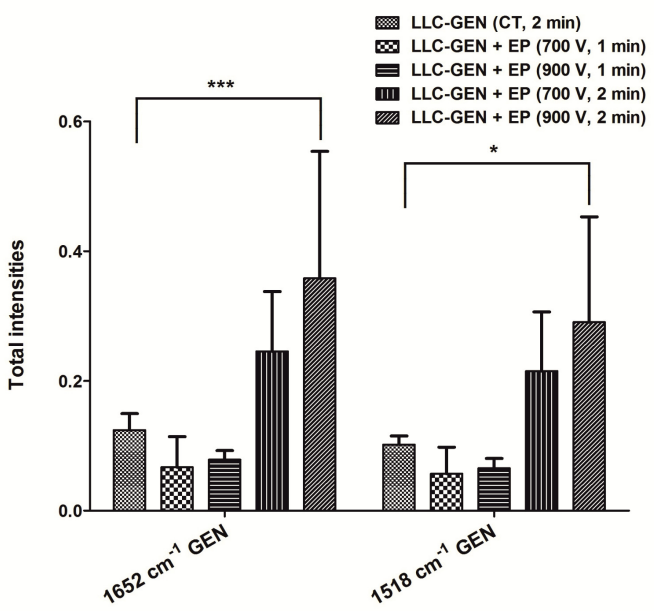

Fig. 3. Total intensities of GEN at 1652 cm^{-1} and at 1518 cm^{-1}. Conventional treatment (CT) was used as a control. $p < 0.001$*** and $p < 0.05$* vs. EP-treated group.

3.2. Raman spectroscopy

The deeper skin penetration of LLC-GEN containing the lipophilic ingredients CRH40 and IPM was studied in Raman scattering experiments. Raman chemical mapping was employed to confirm the localization of GEN at various depths of the skin specimens. Since ATR-FTIR demonstrated that EP treatment at 900 V ensured deeper penetration than that at 700 V, EP treatments at 900 V for 1 and 2 min were chosen for comparison with conventional treatment by Raman spectroscopy.

Figure 4 depicts the experimental Raman spectra of pure CRH40, IPM and GEN in the wavenumber range 2000-200 cm^{-1}. As model solution, GEN was dissolved in CRH40 and IPM containing LLC (GEN content 3 wt.%) to observe the physical state of GEN. Six common characteristic ranges can be seen in the spectra of CRH40 and IPM, with peaks centred at 1733, ~1442-1437, 1300, 1063 and 843-823 cm^{-1}, and the spectra of CRH40, IPM and the LLC-GEN composition are very similar. Table 2 lists the Raman bands of the components and the LLC-GEN composition. The lipid components used in this study have similar chemical structures and therefore similar Raman bands. The Raman spectrum of the LLC-GEN is basically the sum of the individual spectra, with minor shifts at around 1440 and 1079 cm^{-1} (Fig. 4(c)), indicating that the CH_2-CH_3 bonds of the LLC ingredients were affected by the interaction. Only a few Raman peaks of GEN were observed in the spectrum of LLC-GEN, at around 1617, 1062, 991, 887 and 789 cm^{-1}. For GEN, two characteristic peaks, centred at 1617 and 789 cm^{-1}, were assigned to the vibration of the C = C bond in ring B and the C-C-C, C-C and C = O bonds in ring C of the isoflavonoid molecule. These bands, free from interference from LLC ingredient bands, were chosen to confirm the localization of GEN in the skin specimen.

Raman spectra were acquired from skin treated with LLC-GEN and from non-treated intact *ex vivo* skin (Fig. 5), both perpendicular to the SC at equivalent depth (1000 μm). In the Raman spectrum of the treated skin, characteristic peaks of GEN and the LLC ingredients were observed at around 1670-1650 and 1470-1410 cm^{-1}, respectively. The band of interest

#253195 Received 2 Nov 2015; revised 18 Nov 2015; accepted 18 Nov 2015; published 8 Dec 2015

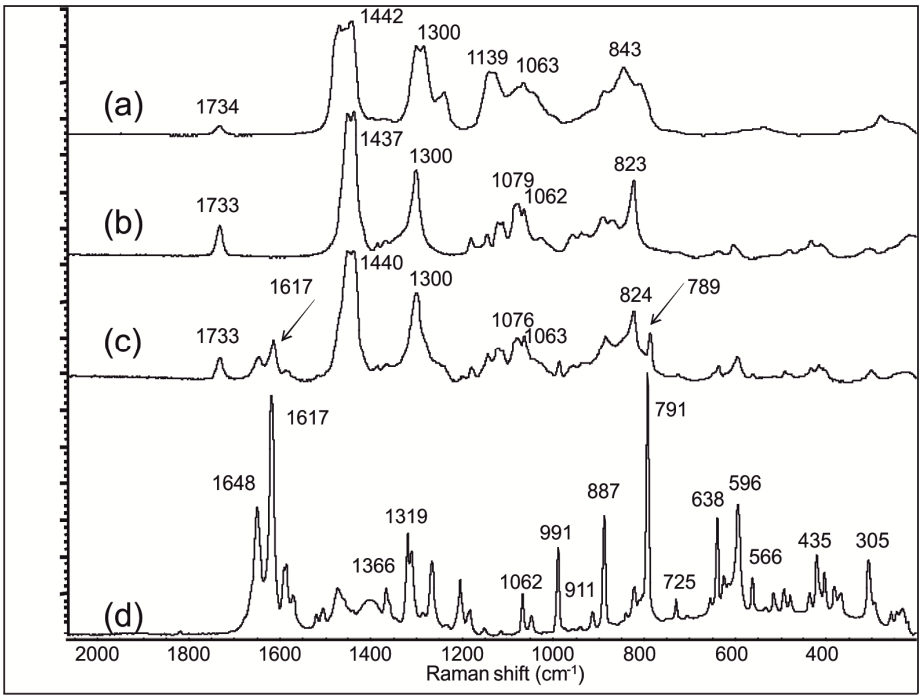

Fig. 4. Experimental Raman spectra of Cremophor RH 40 (a), isopropyl myristate (b), LLC-GEN composition (c) and pure GEN (d).

Table 2. Observed Raman peaks and peak assignments of individual components and LLC-GEN (*str* = stretching, *def* = deformation, *tw* = twisting).

Assignment	Cremophor RH 40	Isopropyl myristate	LLC-GEN	GEN
str C = O (ester)	1734	1733	1733	-
str C = C (ring A)	-	-	1648	1648
str C = C (ring B)	-	-	1617	1617
def CH2-CH3	1442	1437	1440	-
str C = C	-	-	-	1366
	-	-	-	1319
def CH2 and *tw* CH3	1300	1300	1300	-
str C-C	1139	-	-	-
		1079	1076	-
str O-C	1063	1062	1063	1062
str C = C and C-C-C (ring A)	-	-	991	991
str C = C (ring A) and C-C-C (ring C)	-	-	887	887
str C-CH (aromatic ring)	843	-	-	-
	-	823	824	-
str C-C-C (C ring), *str* C = O	-	-	789	791
str C-C-C and C = C (ring A)	-	601	596	596
str C-C-C (rings A and C)	-	-	-	566

centred at 1440 cm^{-1} was assigned to the vibration of the amide functional group due to C = O stretching and $–CH_2$, $-CH_3$ bending of the skin lipid constituents. The C = C stretching

#253195 Received 2 Nov 2015; revised 18 Nov 2015; accepted 18 Nov 2015; published 8 Dec 2015

observed at 1617 cm^{-1} arose predominantly from the GEN isoflavonoid. The chemical mapping therefore confirmed the presence of the characteristic GEN band at around 1617 cm^{-1}. This peak is close to the vibrations of the native skin components. The skin component peaks at 1608 and 1453 cm^{-1} are well known to be associated with the C = C vibration of phenylalanine, the CH_2 scissoring of lipids and the CH_2, CH_3 deformation of proteins in the native skin.

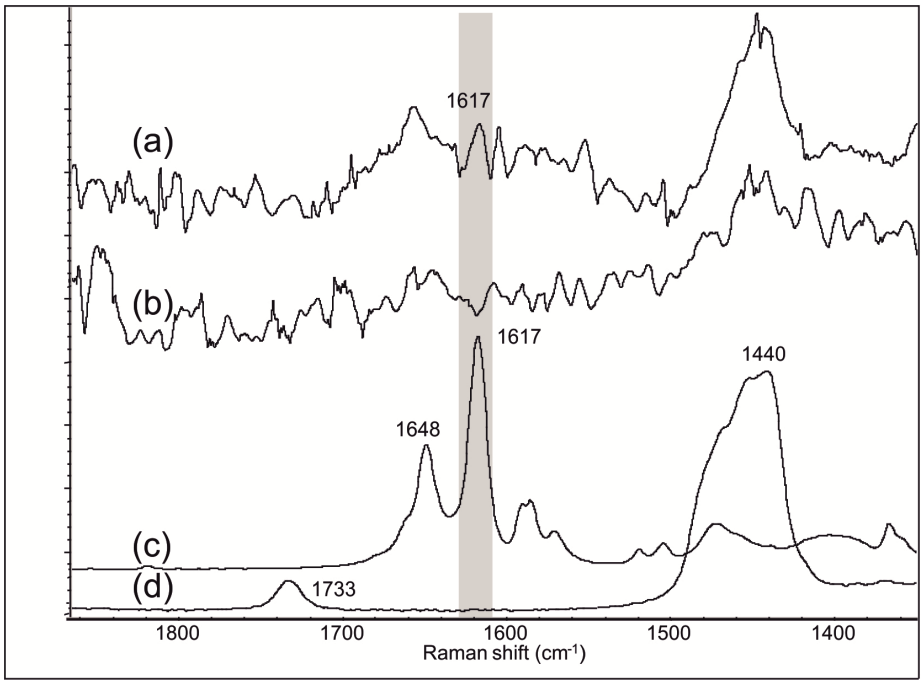

Fig. 5. Raman spectra of GEN-treated skin (900 V, 2 min, 1000 μm depth) (a), non-treated skin specimen as control (1000 μm depth) (b), pure GEN (c) and GEN-free LLC composition (d) in the range 1900-1350 cm^{-1}.

Figure 6 displays qualitative distribution maps of the LLC components and GEN in animal skin specimens after different EP protocols, at 10-fold magnification. It was of interest to determine whether GEN diffusion is limited to the SC or to the epidermis or dermis. As discussed in the Materials and methods section, as the skin specimens were planar, there was no need for the z-axis and adjustment of the depth values. 1300 μm deep sections of the skin specimen were investigated, from corresponding top to bottom to the SC → epidermis → dermis. In order to confirm GEN diffusion, the chemical maps were resolved. The characteristic bands obtained for GEN at around 1617 cm^{-1} were used to visualize the spatial distribution of GEN from the Raman chemical mapping. The resolution of the chemical map and hence the identification of the ingredients present were achieved by using a multivariate curve resolution – alternating least squares chemometric method. This method furnishes the response profiles of different components in complex samples, and provides information about the composition.

The presence of bands due to GEN and the LLC components in the upper layer of the skin (0-1000 μm) clearly indicates a good distribution following conventional treatment of the LLC-GEN composition (Fig. 6(a)). After the 900 V process for 1 min, GEN was accumulated in the middle section of the dermis (Fig. 6(b)). The penetration of GEN into the dermis was slowed by the dermis a being dense network of collagen fibres. The GEN and LLC component contents of the skin specimen (to a depth of 1300 μm) were relatively low after the 900 V EP process for 2 min (Fig. 6(c)), indicating that the GEN penetrated into the deep

#253195 Received 2 Nov 2015; revised 18 Nov 2015; accepted 18 Nov 2015; published 8 Dec 2015

layer of the dermis. Although the difference between the EP processes for 1 and 2 min may seem minor, the slower diffusion of GEN may be presumed because of the enrichment of the LLC components (as vehicles of GEN) in the 1000-1300 µm deep section. In the absence of the EP process, the epidermal and upper dermal regions serve as a tight barrier, impeding deep GEN delivery. Thus, slow diffusion of the GEN took place.

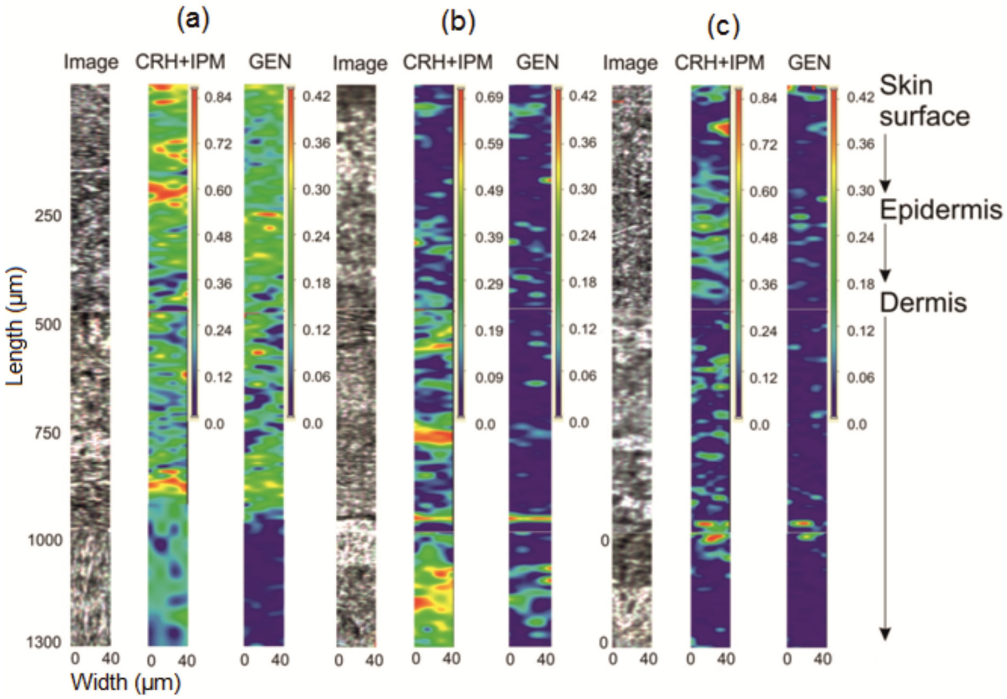

Fig. 6. Qualitative Raman maps of GEN distribution in animal skin specimens following different EP protocols (at 10-fold magnification). Conventionally treated skin as control (a), skin treated with EP at 900 V for 1 min (b) and skin treated with EP at 900 V for 2 min (c). Image: LLC-GEN composition, CRH + IPM: Cremophor RH 40 + isopropyl myristate, GEN: Genistein. Colour coding of content: red>yellow>green>blue.

4. Conclusions

In summary, the results of this study have demonstrated that our newly developed LLC formulation is a suitable carrier for the poor water soluble GEN. The penetration through the skin was ensured already by LLC-GEN alone application. However the combination of LLC nanocarrier system with EP was resulted rapid and more effective transdermal drug transport than alone LLC-GEN formulation. The synergistic effect of EP was verified by both the ATR-FTIR and the Raman spectroscopy. It could be concluded from our study that combination of LLC an EP process is very promising, but the optimization of drug penetration is necessary.

Acknowledgments

The authors are grateful to the Dr Derm Equipment for providing the Mezoforte Duo Mez 120905-D device. Dr. Corina Danciu was financed by the UMFT grant - Parteneriate încercetarea fundamentalăinovativă-PIII-C2-PCFI-2015/2016 acronim FLAVOFORM.

VI.

Journal of Pharmaceutical Sciences xxx (2016) 1–7

Contents lists available at ScienceDirect

Journal of Pharmaceutical Sciences

journal homepage: www.jpharmsci.org

Research Article

Investigation of the Efficacy of Transdermal Penetration Enhancers Through the Use of Human Skin and a Skin Mimic Artificial Membrane

Boglárka Balázs [1, 2], Gábor Vizserálek [3], Szilvia Berkó [1], Mária Budai-Szűcs [1], András Kelemen [4], Bálint Sinkó [3, 5], Krisztina Takács-Novák [3], Piroska Szabó-Révész [1], Erzsébet Csányi [1, *]

[1] *Department of Pharmaceutical Technology, University of Szeged, Szeged H-6720, Hungary*
[2] *Gedeon Richter Plc., Budapest H-1103, Hungary*
[3] *Department of Pharmaceutical Chemistry, Semmelweis University, Budapest H-1092, Hungary*
[4] *Department of Applied Informatics, University of Szeged, Szeged H-6720, Hungary*
[5] *SinkoLAB Scientific, Sopron H-9400, Hungary*

ARTICLE INFO

Article history:
Received 24 August 2015
Revised 27 October 2015
Accepted 19 November 2015
Available online xxx

Keywords:
skin
transdermal
transdermal drug delivery
permeability
permeation enhancers
surfactants
hydrogels
in vitro models

ABSTRACT

The aim of this study was to investigate the behavior of promising penetration enhancers through the use of 2 different skin test systems. Hydrogel-based transdermal formulations were developed with ibuprofen as a nonsteroidal anti-inflammatory drug. Transcutol and sucrose esters were used as biocompatible penetration enhancers. The permeability measurements were performed with *ex vivo* Franz diffusion cell methods and a newly developed Skin Parallel Artificial Membrane Permeability Assays (PAMPA) model. Franz diffusion measurement is commonly used as a research tool in studies of diffusion through synthetic membranes *in vitro* or penetration through *ex vivo* human skin, whereas Skin PAMPA involves recently published artificial membrane-based technology for the fast prediction of skin penetration. It is a 96-well plate-based model with optimized artificial membrane structure containing free fatty acid, cholesterol, and synthetic ceramide analog compounds to mimic the stratum corneum barrier function. Transdermal preparations containing 2.64% of different sucrose esters and/or Transcutol and a constant (5%) of ibuprofen were investigated to determine the effects of these penetration enhancers. The study demonstrated the good correlation of the permeability data obtained through use of human skin membrane and the *in vitro* Skin PAMPA system. The Skin PAMPA artificial membrane serves as quick and relatively deep tool in the early stages of transdermal delivery systems, through which the enhancing efficacy of excipients can be screened so as to facilitate the choice of effective penetration components.

Introduction

Transdermal drug delivery has received increased attention in recent years thanks to its numerous advantages over the oral and injection routes, such as avoidance of the hepatic “first-pass” metabolism, sustained drug delivery, protection of the gastrointestinal tract from drugs, and good patient compliance. The main penetration barrier for most drugs is the stratum corneum (SC), the outermost 10-15 μm thick zone of the epidermis. The SC consists of several layers of almost nonpermeable, nonviable cornified cells (corneocytes) and intercellular lipid domains. These lipids comprise approximately 50% ceramides, 25% cholesterol, 15% free fatty acids, and some minor components.[1]

The strategies most widely applied with the aim of improving drug penetration involve the use of chemical penetration enhancers and skin hydration.[2] In this respect, we report here on the development of hydrogel formulations containing penetration enhancers for the transdermal delivery of ibuprofen (IBU), a nonsteroidal anti-inflammatory drug frequently used for the treatment of musculoskeletal injuries. The transdermal delivery of IBU is a convenient way to minimize the potential risk of adverse gastrointestinal events (e.g., bleeding, ulceration, and perforation of the stomach).[3] The physicochemical properties of IBU are

*Correspondence to: Erzsébet Csányi (Telephone: +36-62-545-573; Fax: +36-62-545-571).
E-mail address: csanyi@pharm.u-szeged.hu (E. Csányi).

http://dx.doi.org/10.1016/S0022-3549(15)00172-0
0022-3549/

appropriate for its development as a transdermal gel formulation,[4] but the use of a penetration enhancer is unescapable because of the highly structured SC.[1]

Transcutol (TR) and sucrose fatty acid esters (SEs) were chosen as penetration enhancer excipients. TR is a powerful solubilizing agent and enhances the percutaneous penetration of various drugs, especially when it is used in combination with suitable surfactants.[5,6] SEs, a new generation of nonionic surfactants, are likewise favorable penetration enhancers.[7] They have low toxicity, good biocompatibility, and excellent biodegradability, and they cause little dermatologic damage.[8,9] The extent of the ability of the SEs to promote drug release *in vitro* has been reported to depend on the hydrophilic-lipophilic balance (HLB) value and the C atom number of the fatty acid chain in the SEs.[10] The effectiveness of SEs in combination with TR has also been demonstrated in the experiments on porcine ear skin and human skin.[6,11]

The efficacy of a surfactant in enhancing transdermal delivery is dependent on its structure, the physicochemical properties of the drug, and the nature of the vehicle, the main factors defining the surfactant–skin interaction.[12,13] Numerous studies have demonstrated that SEs and TR interact with the skin.[6,11,14,15] However, simple *in vitro*[10] or *ex vivo* animal membrane diffusion measurements[16] are not sufficient to allow an evaluation of the penetration-enhancing effects of different SEs. The SC in animals differs from the human SC in thickness, the number of corneocyte layers, the hair density, the water content, the lipid profile, and the morphology.[17] To select the best formulation for a clinical study, it is important to investigate transdermal formulations with *ex vivo* human skin penetration methods.

The transepidermal water loss (TEWL) is an indicator of the integrity of the skin barrier, and measurement of the TEWL is an easy and rapid noninvasive means of examining the effects of new transdermal systems.[18,19] For penetration investigations, measurements were made across excised human epidermis with a vertical Franz diffusion cell.[20] Because the use of human skin in research encounters ethical, health, and supply problems,[17] our transdermal gels were additionally tested in newly developed Skin Parallel Artificial Membrane Permeability Assays (Skin PAMPA),[21] developed as a rapid, reproducible, and cost-efficient system for the prediction of skin penetration. The Skin PAMPA was designed to be biomimetic, that is, the same or similar components have been applied as present in the most important barrier of human skin. As the main barrier of the human skin, it is known to be the outermost layer of epidermis, the SC, Skin PAMPA has been designed to mimic the features of this layer. SC composes of corneocytes embedded into a multilamellar lipid layer. The lipid layer consists of a mixture of ceramides, cholesterol, and free fatty acids as major components and provides the main route of penetration, the paracellular pathway. The Skin PAMPA membrane was created by using free fatty acid, cholesterol, and a synthetic ceramide analog compound (long-chain tartaric acid diamide derivative named certramide) to mimic the features of ceramide in the lipid matrix.[22,23] The optimized artificial membrane mimics molecular transport through the SC, and the commercially already available Skin PAMPA™ system can serve as a good alternative tool for penetration studies of transdermal formulations.[24]

The aims of the present study were to compare different types of SEs (alone or in combination with TR) from the aspect of their ability to enhance the delivery of IBU through human skin and to prove the usefulness of the Skin PAMPA model as a valuable tool in research on transdermal systems. The Skin Pampa model has never been used earlier to investigate transdermal penetration enhancers but the use of it could offer such advantages as a simple and cost-effective early phase screening system of penetration enhancers.

Materials and Methods

Sample Preparation

A penetration-enhancing free hydrogel (control gel) was prepared by the following procedure. A 5 wt% IBU (Sigma-Aldrich, St Louis, MO) was dissolved in polyethylene glycol 400 (20 wt%; Hungaropharma Ltd., Budapest, Hungary) and this solution was added to 3 wt% Carbopol 971 (Lubrizol Corporation/Azelis, Budapest, Hungary) hydrogel prepared with distilled water. The pH was adjusted to 7.0 by adding trolamine (7 wt%; Hungaropharma Ltd.). Sucrose esters, sucrose laurate D-1216 (SL), and sucrose myristate C-1416 (SM) were purchased from Mitsubishi-Kagaku Foods Corporation, Tokyo, Japan. To compare the 2 SEs, 2.64 wt% was incorporated in Carbopol 971-based hydrogel (SL gel and SM gel). A 2.64 wt% was chosen because this gave the maximum SE concentration-containing hydrogel which did not require a centrifugation process to remove the bubbles. Similar compositions were prepared by using 10 wt% TR (Gattefossé and Lubrizol Corporation/Azelis, Budapest, Hungary) (TR gel); 2.64 wt% SE + 10% TR-containing gels too were prepared (SL + TR and SM + TR gel).

TEWL Measurements

Measurements were performed under standardized conditions (room temperature of 21°C-23°C and 40%-50% relative humidity). Seven healthy female volunteers aged between 23 and 60 years with no history of dermatologic diseases or allergy participated in the experiment. Informed consent was obtained from all these volunteers, and the study was approved by the local ethics committee (the Regional and Institutional Human Medical Biological Research Ethics Committee at the University of Szeged). The volunteers were asked not to apply any moisturizer or cosmetic product for at least 24 h before the process. They were given 30 min to adapt to the measurement room conditions. During the experiment, samples were applied to the dorsal region of the hand of all the subjects. TEWL values were determined on the same area of the skin before and after 30 and 150 min of the sample application. The measured values were compared with the values detected on the nontreated skin; the changes in TEWL were expressed in percentage.[25-27] Measurements were performed with a Tewameter® TM 300 instrument (Courage and Khazaka Electronic GmbH, Cologne, Germany).

Drug Diffusion and Penetration Investigations

Preparation of Heat-Separated Epidermis

Excised human skin was obtained during abdominal plastic surgery on a Caucasian female patient (aged between 30 and 40 years). This was approved in advance by the Ethical Committee of the Human Investigation Review Board at Albert Szent-Györgyi Clinical Centre, University of Szeged. The subcutaneous fat tissue was separated from the outer skin layers after the excision, and the skin was stored at −20°C overnight. Then, after thorough defrosting, membrane separation was achieved with a previously reported method.[28] Individual portions were immersed in water at 60°C for 90 s. After removal of the skin from the water, it was placed SC side up on a filter paper, and the epidermis (comprising the SC and the viable epidermis) was gently removed from the underlying dermis with the use of forceps. The latter was discarded, and the epidermal membrane was floated onto the surface of phosphate buffer solution (pH = 7.4) for at least 20 min and then placed on a supporting Porafil membrane (cellulose acetate, pore diameter 0.45 μm).[29,30]

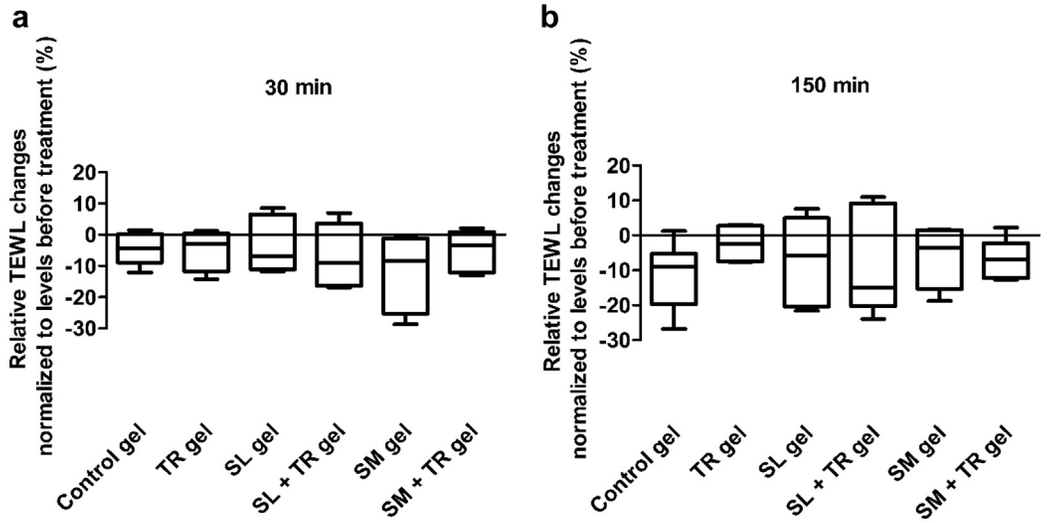

Figure 1. TEWL measurement after single application of 6 ibuprofen-free topical formulations: (a) 30 min and (b) 150 min after treatment with control gel, TR gel, SL gel, SL + TR gel, SM gel, and SM + TR gel. Values are given as percentages referred to TEWL before treatments. The plots are medians with 25th and 75th percentiles.

Franz Diffusion Cell Method

Membrane permeability studies were carried out with a vertical Franz diffusion cell system (Hanson Microette TM Topical & Transdermal Diffusion Cell System; Hanson Research Corporation, Chatsworth, CA). The surface area for diffusion measured 1.767 cm^2. A stirring rate of 450 rpm was used. The donor phase was 0.30 g of sample, which was placed on the epidermis supported on the cellulose acetate membrane (Porafil; Machenerey-Nagel, Germany, and Pall Life Sciences, Washington, NY). Phosphate buffer solution (pH = 7.4) was used as an acceptor phase.[4] The receptor medium temperature was maintained at 37 ± 0.5°C throughout the experiments to support the physiological skin temperature (32 ± 0.5°C) on the membrane in the Franz cell.[31] Experiments were performed for 16 h. Samples of 0.8 mL were taken from the acceptor phase by the autosampler (Hanson Microette Autosampling System; Hanson Research Co., Chatsworth, CA) and replaced with fresh receiving medium. The absorbance of the IBU content was measured with a UV spectrophotometer (Helios α Thermospectronic UV-spectrophotometer v4.55, Unicam; Thermo Fisher Scientific, Waltham, MA) at a wavelength of λ = 264 nm via a previously obtained calibration plot. The concentration of IBU and the measured absorbance correlated linearly. Five parallel measurements were made of the amount of IBU that penetrated over a period. Results were expressed as mean ± SD.

PAMPA Method

The Skin PAMPA™ sandwiches and the stirring bars (P/N: 110211) were purchased from Pion Inc. (Billerica, MA). The UV plates were from Greiner Bio-One GmbH (Kremsmünster, Austria; UV-star micro plate, clear, flat bottom, half area). Standard Britton-Robinson buffers were made in-house, and 0.2 M sodium hydroxide was used to adjust the pH to 7.4 to serve the acceptor solution. The Skin PAMPA™ sandwiches were used after an overnight hydration (Hydration Solution, Pion Inc. P/N: 120706). The bottom part of the original Skin PAMPA™ sandwich was replaced with Formulation Plate purchased from Pion Inc. (P/N:120806). Seventy microliters of gel was transferred to the Formulation Plate. The top plate was filled with 250 μL of fresh acceptor solution, and stirring bars were applied in every well to avoid the effect of the unstirred water layer. The Gut-Box™ from Pion Inc. was used for stirring. The resultant system was incubated at 32°C. The acceptor solution was sampled after 0.5, 1, 2, 3, 4, 5, 6, 7, 8, 9, 10, 12, and 16 hours of incubation. After each individual incubation period, 150 μL from the acceptor compartment was transferred to UV plates, and the transferred volume of receiving medium was replaced with fresh acceptor solution. UV absorption (230-500 nm) was measured with a Tecan Infinite M200 instrument driven by Magellan 6 software (Tecan Group Ltd., Männedorf, Switzerland). Calibration for the quantitative analysis was performed with IBU as standard compound. The calibration curve (Beer-Lambert law: $A = A^{1\%}_{1cm} * c * l$) was prepared by using 8 dilutions in Britton-Robinson buffer of pH 7.4. The absorption maximum was found at 264 nm. The linearity range was 100-600 μg/mL; the specific absorbtivity ($A^{1\%}_{1cm}$) was 10.872; $R^2 = 0.9986$. Calibration plots were constructed by least-square linear regression analysis. Five parallel measurements were performed for all formulations prepared for this study.

Dissolution Analysis

Penetration parameters were obtained from the cumulative amount of IBU penetrated per cm^2 versus time plots (Q). The transdermal flux (J) was calculated from the slope of the concentration versus time profile in the receiver compartment and expressed in μg/cm^2/h. For the linear regression analysis, the linear range of the incubation period from 1 to 6 h was selected, and this range was used to calculate the flux data of the compounds.

The effectiveness of a penetration enhancer was determined by comparing the flux of IBU in the presence and the absence of

Table 1
Penetration Parameters of Ibuprofen Through Human Epidermis After 16 h

Formulation	Q (μg/cm^2)	J (μg/cm^2/h)	EF
Control gel	463.95 ± 110.50	42.72	–
TR gel	193.36 ± 87.13	14.23	0.33
SL gel	866.79 ± 320.42	67.93	1.59
SM gel	889.22 ± 348.09	54.28	1.27
SL + TR gel	825.08 ± 384.67	54.38	1.27
SM + TR gel	1527.19 ± 764.62	91.59	2.14

Q, cumulative amount of IBU penetrated per cm^2 versus time plots, average values ± SD, n = 5; J, slope of the concentration versus time profile in the receiver compartment; EF, flux of penetrant from the gel containing an enhancer divided by the flux of penetrant from the control gel without an enhancer.

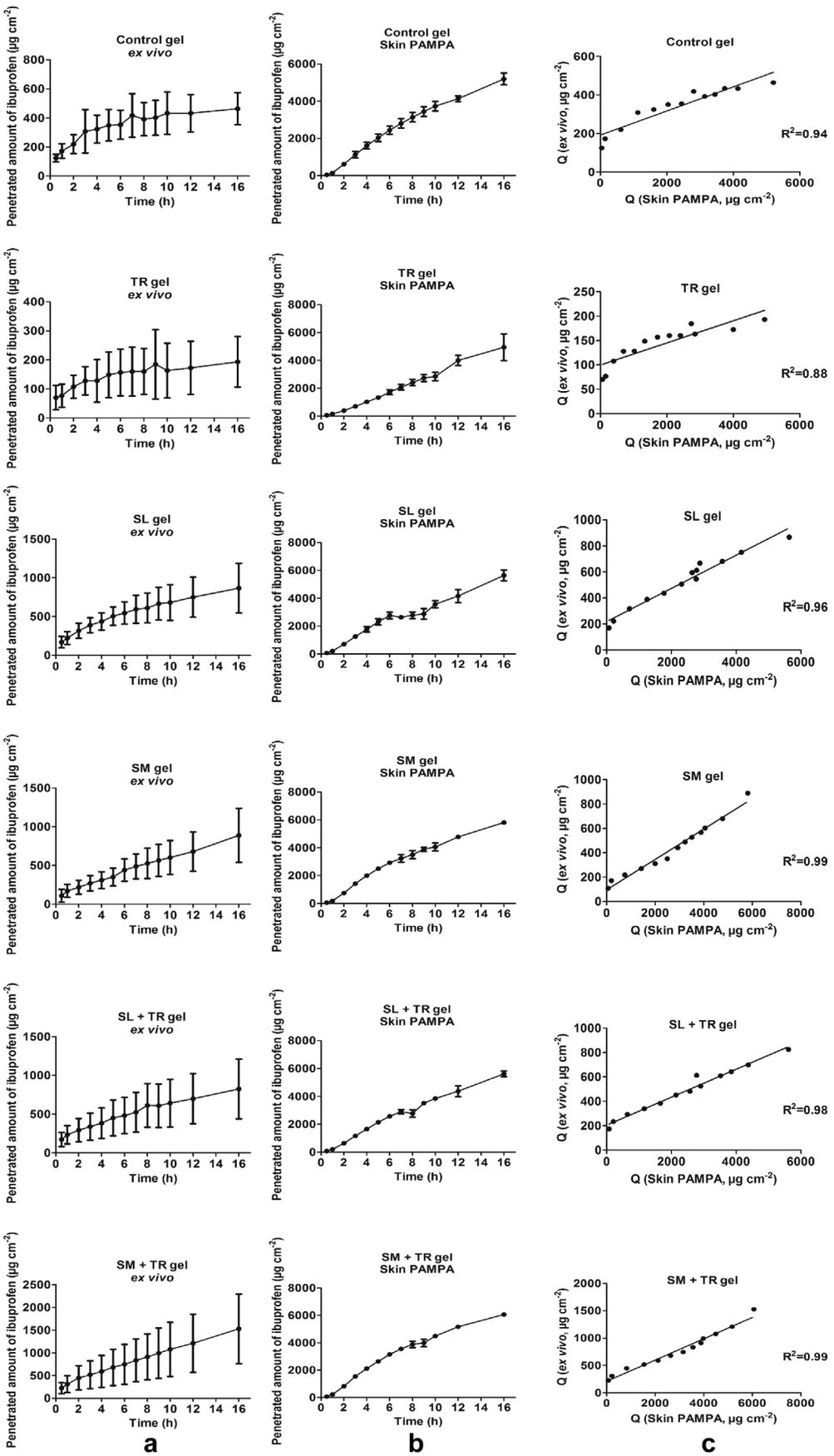

Figure 2. Ibuprofen penetration profiles of transdermal formulations (a) with the *ex vivo* Franz cell method, (b) the *in vitro* Skin PAMPA system, and (c) the correlations between the amounts of drug penetrated through human skin and Skin PAMPA.

the enhancer. This was defined as the enhancement factor (EF), which was calculated via the following equation.[32]

$$\text{EF} = (\text{flux of penetrant from the gel containing an enhancer})/(\text{flux of penetrant from the control gel without an enhancer}). \quad (1)$$

Statistics

Results are presented as means ± SD. Two-way ANOVA was used to determine the statistical difference between the data for the various preparations and the control gel; ** and *** indicate $p < 0.01$ and $p < 0.001$. Statistical analysis was performed through the use of GraphPad Prism software (Graph-Pad Software Inc., La Jolla, CA).

Correlation

The correlation between Skin PAMPA model and human epidermis was calculated by the following formula (Eq. 2):

$$R = \frac{\sum(x-\bar{x})(y-\bar{y})}{\sqrt{\sum(x-\bar{x})^2 \sum(y-\bar{y})^2}} \quad (2)$$

where R is the correlation, x and y denote the amount of penetrated drug as a function of time t in case of human epidermis and the Skin PAMPA model, respectively, and are the average values of x and y.

Results and Discussion

TEWL measurement is the most appropriate noninvasive model with which to study the skin barrier function and the effects of penetration enhancers. Application of the control formulation leads to lower TEWL values than the level before treatment. Even after 150 min, the skin was well protected and lastingly by the control gel. This phenomenon can be seen in the cases of TR, SM, and the combination SM + TR. Treatment with SL or SL + TR-containing gels resulted in only slight increases of TEWL. The changes were not statistically significant as compared with the control gel. The skin barrier structure remained basically unaltered for all the tested formulations. Although TR and the SEs caused minimal modifications in the SC barrier structure,[6,15] these hydrogel-based trandsdermal preparations protected the special SC structure (Fig. 1).

The *in vitro* and *in vivo* skin permeability of IBU is improved by the use of a hydrophilic vehicle alone,[33] but it is increased even more by the application of penetration enhancers such as SEs.[15] Table 1 presents the penetration parameters of IBU through excised human epidermis. The SE gels increased the IBU penetration through the skin as appreciably compared with the enhancer-free control gel, but the TR gel did not enhance the IBU penetration. TR is thought to give rise to its penetration-enhancing function by increasing the solubility of the applied drug. However, TR has also been observed to display an accumulation property by increasing the skin accumulation of topically applied drugs without a concomitant increase in transdermal penetration. TR causes the swelling of intercellular SC lipids, and lipophilic drugs such as IBU are trapped within the swollen SC lipids.[34]

As regard SEs, SL (C = 12, HLB = 16) and SM (C = 14, HLB = 16) were selected because SEs with lower C numbers and higher HLB values increase drug release more than SEs with longer fatty acids and lower HLBs.[10] SL has been reported to maximize the effect of a surfactant on membrane permeability.[35] SEs may act by disrupting the ceramide–cholesterol or cholesterol–cholesterol interaction.

Table 2
Penetration Parameters of Ibuprofen Through the Skin PAMPA Model After 16 h

Formulation	Q (μg/cm^2)	J (μg/cm^2/h)	EF
Control gel	5204.95 ± 311.23	432.35	–
TR gel	4941.95 ± 966.97	329.95	0.76
SL gel	5642.38 ± 383.43	517.06	1.20
SM gel	5812.12 ± 150.72	512.81	1.19
SL + TR gel	5616.67 ± 208.33	483.72	1.12
SM + TR gel	6062.98 ± 121.23	563.1	1.30

Q, cumulative amount of IBU penetrated per cm^2 versus time plots, average values ± SD, n = 5; J, slope of the concentration versus time profile in the receiver compartment; EF, flux of penetrant from the gel containing an enhancer divided by the flux of penetrant from the control gel without an enhancer.

Increase of the carbon chain length of the fatty acids results in their molecular weights increasing, and their mobility within the skin layers is also expected to decrease, which may explain their lower penetration enhancement effect.[16] *Ex vivo* fluxes (representing the absorption rate per unit area) reveal that SL induces faster IBU release than does SM, whereas the amount of penetrated IBU after 16 h was higher in the case of the SM gel. The *ex vivo* drug release behavior data indicated that SL was not a better penetration enhancer for IBU than SM (Table 1).

In contrast with the application of TR alone, it has been reported that its combination with SE resulted in facilitated surfactant absorption into the deeper layers of the SC. This synergistic enhancement between SE and TR affects only the penetration depth of the formulation and does not increase the amount of drug that penetrates.[11] The SM + TR gel exhibited the best penetration parameters (Table 1) and penetration profile for IBU (Fig. 2a). The SL + TR gel resulted in a lower penetration than that with the SL gel, but the difference was not statistically significant (Fig. 2a). A possible reason for this phenomenon could be that the TR depot effect predominated in the case of the SL + TR gel because SL is not able to cause so much lipid disruption. In contrast with SL, SM may cause a greater extent of lipid alteration through its higher carbon chain and this prevents the TR depot effect. Furthermore, SM in combination with TR proved to penetrate the skin well, and there was a marked increase in IBU release from the SM + TR gel as

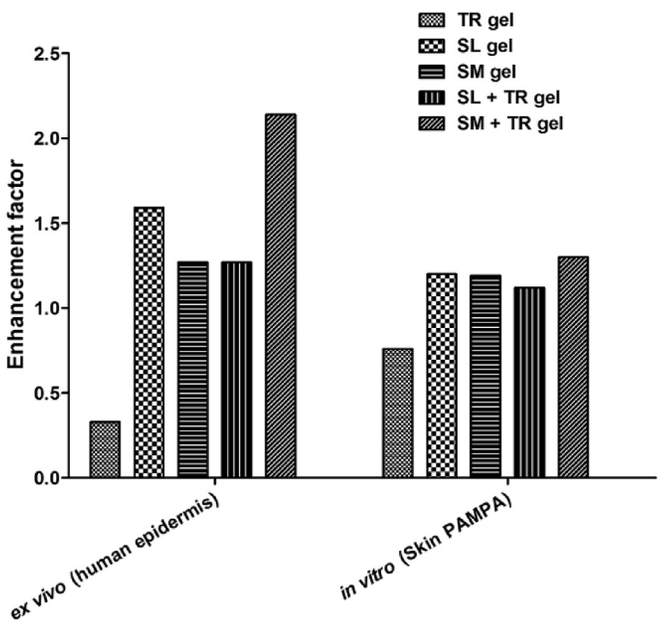

Figure 3. *Ex vivo* (human epidermis) and *in vitro* (Skin PAMPA) enhancement factors of different formulations.

compared with the control gel. The *ex vivo* statistical analysis indicated that only the SM + TR gel resulted in a significantly ($p < 0.001^{***}$) higher penetrated IBU amount relative to the control gel after 7 h (Fig. 2a).

Table 2 presents the penetration data on the different transdermal formulations tested with the Skin PAMPA system. Lower SD and higher penetration data are observed with the PAMPA model than with the Franz cell method, which may be caused by the differences in the membrane structure in the 2 procedures. However, the penetration profiles obtained with the Skin PAMPA and *ex vivo* Franz cell methods were in good agreement in most cases (Figs. 2a and 2b). The differences between the PAMPA and Franz cell results clearly indicate the TR depot phenomena which can not be observed through the synthetic membrane.[36] The decreased amount of IBU penetrated from the TR gel relative to the control gel was statistically significant after 3 h ($p < 0.001^{***}$; Fig. 2b). The penetration-enhancing effect of the SEs is clear. Although SL rather hampers the penetration through the synthetic membrane, it increases the penetration of IBU efficiently through the Skin PAMPA or the human epidermis.[36] The SM gel caused only a slightly lower flux than that with the SL gel, yielding a significantly higher penetration profile as compared with the control gel after 4 h ($p < 0.01^{**}$) and as compared with the SL gel after 7 h ($p < 0.001^{***}$; Fig. 2b). The combination SL + TR also demonstrated a lower penetration profile, as can be seen in the case of the *ex vivo* result. The penetration profile of IBU from the SM + TR gel showed the earliest significantly increased diffused IBU amount ($p < 0.001^{**}$) after 3 h as compared with the control gel and after 7 h as compared with the SM gel (Fig. 2b). The highest average penetration profile of IBU was seen with this gel. This result was verified by both the Skin PAMPA and the Franz cell method.

The determination coefficients (R^2) of linear regression of the correlation between the amount of IBU penetrated through the human skin and the amount of IBU penetrated through the Skin PAMPA indicated a good correlation. The determination coefficients between the *in vitro* PAMPA and the *ex vivo* Franz cell methods were in the range 0.88-0.99 (Fig. 2c). These EF values observed with the *ex vivo* and *in vitro* methods were of the same order of magnitude in all 5 cases (Fig. 3).

Conclusions

In summary, the results of this study have demonstrated that the *in vitro* Skin PAMPA system is a convenient rapid method for investigations of penetration enhancers to select the best one for *ex vivo* human skin and *in vivo* animal studies. The findings with the new artificial PAMPA membrane correlated closely with those with an *ex vivo* human skin membrane. It can serve as an effective prediction model for the monitoring of penetration enhancers and of drug penetration through the skin. From this aspect, this method could be the first, rapid, cost-effective, and simple system with which to test transdermal formulations. However, a better understanding of the penetration-enhancing effects of excipients necessitates the application of both *ex vivo* and *in vitro* methods. Our results indicate that TR as cosolvent with SM significantly improved the penetration of the surfactant into the skin and promoted attainment of the maximum penetration effect. SM + TR could be a potential nontoxic biocompatible penetration enhancer combination for IBU in transdermal delivery systems.

Acknowledgments

The authors wish to thank the Mitsubishi-Kagaku Foods Corporation (Tokyo, Japan) for providing samples of sugar-esters and Lubrizol Corporation/Azelis (Budapest, Hungary) for providing Carbopol samples.

References

1. Prausnitz MR, Elias PM, Franz TJ, et al. Skin barrier and transdermal drug delivery. In: Bolognia JL, Jorizzo JL, Schaffer JV, eds. *Dermatology*. 3rd ed. St. Louis: Elsevier Health Sciences; 2012:2065-2073.
2. Barry BW. Novel mechanisms and devices to enable successful transdermal drug delivery. *Eur J Pharm Sci*. 2001;14(2):101-114.
3. Rhee YS, Chang SY, Park CW, Chi SC, Park ES. Optimization of ibuprofen gel formulations using experimental design technique for enhanced transdermal penetration. *Int J Pharm*. 2008;364(1):14-20.
4. Potthast H, Dressman JB, Junginger HE, Midha KK. Biowaiver monographs for immediate release solid oral dosage forms: ibuprofen. *J Pharm Sci*. 2005;94(10):2121-2131.
5. Touitou E, Levi-Schaffer F, Dayan N, Alhaique F, Riccieri F. Modulation of caffeine skin delivery by carrier design: liposomes versus permeation enhancers. *Int J Pharm*. 1994;103(2):131-136.
6. Cázares-Delgadillo J, Naik A, Kalia YN, Quintanar-Guerrero D, Ganem-Quintanar A. Skin permeation enhancement by sucrose esters: a pH-dependent phenomenon. *Int J Pharm*. 2005;297(1–2):204-212.
7. Mitsubishi-Kagaku Foods Corporation. *Ryoto Sugar Ester Technical Information. Nonionic Surfactant/Sucrose Fatty Acid Ester/Food Additive*; 1982. http://www.mfc.co.jp/english. Accessed December 30, 2015.
8. Youan BC, Hussain A, Nguyen NT. Evaluation of sucrose esters as alternative surfactants in micro-encapsulation of proteins by the solvent evaporation method. *AAPS PharmSci*. 2003;5(2):123-131.
9. Kanikkannan N, Singh M. Skin permeation enhancement effect and skin irritation of saturated fatty alcohol. *Int J Pharm*. 2002;248(1–2):219-228.
10. Csóka G, Marton S, Zelko R, Otomo N, Antal I. Application of sucrose fatty acid esters in transdermal therapeutic systems. *Int J Pharm*. 2007;65(2):233-237.
11. Ayala-Bravo HA, Quintanar-Guerrero D, Naik A, Kalia YN, Cornejo-Bravo JM, Ganem-Quintanar A. Effects of sucrose oleate and sucrose laureate on in vivo human stratum corneum permeability. *J Pharm Res*. 2003;20(8):1267-1273.
12. Bonina F, Carelli V, DiColo G, Montenegro L, Nanniperi E. Vehicle effects on in vitro skin permeation of and stratum corneum affinity for model drugs caffeine and testosterone. *Int J Pharm*. 1993;100(1–3):41-47.
13. Touitou E, Levi-Schaffer F, Shaco-Ezra N, Ben-Yossef R, Fabin B. Enhanced permeation of theophylline through the skin and its effect on fibroblast proliferation. *Int J Pharm*. 1991;70(1–2):159-166.
14. Ritschel WA, Panchagnula R, Stemmer K, Ashraf M. Development of an intracutaneous depot for drugs. Binding, drug accumulation and retention studies, and mechanism of depot. *Skin Pharmacol*. 1991;4(4):235-245.
15. Csizmazia E, Eros G, Berkesi O, Berkó S, Szabó-Révész P, Csányi E. Ibuprofen penetration enhance by sucrose ester examined by ATR-FTIR in vivo. *Pharm Dev Technol*. 2012;17(1):125-128.
16. El-Laithy HM. Novel transdermal delivery of Timolol maleate using sugar esters: preclinical and clinical studies. *Eur J Pharm Biopharm*. 2009;72(1):239-245.
17. El Maghraby GM, Barry BW, Williams AC. Liposomes and skin: from drug delivery to model membranes. *Eur J Pharm Sci*. 2008;34(4–5):203-222.
18. Tanojo H, Boelsma E, Junginger HE, Ponec M, Bodde HE. In vivo human skin barrier modulation by topical application of fatty acids. *Skin Pharmacol Appl Skin Physiol*. 1998;11(2):87-97.
19. Yilmaz E, Borchert HH. Effect of lipid-containing, positively charged nanoemulsions on skin hydration, elasticity and erythema—an in vivo study. *Int J Pharm*. 2006;307(2):232-238.
20. Netzlaff F, Kaca M, Bock U, et al. Permeability of the reconstructed human epidermis model Episkin in comparison to various human skin preparations. *Eur J Pharm Biopharm*. 2007;66(1):127-134.
21. Sinkó B, Garrigues TM, Balogh GT, et al. Skin-PAMPA: a new method for fast prediction of skin penetration. *Eur J Pharm Sci*. 2012;45(5):698-707.
22. Sinkó B, Kökösi J, Avdeef A, Takács-Novák K. A PAMPA study of the permeability-enhancing effect of new ceramide analogues. *Chem Biodivers*. 2009;6(11):1867-1874.
23. Sinkó B, Pálfi M, Béni S, Kökösi J, Takács-Novák K. Synthesis and characterization of long-chain tartaric acid diamides as novel ceramide-like compounds. *Molecules*. 2010;15(2):824-833.
24. Vizserálek G, Berkó S, Tóth G, et al. Permeability test for transdermal and local therapeutic patches using Skin PAMPA method. *Eur J Pharm Sci*. 2015;76:165-172.
25. Nicander I, Ollmar S. Clinically normal atopic skin vs. non-atopic skin as seen through electrical impedance. *Skin Res Technol*. 2004;10(3):178-183.
26. Savic S, Tamburic S, Savic M, Cekic N, Milic J, Vuleta G. Vehicle-controlled effect of urea on normal and SLS-irritated skin. *Int J Pharm*. 2004;271(1–2):269-280.
27. Betz G, Aeppli A, Menshutina N, Leuenberger H. In vivo comparison of various liposome formulations for cosmetic application. *Int J Pharm*. 2005;296(1–2):44-54.
28. Kligman AM, Christophers E. Preparation of isolated sheets of human stratum corneum. *Arch Dermatol*. 1963;88:702-705.
29. Brain KR, Green DM, Lalko J, Api AM. In vitro human skin penetration of the fragrance material geranyl nitrile. *Toxicol In Vitro*. 2007;21(1):133-138.

30. Schroeder IZ, Franke P, Schaefer UF, Lehr CM. Delivery of ethinylestradiol from film forming polymeric solutions across human epidermis in vitro and in vivo in pigs. *J Control Release*. 2007;118(2):196-203.
31. Mura S, Manconi M, Sinico C, Valenti D, Fadda AM. Penetration enhancer-containing vesicles (PEVs) as carriers for cutaneous delivery of minoxidil. *Int J Pharm*. 2009;380(1–2):72-79.
32. Yan KS, Yan TX, Guo H, et al. Evaluation of transdermal permeability of pentoxifylline gel: in vitro skin permeation and in vivo microdialysis using Wistar rats. *Drug Discov Ther*. 2007;1(1):78-83.
33. Lee CK, Uchida T, Kitagawa K, Yagi A, Kim NS, Goto S. Effect of hydrophilic and lipophilic vehicles on skin permeation of tegafur, alclofenac and ibuprofen with or without permeation enhancers. *Biol Pharm Bull*. 1993;16(12):1264-1269.
34. Godwin DA, Kim NH, Felton LA. Influence of Transcutol CG on the skin accumlation and transdermal permeation of ultraviolet absorbers. *Eur J Pharm Biopharm*. 2002;53(1):23-27.
35. Park ES, Chang SY, Hahn M, Chi SC. Enhancing effect of polyoxyethylene alkyl ethers on the skin permeation of ibuprofen. *Int J Pharm*. 2000;209(1–2):109-119.
36. Csizmazia E, Erős G, Berkesi O, Berkó S, Szabó-Révész P, Csányi E. Penetration enhancer effect of sucrose laurate and Transcutol on Ibuprofen. *J Drug Deliv Sci Tec*. 2011;21(5):411-415.